uOttawa

L'Université canadienne
Canada's university

FACULTÉ DES ÉTUDES SUPÉRIEURES ET POSTOCTORALES

uOttawa

L'Université canadienne
Canada's university

FACULTY OF GRADUATE AND POSDOCTORAL STUDIES

Tyler J. Sylvestre

AUTEUR DE LA THÈSE / AUTHOR OF THESIS

M.Sc. (Geography)

GRADE / DEGREE

Department of Geography

FACULTÉ, ÉCOLE, DÉPARTEMENT / FACULTY, SCHOOL, DEPARTMENT

Spatial Patterns of Snow Accumulation Across the Belcher Glacier Basin, Devon Island, Nunavut, Canada

TITRE DE LA THÈSE / TITLE OF THESIS

Luke Copland

DIRECTEUR (DIRECTRICE) DE LA THÈSE / THESIS SUPERVISOR

CO-DIRECTEUR (CO-DIRECTRICE) DE LA THÈSE / THESIS CO-SUPERVISOR

EXAMINATEURS (EXAMINATRICES) DE LA THÈSE / THESIS EXAMINERS

Laurence Gray

Konrad Gajewski

Gary W. Slater

Le Doyen de la Faculté des études supérieures et postdoctorales / Dean of the Faculty of Graduate and Postdoctoral Studies

Spatial Patterns of Snow Accumulation across the Belcher Glacier Basin, Devon Island, Nunavut, Canada

Tyler Jeremy Sylvestre

Thesis submitted to the
Faculty of Graduate and Postdoctoral Studies
In partial fulfillment of the requirements
For the MSc Degree in Physical Geography

Department of Geography
Faculty of Arts
University of Ottawa

Supervisor: Dr. Luke Copland
Laboratory of Cryospheric Research
Department of Geography, University of Ottawa

Committee Members
Dr. Konrad Gajewski
Department of Geography, University of Ottawa

Dr. Laurence Gray
Canada Centre for Remote Sensing, Natural Resources Canada

© Tyler J. Sylvestre, Ottawa, Canada, November 2009

Library and Archives Canada

Published Heritage Branch

395 Wellington Street
Ottawa ON K1A 0N4
Canada

Bibliothèque et Archives Canada

Direction du Patrimoine de l'édition

395, rue Wellington
Ottawa ON K1A 0N4
Canada

Your file *Votre référence*
ISBN: 978-0-494-61270-5
Our file *Notre référence*
ISBN: 978-0-494-61270-5

NOTICE:

The author has granted a non-exclusive license allowing Library and Archives Canada to reproduce, publish, archive, preserve, conserve, communicate to the public by telecommunication or on the Internet, loan, distribute and sell theses worldwide, for commercial or non-commercial purposes, in microform, paper, electronic and/or any other formats.

The author retains copyright ownership and moral rights in this thesis. Neither the thesis nor substantial extracts from it may be printed or otherwise reproduced without the author's permission.

AVIS:

L'auteur a accordé une licence non exclusive permettant à la Bibliothèque et Archives Canada de reproduire, publier, archiver, sauvegarder, conserver, transmettre au public par télécommunication ou par l'Internet, prêter, distribuer et vendre des thèses partout dans le monde, à des fins commerciales ou autres, sur support microforme, papier, électronique et/ou autres formats.

L'auteur conserve la propriété du droit d'auteur et des droits moraux qui protège cette thèse. Ni la thèse ni des extraits substantiels de celle-ci ne doivent être imprimés ou autrement reproduits sans son autorisation.

In compliance with the Canadian Privacy Act some supporting forms may have been removed from this thesis.

While these forms may be included in the document page count, their removal does not represent any loss of content from the thesis.

Conformément à la loi canadienne sur la protection de la vie privée, quelques formulaires secondaires ont été enlevés de cette thèse.

Bien que ces formulaires aient inclus dans la pagination, il n'y aura aucun contenu manquant.

Canada

Abstract
In May 2008, high frequency ground penetrating radar (GPR) surveys were conducted on the Belcher Glacier Basin, Devon Ice Cap, and validated with avalanche probe measurements to map the thickness and spatial variability of winter (2007-8) snow. The GPR record was combined with field measurements using a neutron density probe and correlated with NCEP-NCAR climate reanalysis, QSCAT satellite records, and airborne ASIRAS data to derive multi-year snow accumulation patterns across the basin from 2005-7. The distinct characteristics of the GPR record from the surface to 3 m depth were related to the 2007 and 2005 summer surfaces. GPR derived depths to these surfaces and the assessment of the average annual accumulation rate across this basin correlate very well with previous snow accumulation assessments in other parts of Devon Ice Cap (Mair et al. 2005, Colgan et al. 2008 and Koerner 1977). The complex radar returns in the LSS-05 depth range appear to be related to extensive melt processes during summer 2005, together with a large rain event in summer 2006, which produced large quantities of meltwater at all elevations of Devon Ice Cap. The major broad-scale control factor in determining annual and multiyear snow depth patterns for the basin is elevation, with surface topography and distance from the moisture source being locally important. GPR enabled the position of the basin-wide snow line to be determined by observing internal layers emerging at the surface, with the superimposed ice facies and equilibrium line altitude inferred below this altitude.

Acknowledgements

This paper is a contribution to the International Polar Year project GLACIODYN, The Dynamic Response of Arctic Glaciers to Global Warming. The work was funded by the University of Ottawa, National Science and Engineering Research Council of Canada (NSERC), the Northern Scientific Training Program (NSTP), the Canadian Foundation for Innovation (CFI) and the Ontario Research Fund (ORF). We thank the Polar Continental Shelf Project (PCSP) for logistical support (this thesis is PCSP contribution # 04409). We thank John Sekerka and Mike Demuth (NGP-GSC) for assistance with collecting and processing the neutron probe data, Wesley Van Wychen and Emilie Herdes for their dedication and hard work in the field (2008), Wilhelmina Clavano for processing the SPOT DEM and SPIRIT project (SPOT 5 stereoscopic survey of Polar Ice: Reference Images and Topographies, Université de Toulouse, France), Gabriel Wolken for providing Quickscat (QSCAT) data, and Laurence Gray for ASIRAS data at the Canada Centre for Remote Sensing.

__Table of Contents__

List of Tables

List of Figures

List of Acronyms

ACIA – Arctic Climate Impact Assessment

ASIRAS – Airborne Synthetic Aperture Radar (SAR) / Interferometric Radar Altimeter System

ASTER – Advanced Spaceborne Thermal Emission and Reflection Radiometer

BH # – Borehole number

DEM – Digital Elevation Model

ELA – Equilibrium Line Altitude

ESA – European Space Agency

FMCW – Broadband Microwave Frequency Modulated Continuous Wave

GCM – Global Climate Model

GCP – Ground Control Point

GIS – Geographic Information System

GPR – Ground Penetrating Radar

GPS – Global Positioning System

IDW – Inverse Distance Weighting

IPCC – Intergovernmental Panel on Climate Change

IPY – International Polar Year

IRH – Internal Reflector Horizon

LSS – Last Summers Surface

MHz – Megahertz

MODIS – Moderate Resolution Imaging Spectroradiometer

NASA – National Aeronautics and Space Administration

NCEP / NCAR – National Centers for Environmental Prediction / National Center for Atmospheric Research

NE – Northeast

NGP – GSC – National Glaciology Program at the Geological Survey of Canada

NOW – North Open Water Polynya

NW – Northwest

PC # – Principal Component number

PCA – Principal Component Analysis

PDD – Positive Degree Days

QEI – Queen Elizabeth Islands

QSCAT – SeaWinds Scatterometer on the QuikSCAT satellite

S.D. – Standard Deviation

SE – Southeast

SEC2 – Spherical Exponential Calibrated Compensation Gain

SMB – Surface Mass Balance

SPOT – Système Pour l'Observation de la Terre

SW – Southwest

SWE – Snow water equivalent

TWT – Two-Way Travel time

CHAPTER 1 – Introduction

1.1 Introduction

Evidence of climate change since the 1960s in the Queen Elizabeth Islands (QEI) of the Canadian High Arctic is reflected in region-wide declines in cryospheric variables such as glacier area and surface mass balance (SMB) (Fig 1.1) (Braun *et al.* 2004; Burgess and Sharp, 2004; Huss *et al.* 2008; Sneed *et al.* 2008), ice shelves (Copland *et al.* 2007), permafrost (Lewkowicz, 2007), and sea ice (Maslanik *et al.* 2007). Over the same period, surface air temperatures (> 65°N) have increased on average by 0.09°C per decade, nearly double the background rate of the entire Northern Hemisphere (NASA, 2007) (Fig. 1.2). The QEI and Baffin Island contain ~150,000 km^2 of glaciers, the largest area of terrestrial ice in the polar regions outside of Greenland and Antarctica (Hagen *et al.* 2003). If these glaciers and ice caps were to melt, global sea levels could rise by ~0.5 m (Wang *et al.* 2005).

In a pan-arctic review of glacier mass balance records over the last half-century by Dowdeswell *et al.* (1997), 70% of years sampled had negative SMB. SMB refers to the sum of accumulation processes (snowfall, superimposed ice) minus the sum of ablation processes (surface melt, sublimation, calving). Snow accumulation at any site on a glacier is a function of both external controls such as climatic conditions and distance from moisture sources, and internal localized controls such as topography, elevation and wind redistribution. Despite the widespread evidence of recent cryospheric changes across the QEI, there have been few studies that have quantified glacier changes in detail with regards to snow accumulation patterns, making it difficult to assess its impact on observed terrestrial ice losses (Hagen *et al.* 2003; Mair *et al.* 2005). To address this shortcoming, and to provide accurate predictions of future sea level rise, we therefore need to improve understanding of the spatial and temporal patterns and controls on snowfall across the ice caps of the QEI, including quantification of net snow water equivalent (SWE) and near surface (<15 m) density (Bell *et al.* 2008; Demuth *et al.* 2007)

Snow accumulation data is usually determined from shallow firn cores, snow pits and stake measurements, which means that it is limited in time and space to the local conditions at the probing site (Anschütz *et al.* 2007; Koerner *et al.* 2002; Mair *et al.* 2005). Current estimates

Figure 1.1 Time-series of cumulative net mass balance (mm W.E.) for glaciers and ice caps in the QEI 1960 – 2001. Source: Demuth and Pietroniro, 2008 (based on Koerner's work).

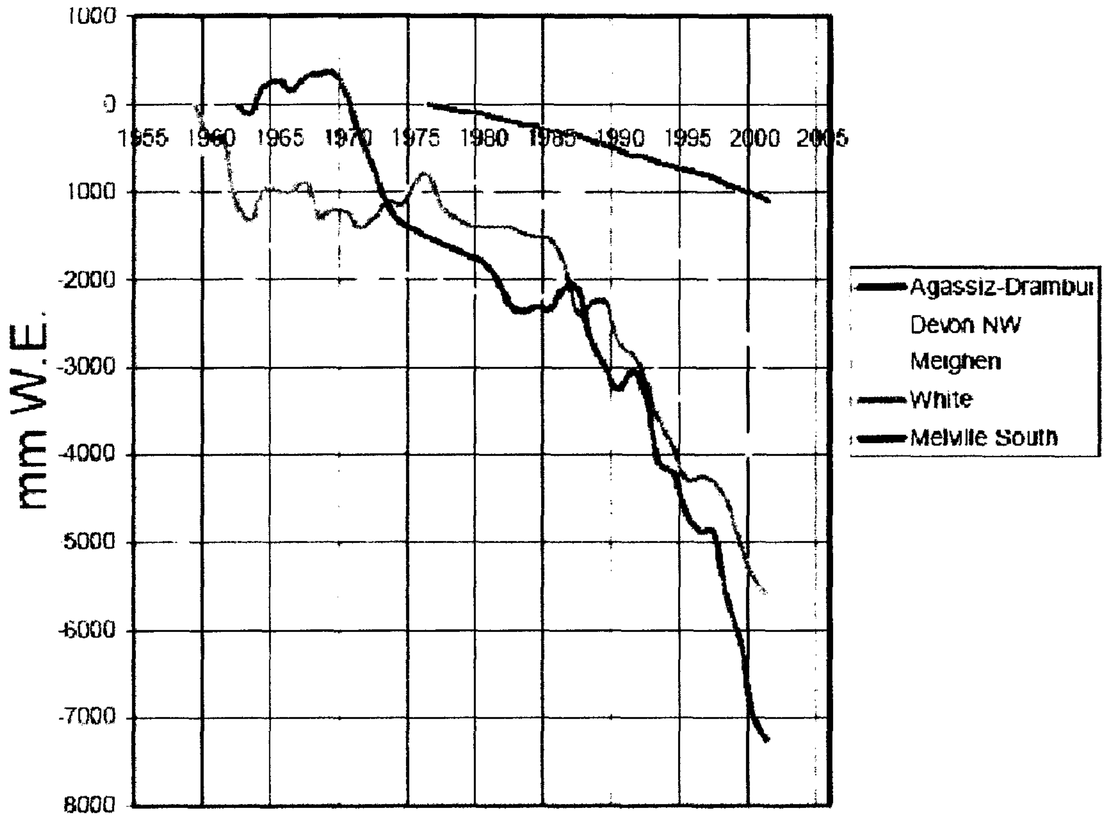

Figure 1.2 Decadal changes in surface air temperature (^{o}C $decade^{-1}$) between 1981 – 2007. Source: NASA (2007).

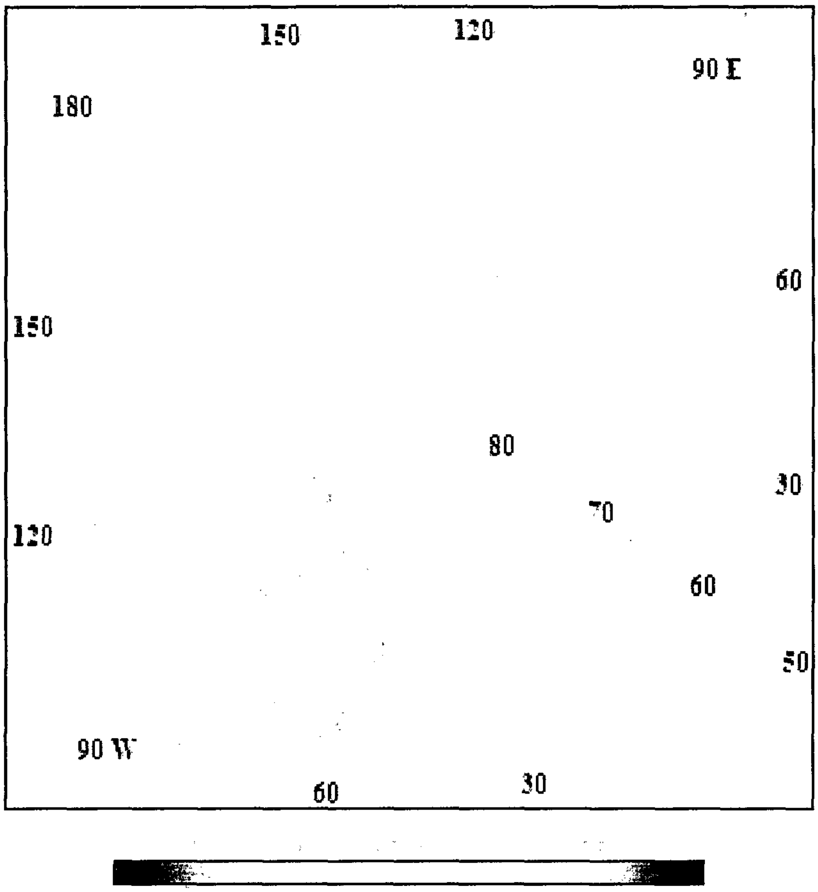

of snow accumulation on ice caps such as the Greenland Ice sheet have large errors (20 – 25%) because extrapolation methods use only a sparse network of point data (Maurer, 2006). Mair *et al.* (2005) undertook a study of snow accumulation patterns in the upper regions of Devon Ice Cap using down-borehole gamma spectroscopy, and stated that "*A fundamental uncertainty concerns the ability of a measurement based on a single core or point to represent the average accumulation rate across a larger area.*" Net accumulation inferred via ice cores is different than annual snowfall measured at a point because runoff due to surface melt can remove part of the local annual accumulation, and meteorological records of snowfall usually come from distant settlements which are not spatially and temporally representative of snow accumulation on a glacier (Colgan *et al.* 2008). In addition, quantifying snowfall in the polar regions is difficult due to generally low precipitation totals and wind redistribution (Colgan *et al.* 2008).

Ground penetrating radar (GPR) is used to measure the spatial distribution of internal glacier properties such as snow layers and accumulation variability (Pälli *et al.* 2002). Snow layers or Internal Reflector Horizons (IRHs) in GPR surveys result from differences in dielectric constant between materials, and are formed by processes such as spatial variations in accumulation, changes in surface slope, internal accumulation through melting and refreezing, and redistribution by wind action (Maurer, 2006). GPR has been used to map variability in SMB and accumulation over large areas by connecting internal layers found in snow pits and core sites at different locations on the same ice cap such as Austfonna, Svalbard (Dunse *et al.* 2009; Taurisano *et al.* 2007), and Potsdam Glacier in Coastal Dronning Maud Land, East Antarctica (Anschütz *et al.* 2006). On Austfonna, high frequency GPR has also been used to determine the location of the equilibrium line altitude (ELA), and to understand temporal changes in glacier facies using repeat surveys (Dunse *et al.* 2009). GPR therefore has the potential to improve upon snow accumulation estimates by providing greater horizontal and vertical coverage than a single point measure (core or stake) can offer. High frequency GPR (250 – 1000 MHz) has been shown to significantly improve upon point accumulation estimates because it enables continuous snow depth measurements over large regions in short time periods with high vertical and horizontal resolutions. Extending the spatial coverage of snow accumulation measurements enables the characterization of spatial variability and distribution of accumulation (Maurer, 2006).

A series of field measurements have been conducted by the National Glaciology Program (of the Geological Survey of Canada; NGP-GSC) on Devon Ice Cap, Nunavut, since the 1960s to assess SMB changes. This has included shallow and deep ice cores (Koerner, 1977), snow pits (Bell *et al.* 2008), gamma-spectrometry measurements (Colgan and Sharp, 2008; Mair *et al.* 2005), installation of automatic weather stations, mass balance stakes, and remote sensing studies (Burgess and Sharp, 2004). Most of these measurements have been focused in the NW (Sverdrup Basin), summit (~1921 m a.s.l) and SW regions (Fig 1.3). Mass balance patterns and changes in the NE (Belcher Glacier) sector have been largely interpolated from these remote point measurements, resulting in uncertainties concerning the ability of these measurements to truly represent the conditions within this region (Mair *et al.* 2005).

The aim of this study is to present the first detailed, *in situ* measurements of snow accumulation patterns across the Belcher Glacier basin. This is mainly based on a series of GPR, avalanche probe and snow pit measurements collected over a horizontal track distance of ~306 km in May 2008. In addition, a high resolution neutron probe was used to make density readings in a series of shallow boreholes drilled across the accumulation area of the glacier. The GPR measurements provide information about the spatial continuity of point measurements by enabling internal layers found in the snow pits and boreholes to be regionally connected across the accumulation zone of the glacier. In turn, this enhances understanding of controls and factors on snow accumulation, and enables the calculation of detailed SWE values.

This study is part of the larger *GLACIODYN: The Dynamic Response of Arctic Glaciers to Global Warming* project, which in turn is part of the International Polar Year (IPY) (http://www.ipy.org/). The aim of the GLACIODYN project is to determine the dynamic response of tidewater glaciers under future climate change scenarios, and incorporates studies on glaciers in Svalbard, Alaska and Greenland, in addition to Belcher Glacier. The Canadian GLACIODYN project is being undertaken with partners from the University of

Figure 1.3. Location of Sverdrup Glacier terminus (blue dot), Summit region (1920 m a.s.l; yellow dot), and the Belcher Glacier basin (outlined in red), on Devon Island Ice Cap, Nunavut (Base image: Landsat 7, July 7, 2000). Inset of QEI with arrow indicating Devon Island.

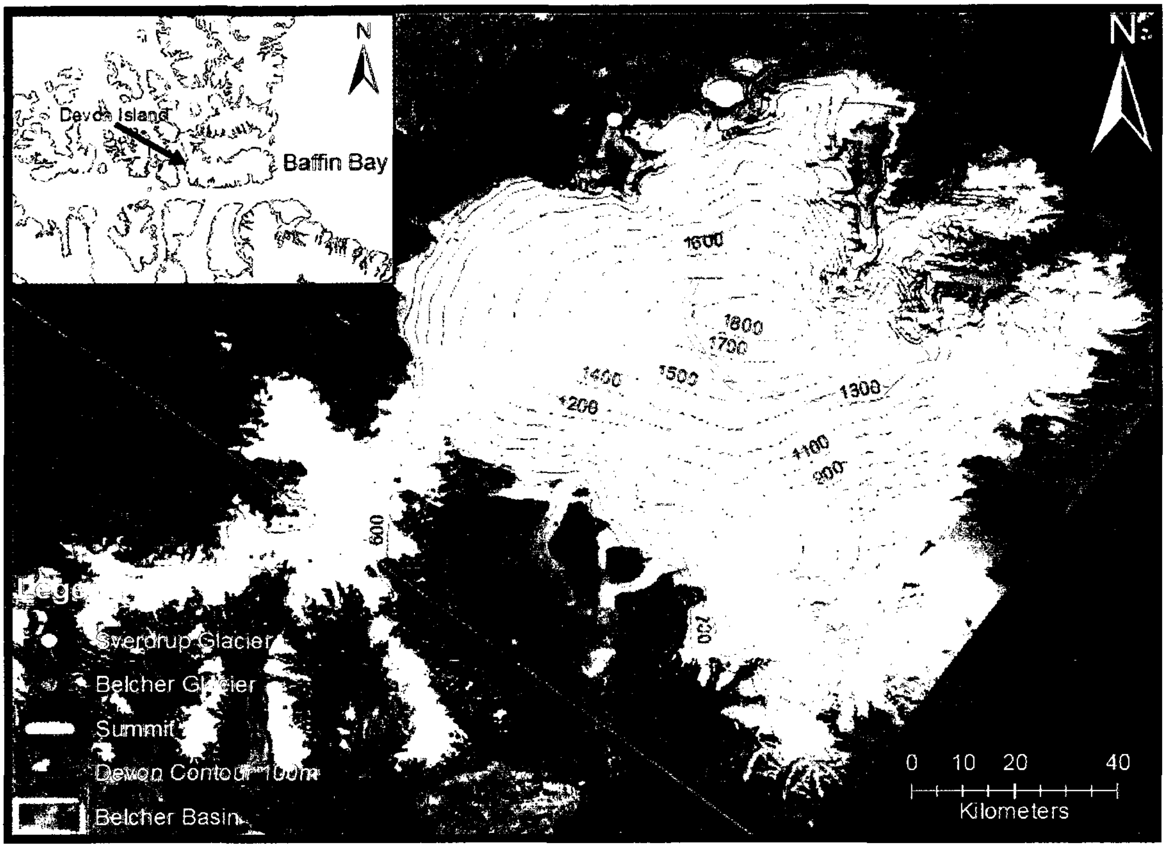

Alberta, University of Ottawa, Memorial University and Simon Fraser University. It involves an intensive field and remote sensing study of the mass balance, hydrology and dynamics of the Belcher Glacier, to provide inputs for a high order coupled model of SMB, ice flow dynamics and hydrology. This study provides snow accumulation information for modeling of the magnitude and spatial distribution of runoff in the Belcher Glacier basin under summer conditions. These data will be used for testing the model hypothesis that changes in the rate of delivery of surface water to the glacier bed can result in major changes in the flow dynamics of the glacier.

1.2 Motivations and Broader Context

Global climate model (GCM) projections show average annual air temperatures in the Arctic could increase to ~3-11°C by 2100 (ACIA, 2004; IPCC, 2007). These models also consistently predict that the most pronounced warming will occur in the winter. This means that the intensity and duration of the melt season on Arctic glaciers will likely also increase (Zwally *et al.* 2002). Furthermore, all IPCC scenarios consistently show that a warmer atmosphere induces a greater moisture holding capacity (Trenberth *et al.* 2003), with each 1°C increase in temperature coinciding with a ~5% increase in precipitation (IPCC, 2007). This could result in a 15-36% mean annual increase in precipitation in the Arctic by 2100. These predictions currently have a high degree of uncertainty, however, due to the lack of detailed information on snowfall and accumulation processes on ice masses in these areas. It therefore remains unclear whether glaciers and ice caps in the QEI will shrink or grow in response to the positive relationship between air temperature and precipitation. This motivates efforts to improve the accuracy of accumulation measurements so that these values can be used in SMB models to better predict glacier changes in a warming Arctic.

A recent study in Greenland by Zwally *et al.* (2002) suggests that changes in glacier geometries, ice flow dynamics and iceberg calving can represent significant influences on glacier contributions to eustatic sea level rise (Colgan and Sharp, 2008; Burgess and Sharp, 2004; Koerner 1977). They found a direct correlation with the timing and quantity of surface melt and increased ice velocities in Greenland, indicating that an increase in the length and intensity of the summer melt season can provide a mechanism for accelerated glacier flow.

Traditionally it was believed that ice sheets, ice caps and large glaciers responded to climate changes over timescales of ~100–1000 years, but the realization that ice motion can respond rapidly via changes in englacial and subglacial hydrology indicates that changes can actually occur at much shorter time scales of ~10–100 years or less (Zwally *et al.* 2002). Rignot and Kanagaratnam (2006) used satellite radar interferometry observations of Greenland to measure widespread acceleration of outlet glaciers south of 66°N in both the east and west margins of the ice sheet between 1996 and 2000. By 2005 similar accelerations had occurred on outlet glaciers up to 70°N. Since the 1990s, annual ice sheet mass loss from Greenland has more than doubled from 90 km^3 a^{-1} to 220 km^3 a^{-1} due in large part to these increased ice velocities (Rignot and Kanagaratnam, 2006).

Given the work on the larger Greenland ice sheet, it is possible that dynamic changes of the smaller glaciers and ice caps of the QEI could allow them to respond more quickly to changing climatic conditions than changes in SMB alone. In general, the relationship between increased surface melting and ice-sheet flow has been given little or no consideration in the QEI. This study will provide the snow distribution information necessary to run improved hydrological and mass balance models to address this question.

1.3 Study Area

1.3.1 Devon Island

Devon Ice Cap covers the eastern portion of Devon Island, Nunavut, Canada (75°30'N, 82°00'W), and has an asymmetrical shape with an east-west trending summit ridge (Fig. 1.3) (Burgess and Sharp, 2004; Colgan and Sharp, 2008; Mair *et al.* 2005). The ice cap is one of the largest in the Canadian Arctic, with a surface area of 14010 km^2. It is estimated that the ice-cap volume is 3980 – 4110 km^3, with a maximum ice thickness of 880 m at the head of its eastward flowing basins (Burgess and Sharp, 2004; Colgan and Sharp, 2008). Its summit is at ~1921 m, with 19% of the cap above 1200 m elevation (Burgess and Sharp, 2004; Colgan and Sharp, 2008). A few long-term (>30 years) weather stations located at the summit (75°20'51.59"N, 82°10'25.81"W) and NW sectors (Sverdrup Glacier; 75°34'56.76"N, 83°04'06.75"W) are maintained by the NGP-GSC and the University of Alberta (Koerner

2005; Koerner, 1977). Summit mean annual air temperature (MAAT) is about -23°C, and mean precipitation is 0.22 m a^{-1} snow water equivalent (SWE) (Koerner, 1977).

The eastern margin of this ice cap faces the North Open Water (NOW) Polynya at the head of Baffin Bay and includes the larger tidewater outlet glaciers of the ice cap (Fig. 1.3) (Burgess and Sharp, 2008). SMB studies show that these glaciers experience high rates of accumulation (up to 500 kg m^{-2} a^{-1}), surface ablation (up to 2000 kg m^{-2} a^{-1}), and mass loss by iceberg calving (Burgess and Sharp, 2004). In the western region of Devon Ice Cap, glaciers tend to terminate on land at elevations of 300-500 m. Burgess and Sharp (2004) explain how the western portion of the island experiences a rain shadow and has very reduced rates of snow accumulation (200 kg m^{-2} a^{-1}) and ablation (1000 kg m^{-2} a^{-1}) compared with the eastern margins of the island.

1.3.2 Belcher Glacier Basin

The Belcher Glacier drainage basin (75°36"N, 81°26"W) lies in the northeast sector of the ice cap, covers 1180 km^2, and is the largest and fastest flowing (up to 300 m a^{-1}) outlet of the ice cap (Fig. 1.4) (Burgess and Sharp, 2004; Dowdeswell *et al.* 2004). The basin faces north east towards the NOW Polynya, which acts as its primary moisture source. Flow stripes on the glacier surface indicate that its motion is largely dominated by basal sliding and bed deformation (Burgess and Sharp, 2004). Crevasse fields and moulins on the glacier surface suggest that supraglacial water channels sink to the glacier bed and connect to subglacial channels.

Figure 1.4 Synthetic aperture radar interferogram of Devon Ice Cap, with surface velocities given in the look direction of the satellite (arrow). The interferogram is overlain on a 1999 Landsat 7 ETM+ image. Source: Dowdeswell *et al.* (2004)

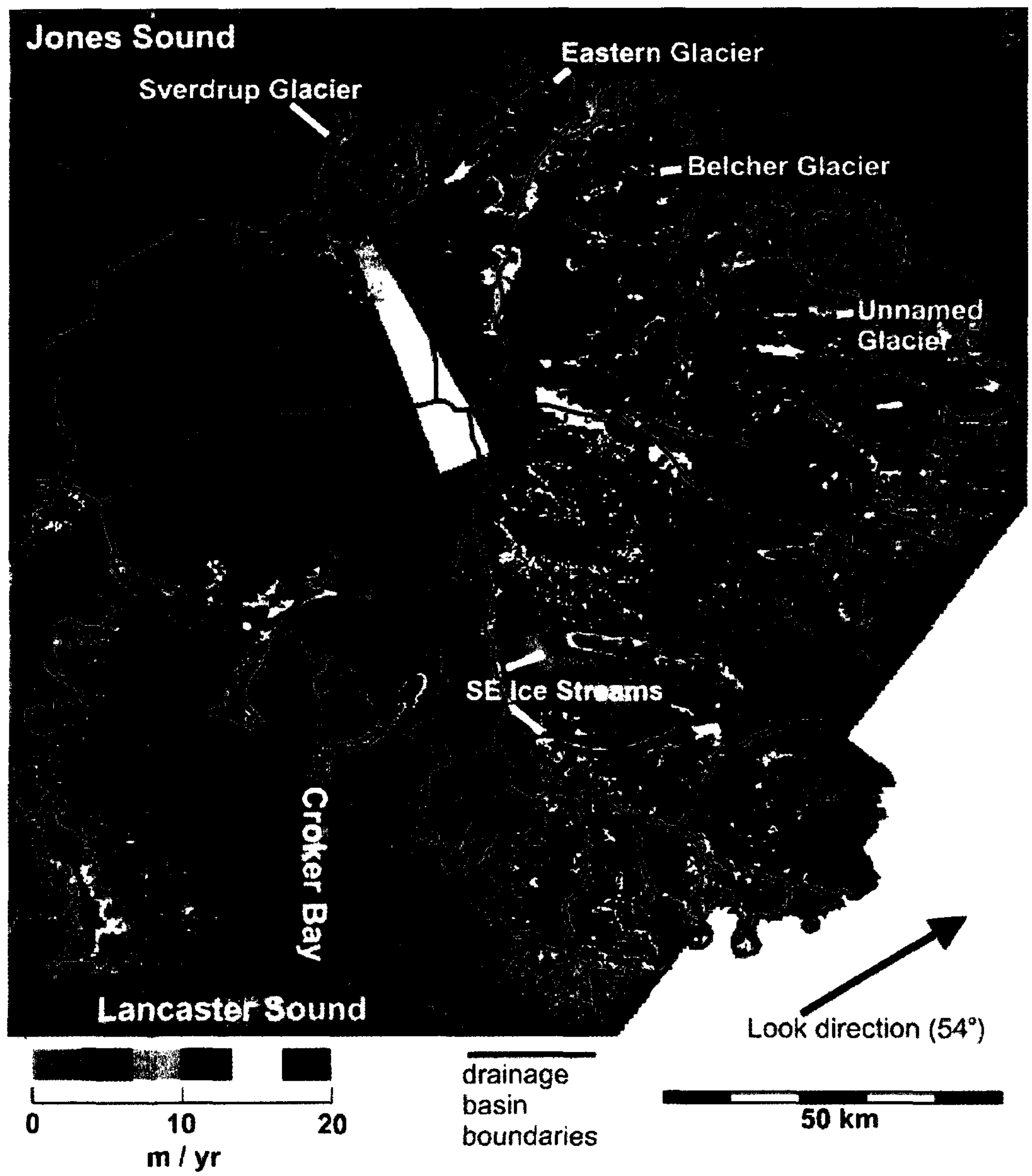

1.4 Thesis Layout

This document is presented in an expanded thesis by article format. Chapter 2 provides a discussion and literature review of current understanding and past work on climate changes and snow accumulation patterns in the QEI and Devon Ice Cap. An evaluation of GPR and its applications to snow and glaciers is also contained in Chapter 2. The third chapter is written in paper format with the intention of submitting it to a peer-reviewed journal such as the *Journal of Glaciology*. Authors for this paper are Tyler Sylvestre and Dr. Luke Copland from the Department of Geography, University of Ottawa, Michael Demuth from Natural Resources Canada, National Glaciology Group, Ottawa, and Dr. Laurence Gray from the Canadian Centre for Remote Sensing, Natural Resources Canada. Tyler Sylvestre did all the field work, writing, data processing and analysis. Dr. Luke Copland reviewed the text, and assisted with field work and data interpretation. Michael Demuth provided the neutron probe, and performed neutron probe calculations. Dr. Laurence Gray processed airborne ASIRAS data flown by European Space Agency (ESA) in support of the CryoSat calibration/validation campaign in 2006. Chapter 4 presents final conclusions derived from this study, and all references are provided as a single list at the end of this chapter. The Appendix provides a brief overview of the spatial scales of snow variability across the Belcher Basin using semivariance analysis.

CHAPTER 2 – Literature Review

2.1 Recent Climate Changes in the QEI

There is widespread evidence of recent cryospheric changes in the Canadian Arctic (Braun *et al.* 2004; Demuth and Pietroniro, 2007; Dowdeswell *et al.* 1997). In this chapter, a detailed review is provided of recent changes to glaciers in the QEI (Dowdeswell *et al.* 1997; Koerner, 2005). For example, a comparison of aerial photography from 1960 with satellite imagery from 2000 by Dowdeswell *et al.* (2007) indicates that the glaciers on Bylot Island experienced area losses of 5% (253 km^2) over this 40 year period. This is consistent with the regional warming trend that has occurred in the Arctic since the 1960s, with glacier retreat on Bylot Island occurring at rates from three to nine times higher in the second half of the 20^{th} century compared to the first half (Fig. 2.1) (Dowdeswell *et al.* 2007).

Short term negative changes such as extreme melt events can play a major role in impacting glacier SMB (Boon *et al.* 2003; Copland *et al.* 2007; Koerner, 1977). For example, Boon *et al.* (2003) describe an extreme melt event on John Evans Glacier, Ellesmere Island, between 28-30 July 2000. Air temperatures reached +8°C during this time, and rates of surface lowering averaged 56 mm day^{-1} along the glacier centerline at 1183 m a.s.l. Melt occurred at all elevations on the glacier during this time, and this single melt event was responsible for 30% of total summer melt at 1183 m and 15% at 850 m. The event thus contributed disproportionately to summer ablation and runoff, and may have had a significant influence on the annual SMB of the glacier. This raises the possibility that increases in the incidence of such events may significantly contribute to interannual variability and longer-term changes in runoff and the SMB of QEI glaciers, where summer melt is typically low.

Other evidence of the impact of short term events is provided by the loss of ice shelves from northern Ellesmere Island. For example, MODIS and ASTER satellite imagery indicate that the entire Ayles Ice Shelf was lost within 5 hours on August 13, 2005 (Copland *et al.* 2007). This change appears to be permanent with no evidence of re-growth. The event occurred during the lowest recorded sea ice extent on record within a region that has experienced

Figure 2.1 Changes in glacier terminus positions on Bylot Island (a – d) since the Neoglacial maximum. End moraines outlined for the 2001 snout area, the 1958/1961 margin and the Neoglacial maximum. Source: Dowdeswell *et al.* (2007).

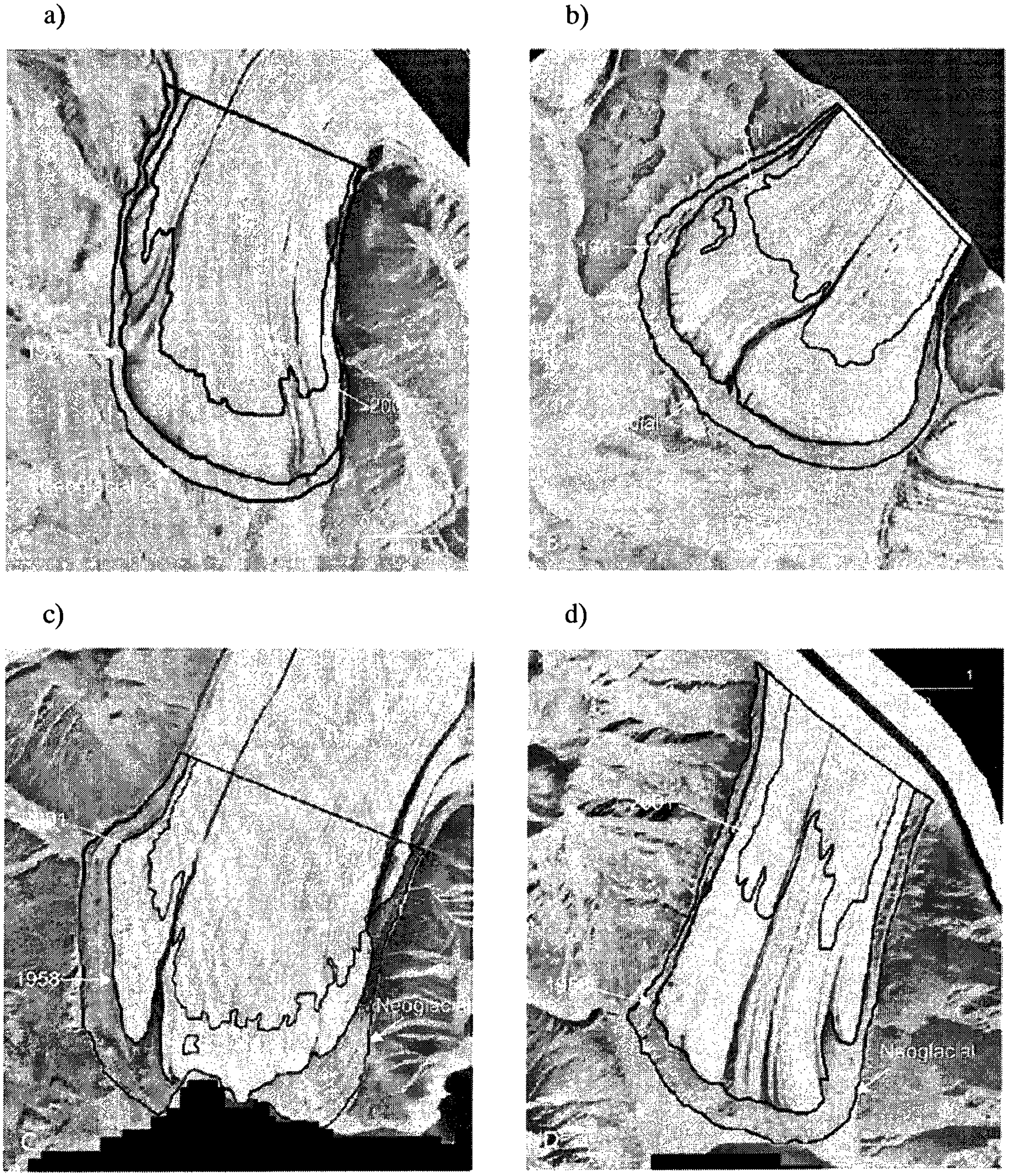

warming of 0.37°C decade^{-1} since 1948, decreases in freezing degree days (FDDs) and rapid increases in positive degree days (PDDs) since the 1990s (Copland *et al.* 2007). The evidence of increasing PDD trends in the QEI compares with the findings of Zwally *et al.* (2002) in Greenland, who showed that summer PDD totals for 1996-1999 increased from 47.6 in 1996, to 60.8 in 1997, to 116.5 in 1998, and were then 94.7 in 1999 (Fig. 1.6c). This suggests that both the intensity and duration of warming is playing a significant role in the QEI, and stresses the importance of accurately quantifying SMB changes in light of these trends.

Overall, QEI glaciers have experienced net SMB deficits and retreat over the last half century, although some ice masses have thickened at higher elevations. This is revealed in both the Meighen (Koerner and Lundgaard, 1995) and Devon Island (Burgess and Sharp, 2005) ice caps. Koerner and Lundgaard (1995) show that the Meighen Ice Cap is mainly stagnant with most accumulation coming from superimposed ice. Its central portion has experienced a positive SMB over the last 34 years, which likely relates to its proximity to the Arctic Ocean (which acts as its moisture source region). Recent trends of less sea ice in the Arctic Ocean means that there is a larger area of open water present, which leads to more moisture availability and therefore more accumulation.

2.2 Recent Changes on Devon Ice Cap

The National Glaciology Program at the Geological Survey of Canada (NGP-GSC) has conducted extensive glaciological monitoring and assessment of the SMB of Devon Ice Cap since 1961 (Burgess and Sharp, 2004; Koerner, 1977; Koerner, 2005; Mair *et al.* 2005). Data has mainly been collected on a NW–SE profile (Fig. 2.2) extending from the Sverdrup Glacier (NW) across the ice cap summit towards Lancaster Sound (SE) using deep (>200 m) and shallow (<25 m) ice cores, snow pits / trenches, manual probing and automated weather stations (Burgess and Sharp, 2004; Koerner, 1977; Mair *et al.* 2005).

Ice cores retrieved at high elevations on Devon Ice Cap in the 1970s show that accumulation varies slightly between 1600-1800 m a.s.l (Koerner, 1977). This suggests that melting governs SMB at this elevation range, as interannual variability in snow accumulation tends

Figure 2.2: Previous studies on Devon Ice Cap focused in the Northwest (Sverdrup Basin), Summit (1920 m a.s.l), and Southeast sites. Borehole locations and point measurement sites along transects on Devon Ice Cap by the Geological Survey of Canada. Source: Koerner (2002)

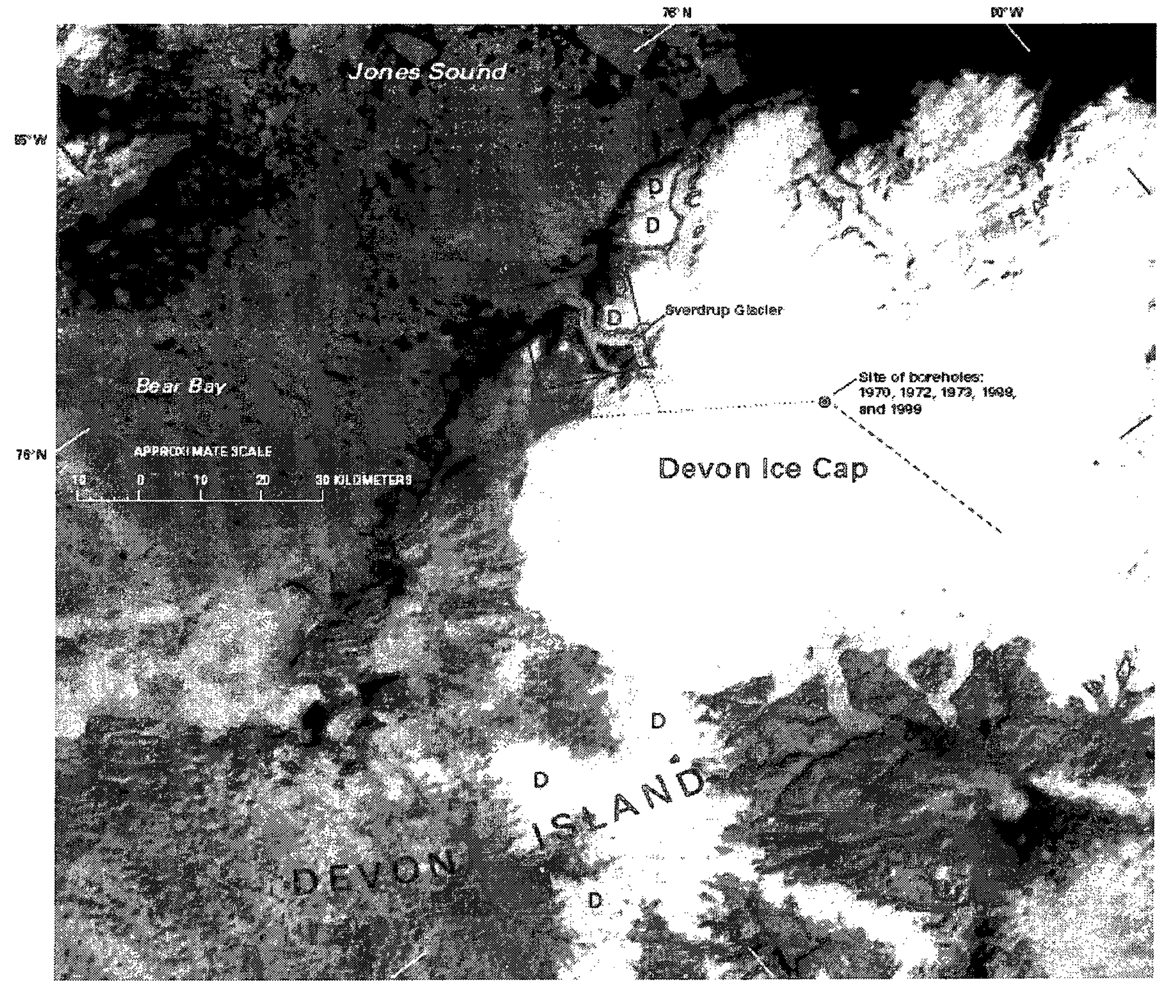

to be low. Other findings since the 1970s show that single negative balance years have a disproportionate effect on SMB trends, and can cancel out several years of positive mass balance. For example, Koerner (2005) showed that for 1960-2005, the warmest years (summers) on record (1962, 1998, and 2001) combine to cancel out the positive balance years for the entire period on the NW side of the ice cap. Warmer summers have increased the melting and depth of meltwater percolation in the accumulation area of Devon Ice Cap, leading to increased near-surface densities (Koerner, 2005). By measuring ice lenses in firn cores, Koerner (1977) showed that the ice cap has experienced a warmer period since 1925 since there was an unusually high percentage of ice content between the surface and 40 m depth, whereas there were very few ice layers between 40 and 95 m depth (Fig. 2.3).

Burgess and Sharp (2004) quantified recent changes in the areal extent of Devon Ice Cap by comparing the positions of ice margins in aerial photographs from 1959/60 and satellite imagery from 1999/2000. Over this 40 year period Devon Ice Cap underwent a net decrease in surface area of 338 ± 40 km^2, with four eastern tidewater glaciers accounting for 10% of this loss (38 ± 4 km^2). The Belcher Glacier (basin 15; Fig. 2.4) has experienced terminus retreat of up to 1300 m since 1960, with increased areas of exposed bedrock within the basin. However, since 1960, adjacent basins (2 and 12: Fig. 2.4) in the NW and west parts of Devon Ice Cap have experienced an ice margin advance by an average of 130 m along an 80 km section. This represents a 10.5 ± 2 km^2 increase in surface area of the ice cap. The ice cap has experienced differential changes in ice cap geometry such as area, volume and variation in terminus position over time, with an overall pattern of ice mass loss since the 1960s (Burgess and Sharp, 2004).

Burgess and Sharp (2008) assessed ice thickness changes of individual glacier drainage basins on Devon Ice Cap between the 1960s and 2000s by comparing surface elevations derived from 1960s aerial photography with airborne laser altimetry survey data collected by NASA in the spring of 2005. Over this period, Belcher Glacier thinned along almost its entire length at a rate of -0.62 ±0.14 m a^{-1} w.e., which equates to a total volume of 11.19 ±1.44 km^3 w.e. Rates of volume change in the accumulation and ablation zones were -0.013 ±0.031 km^3 a^{-1} w.e and -0.274 ±0.070 km^3 a^{-1} w.e., respectively. Furthermore, over half of

Figure 2.3 Ice percentage for three ice cores (>1800 m a.s.l.) drilled on the summit of Devon Ice Cap. Melt increases since 1925 (0-20 m) indicated by greater ice content when compared with deeper sections (20-150 m). Source: Koerner (1977).

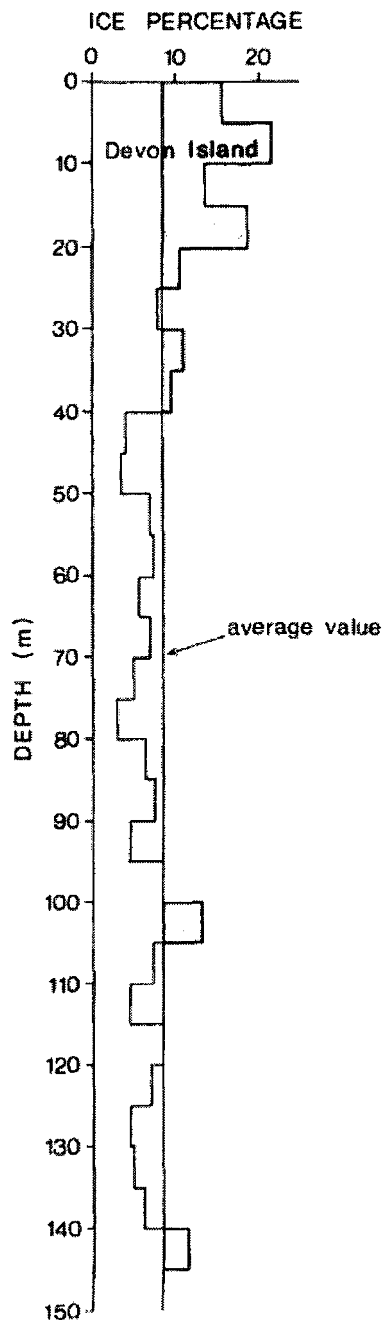

Figure 2.4 Drainage basins of Devon Ice Cap (Belcher Glacier is basin 15).Source: Burgess and Sharp (2004)

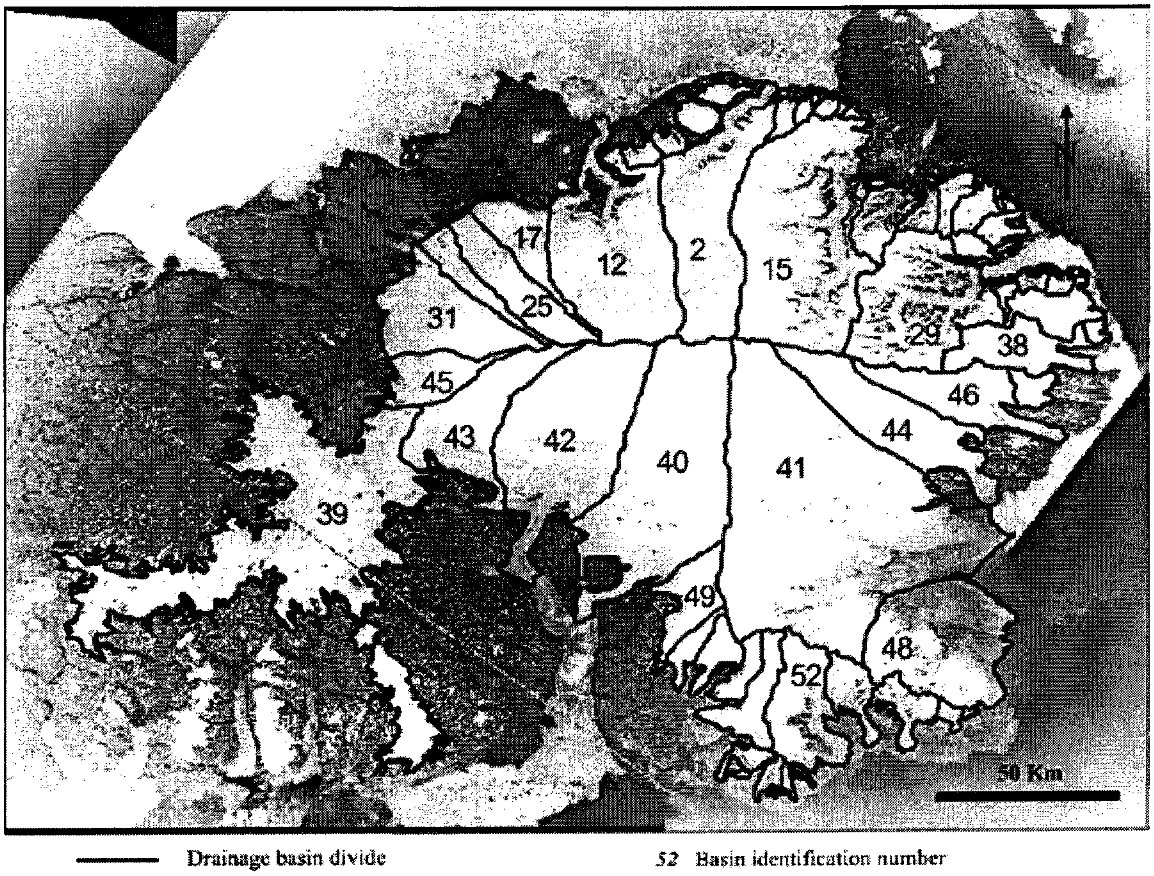

the ice loss from the Belcher basin is related to iceberg calving (-0.21 km^3 a^{-1} w.e.). This represents ~15% of the total mass loss from the entire ice cap since the 1960s. Trends in ice lowering have occurred up to and beyond the long-term ELA to about ~1400 m. The combination of aerial photography and altimetry studies further reveals that the formation of meltwater channels up to 1500 m elevation may provide sufficient surface meltwater to the glacier bed to increase basal lubrication and thus create suitable conditions for speed up of the glacier in its lower reaches. Burgess and Sharp (2008) suggest that most of the surface lowering in the Belcher Glacier basin can be linked to an increased rate of ice flux at lower elevations.

One potential reason for the differential changes in geometry between basins on Devon Ice Cap relates to the existing climate pattern. The North Open Water (NOW) Polynya at the head of Baffin Bay is typically ice free for the entire year and acts as a moisture source for the ice cap, resulting in twice as much precipitation falling over the eastern sector compared with the west (Burgess and Sharp, 2004). Secondly, glaciers on the eastern side of the ice cap typically have low elevation tidewater termini that experience higher rates of surface ablation and mass loss due to iceberg calving than the higher elevation land-terminating glaciers in the west. This means that the eastern part of the ice cap experiences more of a maritime climate, while the western section faces the interior of the QEI and has a more continental climate, being largely unaffected by the moisture source region when compared with the eastern basins.

2.3 Knowledge about Snow Accumulation in the QEI and Devon Ice Cap

2.3.1 Long-term Accumulation Rates in the QEI

Ice core and snow pit data of net winter accumulation for Devon Ice Cap shows a slight increasing trend from 1959 – 1992 (Fig. 2.5) (Koerner, 1977; Dowdeswell *et al.* 1997). This data represents each year when snow accumulation begins (after the summer melt season) until the end of June the following year (Koerner and Lundgaard, 1995). The Dowdeswell *et al.* (1997) pan-arctic study also shows that winter snow accumulation was relatively constant from year to year for 1960–1995, but that it varies more in maritime settings and is significantly less variable than summer mass losses due to melt and iceberg calving. Maps of

Figure 2.5 Snow accumulation above the firn line (1500 m a.s.l.) NW Devon Ice Cap for the period 1961-1993. There is a minor increasing trend over the 33 year period. Source: Koerner and Lundgaard (1995)

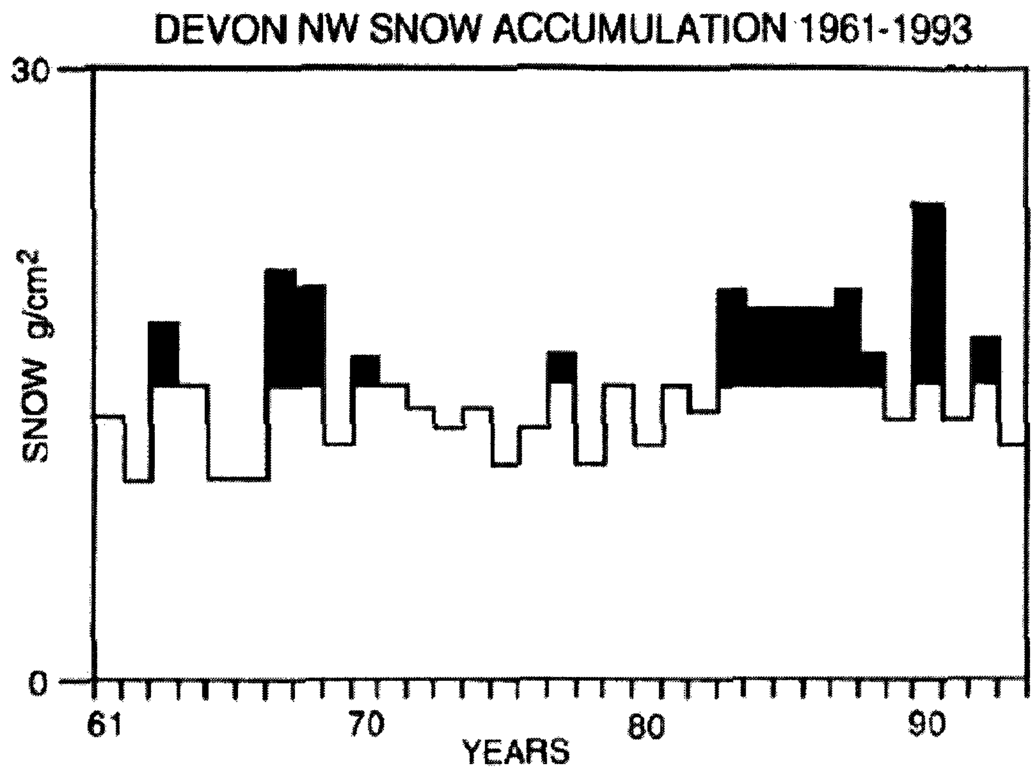

the winter balance in the QEI show a pronounced accumulation gradient running from the southeast to the northwest (Fig 2.6) (Koerner, 2002).

Since surface summer melt varies from year to year, the study of ice layering and snowpack stratigraphy within boreholes can provide a detailed view into summer climate variability (Morris and Cooper, 2004). Meltwater production at the glacier surface eventually percolates through the firn in both uniform and sporadic manners (Koerner, 1977). Uniform percolation will occur in the uppermost layers of the snow profile at high elevations (e.g., at the ice cap summit, ~1921 m a.s.l) to a depth of ~0.5 m, creating a consistent ice lens (Koerner, 1977). Sporadic meltwater percolation typically occurs in an irregular manner at lower elevations, which creates vertical ice tubes/glands and horizontal ice lenses and layers within the snow pack. The path the meltwater takes within the snowpack is termed sporadic because subtle changes in the snow density or grain size and texture will force the percolating water to alter its flow path. Refrozen sporadic percolation features occur frequently in the snow pack during warm summers (Koerner, 1977). Koerner (2005) used ice cores to reveal an inverse elevation-density relationship on Devon Ice Cap, with ice densities typically higher at lower elevations due to higher rates of meltwater percolation compared to the upper accumulation zone.

2.3.2 Long-term Accumulation Studies on Devon Ice Cap

In April and May 2000, Mair *et al.* (2005) drilled eight shallow boreholes in the accumulation zone of Devon Ice Cap to map the spatial distribution of SMB (Fig. 2.7). Core sites ranged in elevation from 1325 m to the summit at ~1920 m. They computed in-situ snow and ice densities of the cores and used a down-borehole gamma spectrometer to detect a 1963 radioactive layer. This 1963 radioactive layer is found in glaciers throughout the Arctic, and is related to nuclear tests conducted in the Russian High Arctic. The peak activity fallout from thermonuclear testing in the Arctic occurred in 1963, originating from major detonations during September-November 1961 at Semipalatinsk (50°N, 80°E) and August–December 1962 at Novaya Zemlya (71-73°N, 55°E) (Pinglot *et al.* 2003). Radioactive species such as ^{137}Cs, and ^{109}Cd were discharged vertically from the explosion of bombs, and transported across the Arctic via atmospheric circulation. These radioactive species attached

Figure 2.6 Accumulation gradient running from the southeast to the northwest across the QEI; green represents ice covered areas, and the concentric circle and dot symbol represents ice-core sites. Source: Koerner (2002)

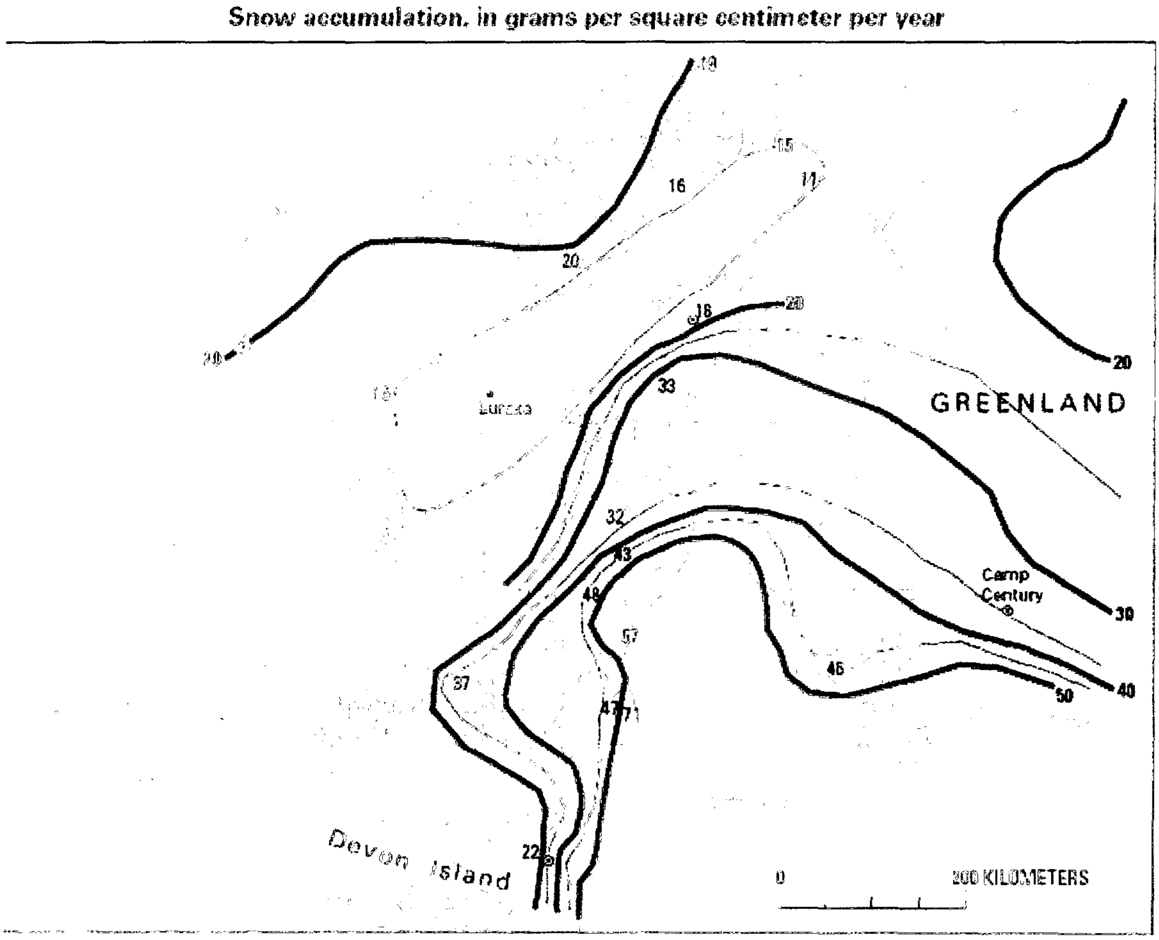

Figure 2.7 Density and ^{137}Cs count rates from ice cores at Devon Ice Cap: (a) summit (1930 m a.s.l); (b) 1640 m a.s.l; (c) 1508 m a.s.l; and (d) 1340 m a.s.l. Source: Mair *et al.* (2005).

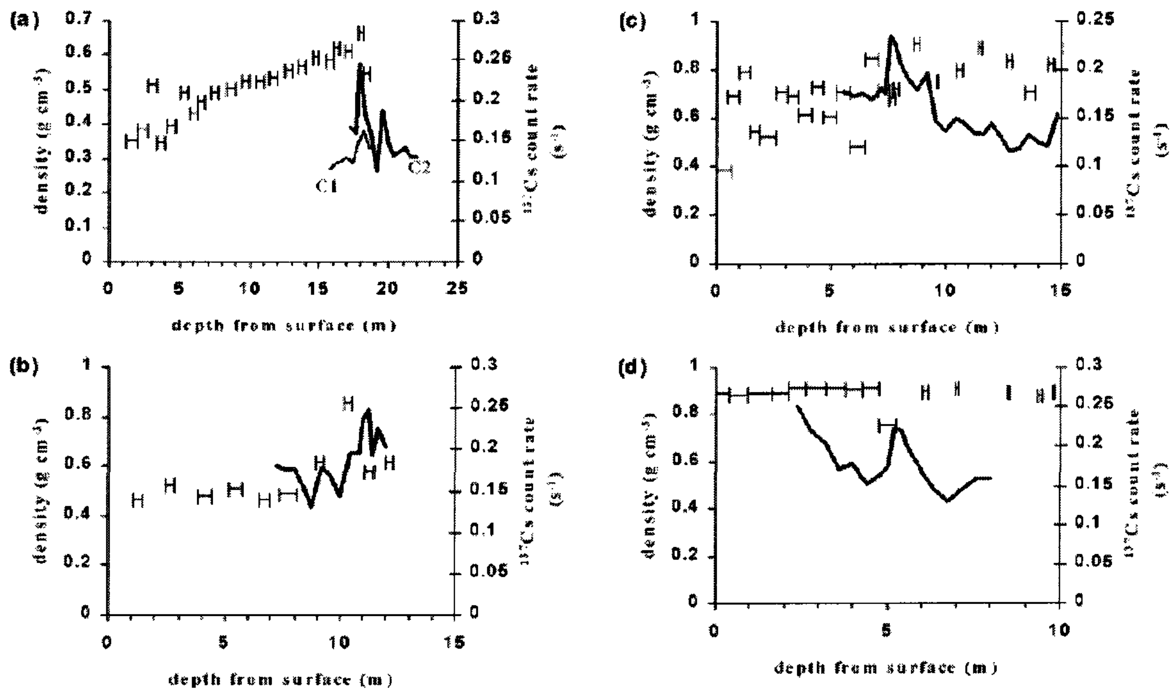

to atmospheric water molecules and were then deposited as snow in 1963, which represents a date marker in the snowpack. When the depth of this layer was determined, and used in combination with snow density calculations above this layer from the retrieved core, Mair *et al.* (2005) could estimate SMB since 1963.

Two gamma profiles from the summit show that the ^{137}Cs peak appears at ~18 m below the surface (Fig. 2.7a). It was assumed this depth represents the 1963 fallout layer, which means that the average SMB at the summit for the period 1963 – 2000 was 0.241 ± 0.03 m w.e. a^{-1}. This compares with laboratory density measurements and major ion concentrations obtained by the NGP-GSC of 0.216-0.234 m w.e. a^{-1} (Mair *et al.* 2005). This showed that using the ^{137}Cs peak is a good method to determine the long-term average SMB of the ice cap, with their results indicating a non-linear relationship between winter accumulation and surface elevation. They conclude that mean annual accumulation reduces dramatically from the summit to 1600 m in the SE, and then gradually decreases towards 1300 m at the equilibrium line. Surface snow densities are low in high altitude regions and gradually increase with depth, with refrozen saturated snow due to meltwater percolation producing densities close to that of ice in the lower altitude areas. Mair *et al.* (2005) show that the pattern in the NW sector reflects wind redistribution of snow from higher altitude regions to lower elevations, where it is deposited.

Shepherd *et al.* (2007) created a map of estimated long–term snow accumulation rates on Devon Ice Cap from annual accumulation patterns derived from summer field measurements, spring snow depths from ten meteorological stations surrounding the ice cap, and information collected by past expeditions in 1962, 1963, 1965 and 1988-2002. (Fig. 2.8). Since the 1960s, it was estimated that snow accumulation was ~0.25 ± 0.05 Gt a^{-1} for the Belcher Glacier catchment (Basin 9 in Fig. 2.8), with runoff of 0.16 ± 0.01 Gt a^{-1}, and a total mass balance of -0.07 ± 0.05 Gt a^{-1}. From in situ measurements and meteorological records this study suggested that snow accumulation in the northwest portion of Devon Ice Cap barely changed from the 40 year mean value of 11 ± 2 cm w.e. a^{-1}.

Figure 2.8 Snow accumulation across Devon Ice Cap derived from a collection of in situ measurements distributed across the ice-cap centre, and meteorological records at sea level from 1962 – 2002. Source: Shepherd *et al.* (2007)

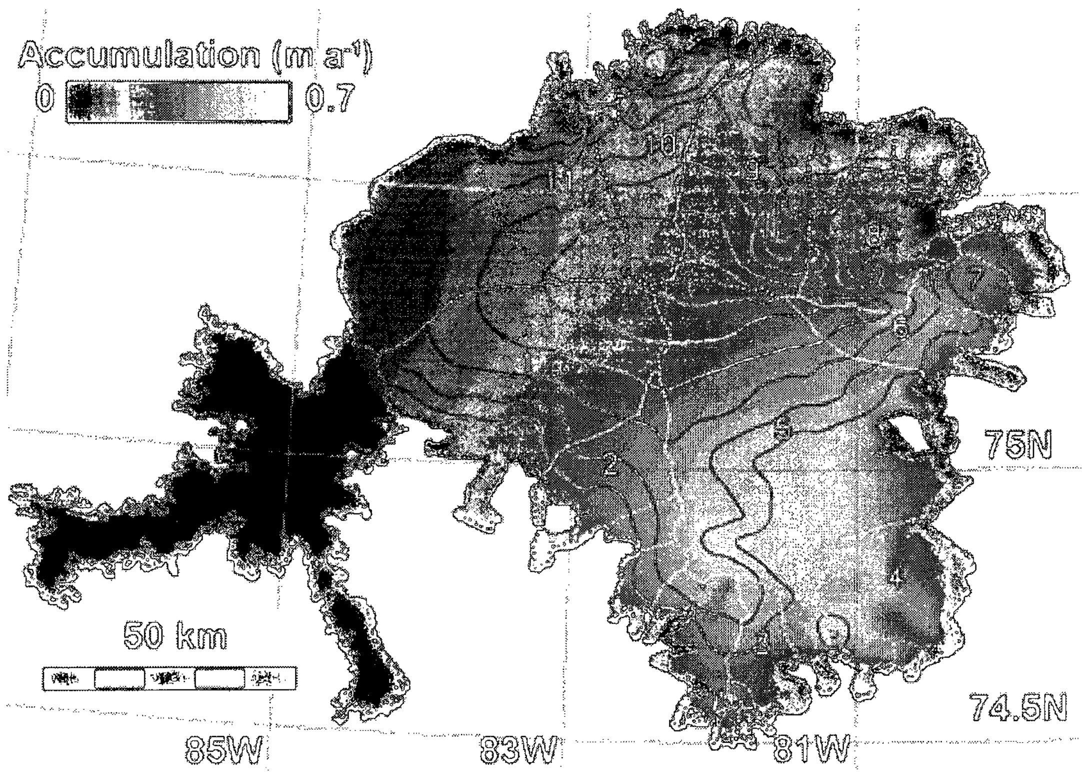

Colgan and Sharp's (2008) study of the mean annual net accumulation of Devon Ice Cap between 1963 and 2003 showed much lower values in the 1989-2003 period compared to 1963-1989 (Colgan and Sharp, 2008). The study was conducted using data from 5 shallow boreholes collected in 2004 and 2005, gamma spectroscopy measurements, ionic chemical analysis, and US National Centers for Environmental Prediction/US National Center for Atmospheric Research (NCEP/NCAR) climate re-analysis data. Standard deviations of the annual net accumulation records indicate that the five cores exhibited similar interannual variability. Overall, they found distinct periods of above average annual net accumulation in 1964–67, 1971–79 and 1984–88, and below average accumulation in 1968–70, 1981–83 and 1989–2003 (Fig. 2.9).

Colgan *et al.* (2008) quantified the mean annual change in surface elevation over 1963-2003 for each drainage basin on Devon Ice Cap using mean annual net accumulation rates determined from 13 shallow firn cores (Fig. 2.10). This was calculated by determining the depth of snow from the surface to the 1963 radioactive layer in the firn cores, and dividing the water equivalent depth of this layer by the number of years elapsed. The authors used multiple linear regression analysis to understand the relationship between snow accumulation, elevation and latitude, and found that the annual specific net accumulation rate in the southern basins (area-average: 0.22 ± 0.02 m w.e. a^{-1}) is significantly ($p < 0.01$) greater than that in the northern basins (area-average: 0.18 ± 0.02 m w.e. a^{-1}). They argue that the main variation in net accumulation rate is a function of latitude rather than elevation, meaning that a strong north-south net accumulation gradient exists across the study region.

2.3.3 Moisture Source Regions

Snow accumulation on Devon Ice Cap is related to its proximity to moisture source areas. These moisture sources are open water locations that have a relatively high probability of being traversed by low-elevation (<500 m) air masses, such as the NOW Polynya at the head of Baffin Bay. Thus, sea ice coverage and its seasonal dynamics play a major role in the distribution of moisture source regions (Burgess and Sharp, 2005; Colgan and Sharp, 2008). During the summers (JASO) when sea ice coverage is low, warmer air masses travelling

Figure 2.9 Devon Ice Cap three year mean of measured surface mass balance (blue) and stacked mean reconstructed net accumulation (red) are shown for the 1963–2003 period, as well as their respective annual records (thin black). The annual maximum and minimum reconstructed net accumulation values are indicated with thin grey lines. A significant decrease ($p < 0.05$; t test) in the mean annual net accumulation after 1988 is shown (dashed line). Source: Colgan and Sharp (2008).

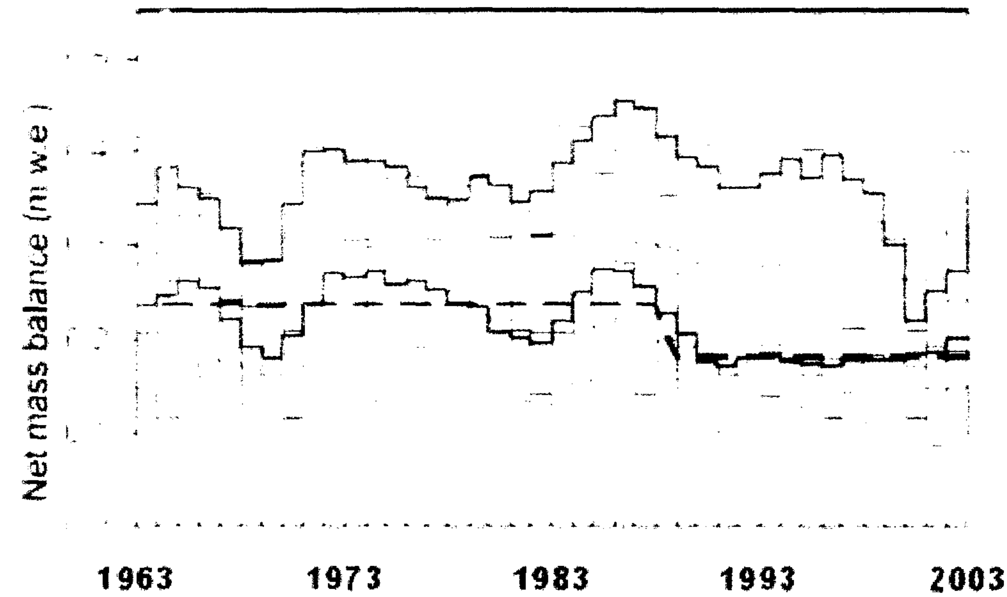

Figure 2.10 Devon Ice Cap (mosaic of Landsat 7 images acquired in July and August 1999, with a 1 km DEM) with the 1200 m contour highlighted and QEI inset. Locations of the shallow firn cores (Mair *et al.* 2005: squares; Colgan and Sharp, 2008: circles) and NASA altimetry flightlines. Source: Colgan *et al.* (2008)

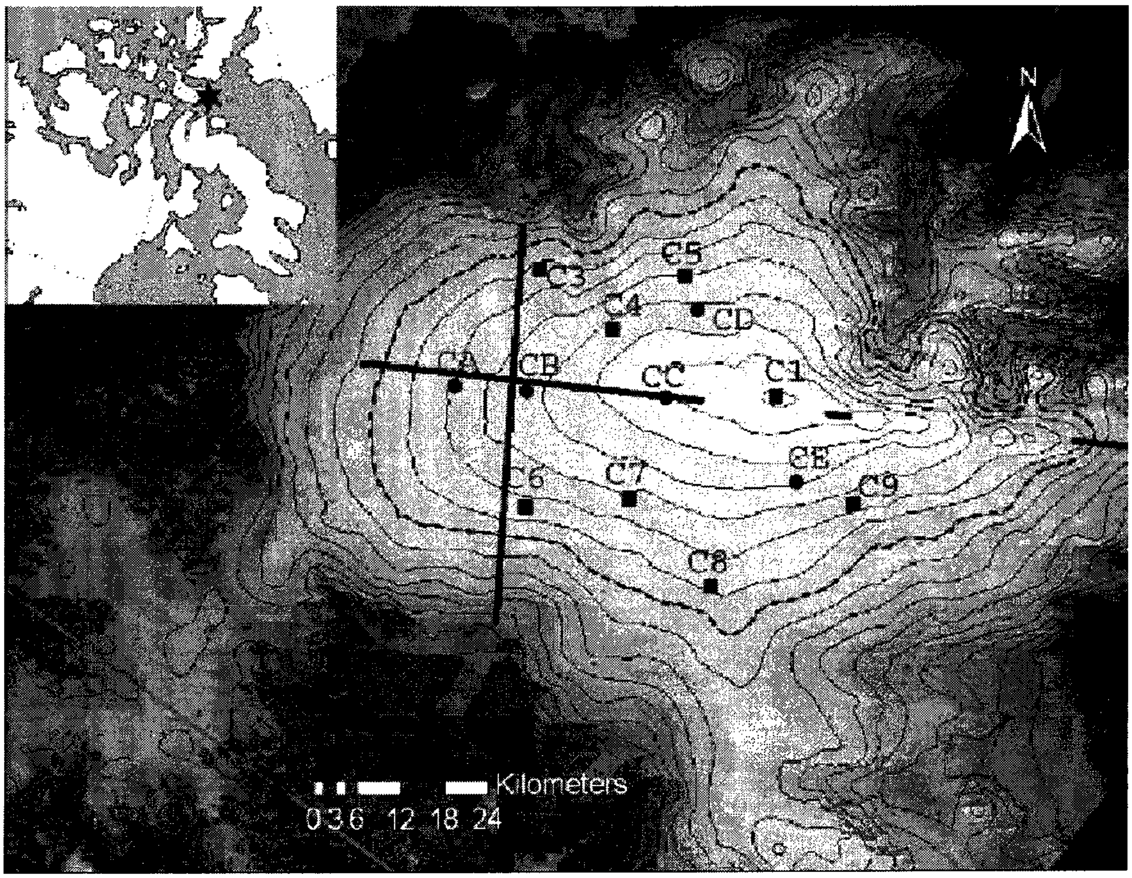

across open water en route to Devon Island can transport more moisture compared with winter (NDJF) (Fig. 2.11) (Colgan and Sharp, 2008; Trenberth *et al.* 2003). As a result, Colgan and Sharp (2008) show that there is twice as much snow accumulation on Devon Ice Cap during the summer versus the spring, and limited accumulation in the winter. Moisture source regions for Devon are the NOW and the Polynya complex of Hells Gate and Cardigan Strait to the NW of Devon Ice Cap, which is kept open throughout the winter (Prach and Smith, 1992).

Bell *et al.* (2008) examined snow pack density properties in spring (pre-melt) and fall (post-melt) 2004/6 across a variety of snow facies (400-1800 m) along the Cryosat Cal/Val experiment line on Devon Island and found considerable interannual and spatial variability (Fig. 2.12). Controls on this spatial variability are shown to be intrinsic or existing features in the snowpack which affect densification during melt, and extrinsic controls such as meteorological conditions, altitude and surface topography. Mid-elevation snow pits had the highest variability in winter accumulation in 2004, ranging from 26.4 cm w.e. at 1259 m to 11.2 cm w.e. at 1328 m, and in 2006 ranging from 31.6 cm w.e. at 1290 m to 9.57 cm w.e. at 1236 m (Fig. 2.13). The average bulk density of the annual snowpack along the transect in spring 2004 and 2006 was 300–350 kg m^{-3}. By autumn 2004, snow depth and accumulation had increased at all sites, with the lowest magnitude increases occurring at lower elevations. The autumn pattern in 2004 was very different from that of 2006 (Figs. 2.13). Above 1290 m the snowpack gained mass during the summer and below this there was a rapid drop in snow accumulation. Spring snowpack profiles in both 2004 and 2006 show low variability over large spatial scales, with low-magnitude changes in density, whereas the end-of-summer/fall density profiles indicate high variability in both 2004 and 2006 (Bell *et al.* 2008).

Bell *et al.* (2008) show that the cool summer of 2004 created an annual snowpack with sporadic melt features and discontinuous ice layers with a higher presence of ice layers towards lower elevations. This agrees with Koerner's (1977) climate-stratigraphy study. Warm late-summer conditions in 2006 produced a very different snowpack that was transformed by high air temperatures (>0°C) at high elevations (>1200 m) for several days in late July and August. The amount of ice in the annual snowpack decreases with lower

Figure 2.11 Relative moisture-source probabilities near Devon Ice Cap in: (a) the winter (NDJF), (b) late-spring/early-summer (MAMJ) and (c) late-summer/early-fall (JASO) seasons, during the 1979–2003 period. Source: Colgan and Sharp (2008)

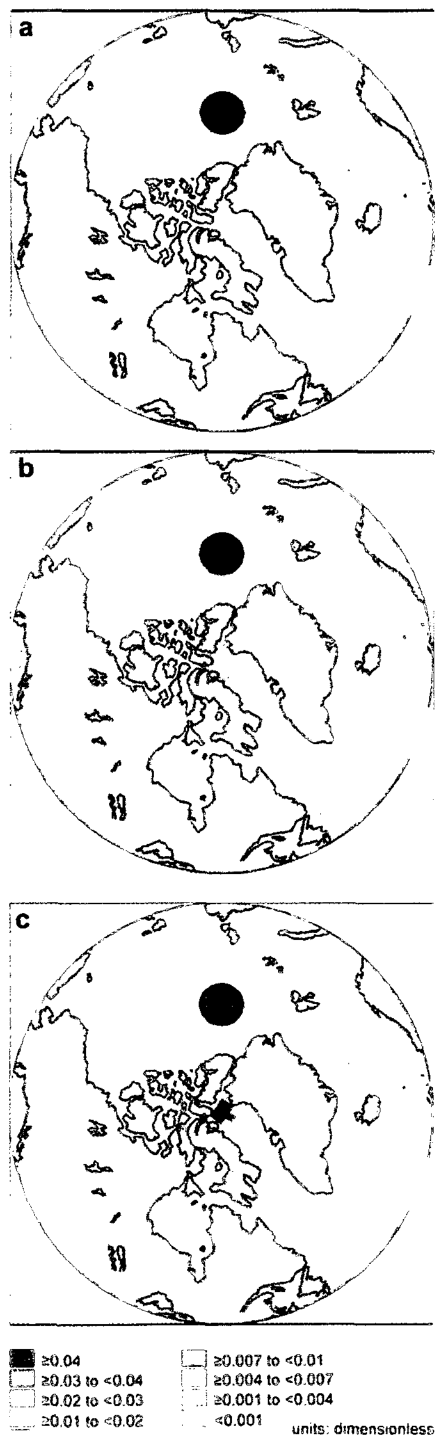

Figure 2.12 Devon Ice Cap and CryoSat reference orbit track showing nested grid sites 1–4 used in the Bell *et al.* (2008) study of spatial and temporal variability in the snowpack of Devon Ice Cap. Source: Bell *et al.* (2008).

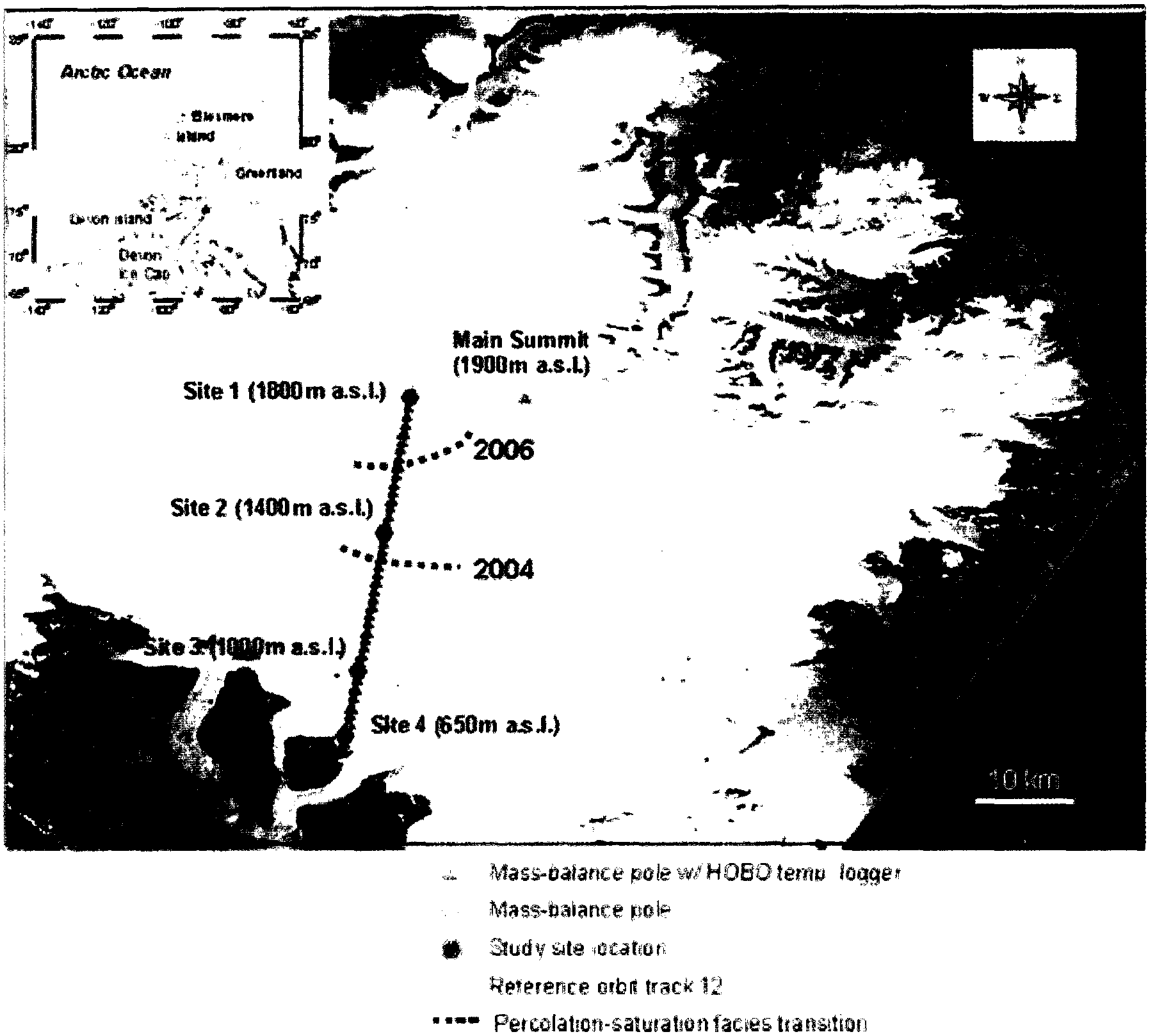

Figure 2.13 Spring and autumn accumulation plotted against elevation from snow-pit measurements along the length of the CryoSat line on Devon ice Cap for (a) 2004 and (b) 2006. Source: Bell *et al.* (2008)

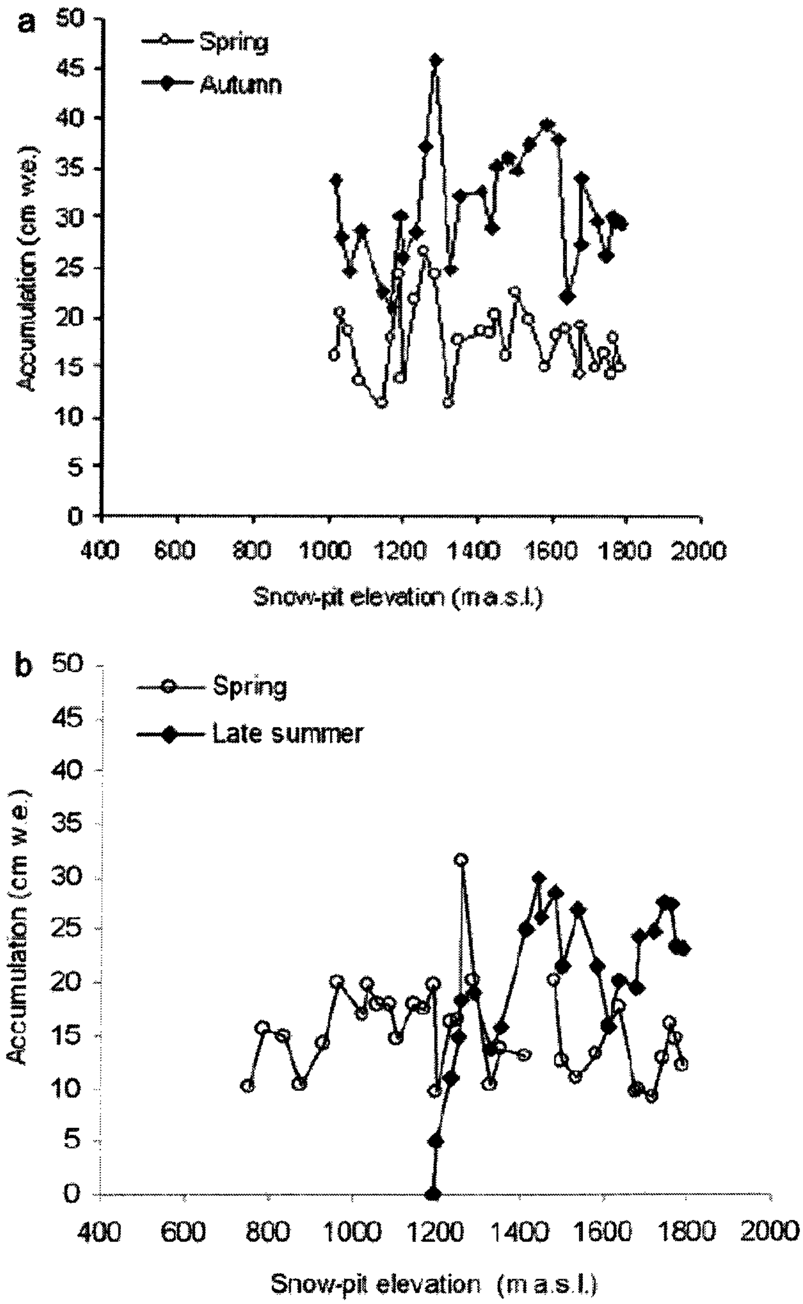

elevation and warmer temperatures. Therefore, ice-layer formation in the 2004 snowpack produced greater stratigraphic variability in the near surface than in 2006 (Bell *et al.* 2008). This information is of interest to the study described here because according to a study by Winther *et al.* (1998) on Svalbard, changes in density are readily identified by the GPR signal in the upper ~75 m of dry snow.

2.4 Use of GPR in Glaciology

GPR has been used in glaciological research to measure the spatial distribution of internal glacier properties such as ice thickness (Copland *et al.* 2003), thermal structure, basal conditions (Irvine-Fynn *et al.* 2006), and internal layering (Pälli *et al.* 2002). GPR can provide information about internal and basal properties of glaciers over short time periods at high resolutions with good areal coverage. GPR can be used to determine subsurface properties by transmitting electromagnetic pulses into the ground and detecting their return. As the pulses travel through the subsurface material, they are reflected at dielectric discontinuities which are expressed as internal reflecting horizons (IRHs) in resulting GPR traces (Annan, 2002). The GPR receiver records and builds an image from these reflections as it is moved across the surface. The GPR records the time between when a pulse is fired from the GPR transmitter into the subsurface, and when it gets back to the receiver. This is known as Two-Way-Travel time (TWT) (Annan, 2002). In order to determine depth, the GPR signal speed through the material in question needs to be known. The relationship between depth and time for a GPR signal is defined as:

$$Depth = (speed) \times (time/2) \qquad \text{(Eq. 1)}$$

The signal speed depends on the dielectric constant (K) of the material in question, which is represented by:

$$K = c^2 / v^2 \qquad \text{(Eq. 2)}$$

where c is the speed of light (3.0×10^8 m s^{-1}) and v is the radar velocity in the material. If K is known for a given material, the velocity of the radar pulse through that material can be estimated. For the purpose of this study, a table of K and estimated v (m ns^{-1}) for water, ice, snow and air are shown (Table 2.1).

Table 2.1 Table of dielectric constants (K) and estimated radar velocity (V) for air, water, snow and ice

Material	K	V (m ns^{-1})
Air	1	0.30
Water	80	0.033
Ice (glacier ice)	3 – 4 (3.20)	0.16
Snow	1.62	0.20

The signal wavelength in the subsurface is approximately equal to the length of the antenna (Annan, 2002). At low frequencies (<50 MHz) the radar wavelength is long and can reach deep into the subsurface (e.g., >4 km in Antarctica). Conversely, at higher frequencies (>100 MHz), the radar wavelength is short and cannot reach as deep into the subsurface, but provides higher resolution returns that can better resolve fine subsurface detail. The depth of fine subsurface detail is limited because GPR signals lose signal strength at an exponential rate in glaciers (Maurer, 2006). Additionally there is a trade off between finer resolutions and the occurrence of radar noise, which interferes with the identification of IRHs.

Dielectric discontinuities in snow and ice are related to changes in density, water content, chemical impurities, and snow crystal orientation (Palli *et al.* 2002). Water produces strong internal reflector horizons but allows little radar penetration due to its high dielectric constant as it absorbs most of the electromagnetic signal. This is why GPR measurements are typically conducted in the spring, prior to the onset of summer melt. According to Winther *et al.* (1998), density variations in dry snow regions are the most important factor in creating dielectric discontinuities in the upper ~75 m of the snowpack and radargram.

2.5 Using GPR for understanding snow accumulation on glaciers

Anschütz *et al.* (2006) used high frequency (500 MHz) GPR measurements on a 50 km transect along the main flow line of Potsdam Glacier in Neuschwabenland, the coastal part of Dronning Maud Land, East Antarctica, in 2003/2004 (Fig. 2.14). The GPR data were compared with shallow firn cores at locations along the radar profiles, IRHs were tracked semi-automatically, and snow-sample data were used to link the firn-core data to the surface. Two internal reflection horizons are traced throughout the GPR profiles and dated against a reference firn core using $\delta^{18}O$ peaks with summer maxima (Fig. 2.14a). Using these layers the authors conclude that the transition zone from very low accumulation to ablation can be identified where internal layers emerge at the surface, such as at the right-hand side of Figs. 2.14a and 2.14b. The spatial variability exceeds the temporal variability for the time periods considered, with high interannual variability found in the firn core data. The GPR-derived accumulation along the main flow line indicates that the spatial representivity of point data provided by the firn cores is limited. Accumulation rates derived from the GPR data show

Figure 2.14 a) GPR from profiles on Potsdam Glacier, East Antarctica. White arrows mark IRHs from accumulation to ablation zones. **b)** Depth of tracked and dated IRHs for IRH 1 (1980); IRH 2 (1970); IRH Ia (1995); IRH Ib (1992); and IRH Ic (1989) identified with arrows. **c)** Upper panel represents accumulation pattern with the solid curve corresponding to 1980–2004, dashed curve: 1970–2004 and dotted curve: 1970–80. Solid line shows linear trend fitted to accumulation pattern; lower panel provides gradient of accumulation and surface slope on main flow-line. Solid line in lower panel corresponds to slope of surface elevation in mm^{-1}, and the dashed line represents slope of accumulation (1980–2004) in kg m^{-2} $a^{-1}m^{-1}$. Source: Anschütz *et al.* (2006)

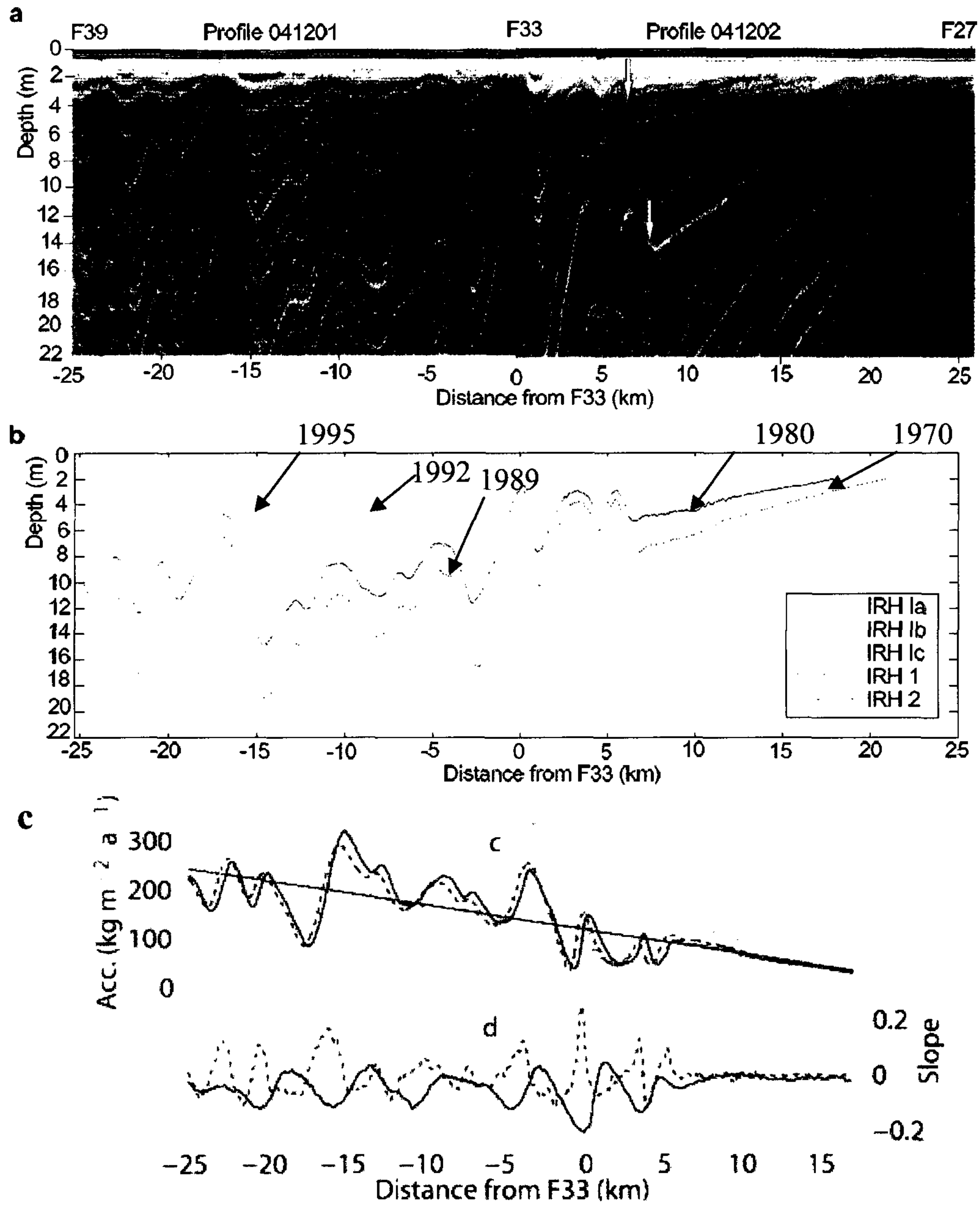

strong spatial gradients of up to 105 kg m^{-2} a^{-1} km^{-1}, with pronounced changes from increasing to decreasing accumulation in the direction of glacier flow, in some cases within less than 1 km (Fig. 2.14c).

Dunse *et al.* (2009) collected 800 MHz GPR along 250 km of profiles across the Austfonna Ice Cap on Nordaustlandet, Svalbard in 2006 and 2007 (Fig. 2.15). This ice cap is very similar to Devon Ice Cap in terms of its dome-shaped topography, the fact that its eastward flowing basins terminate below sea-level, and the fact that there is a NW-SE gradient in snow accumulation that reflects the influence of atmospheric systems from the Barents Sea. By combining GPR data collected in 2004/5 by Taurisano *et al.* (2007) with their own data from 2006/7, Dunse *et al.* (2009) mapped the thickness of winter snow and underlying facies to produce a multi-year sequence of glacier-facies distribution. Glacier facies result from a combination of snow accumulation, metamorphism and ablation of winter snow, and are an expression of SMB changes (Demuth *et al.* 2007; Dunse *et al.* 2009). On Arctic glaciers, the following facies are normally found (in order of increasing altitude) (Benn and Evans, 1998):

(a) ablation zone / ice facies is typically composed of glacier ice that undergoes collective annual losses of mass due to melt, evaporation, sublimation, runoff, and calving processes (Langley *et al.* 2008). Glacier ice tends to be homogeneous and cold, properties which are generally transparent to GPR waves (Dunse *et al.* 2009). Consequently internal GPR signal reflections in the ablation zone / ice facies region do not usually occur.

(b) superimposed ice zone falls within the accumulation area. Accumulation here is characterized by internal refreezing processes, where ice forms at the bottom of the snowpack on top of impermeable ice with varying air-bubble content (Dunse *et al.* 2009). The equilibrium line altitude marks the lower boundary of this zone while the upper boundary of this zone is marked by the snow line (Paterson, 1994). GPR signals are rapidly attenuated in this zone due to the large contrasts in density between snow, firn and ice lenses, resulting in moderate internal reflections.

Figure 2.15 GPR classification of glacier facies along a 30 km long transect from the summit area (F1) into the ablation area (GI) of Etonbreen, Svalbard. Ablation area characterized by low volume backscatter (lower right panel), Accumulation / firn area indicated by high volume backscatter (lower left panel), and superimposed ice region identified by a mix of high and low volume backscatter (lower middle panel). Green line indicates the position of the LSS. Lower panels show close-ups of 2 km GPR data with signal reflection patterns. Source: Dunse *et al.* (2008).

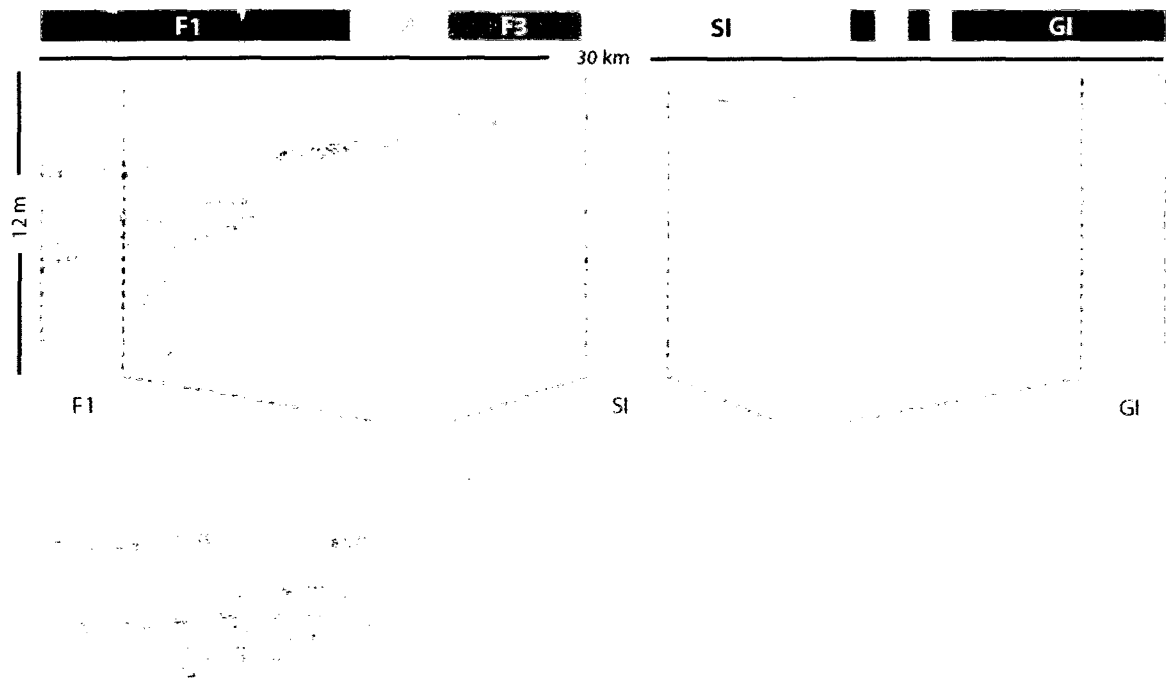

(c) accumulation zone is composed of the dry snow, wet snow and percolation facies (Dunse *et al.* 2009). Surface meltwater infiltrates into the snow and refreezes at the end of the melt season. The snowpack in this zone is composed of a mixture of both wet and dry snow, where the proportion of each depends largely on the temperature conditions during the summer melt season. This zone is typically characterized by strong internal reflections in GPR traces.

In addition to the GPR measurements collected on Austfonna Ice Cap by Dunse *et al.* 2009, firn cores (8–14 m depth), snow pits (to the last summer surface (LSS)), manual probing and neutron-scattering probe measurements were also performed along the GPR survey lines. The neutron probe provides vertical density profiles through a snowpack based on density contrasts between ice, snow and firn and were related to signal reflection patterns found in the GPR data. To determine snow thickness from the GPR surveys, the authors derived the two-way travel time (TWT) of the reflection occurring at the LSS. This information was validated against in situ snow depth data from manual soundings to check that the correct IRH represented the last summer surface.

From the snow pit data on Austfonna, the winter snowpack was shown to have densities between 350 and 450 kg m^{-3} (Fig. 2.16). The GPR profiles over 2004 to 2007 showed that snow thickness typically varied from 0.5 to 1.5 m in the west, and 1.5 to 3 m in the east. The lowest snow accumulation was measured in spring 2004, with a mean thickness of 1.21 m over the entire length of the two transects. In spring 2006, a mean thickness of 2.01 m was measured over the same distance. From the ice core density profiles measured with the neutron probe in the firn area, the LSS was recognizable as a sharp density increase at approximately 1.7 m depth (Fig. 2.17). At 2.6 m depth, density values ranged between 470 to 570 kg m^{-3} (firn), while at depths between 2.6 m and 4.8 m densities were 550 to 850 kg m^{-3} (firn and ice) (Fig. 2.16). At 6 m depth the firn-ice transition was reached (density ~860 kg m^{-3}), with density values and low backscatter in the GPR returns indicating glacier ice below this depth.

Figure 2.16 Comparison of vertical density profiles (from neutron-scattering probe) with GPR signal reflections obtained along ~120m sections at basecamp and Cry-1 sites on Etonbreen, Svalbard. Dashed lines in GPR surveys show the position of the LSS confirmed from snow pits and manual snow-depth soundings. Source: Dunse *et al.* (2008).

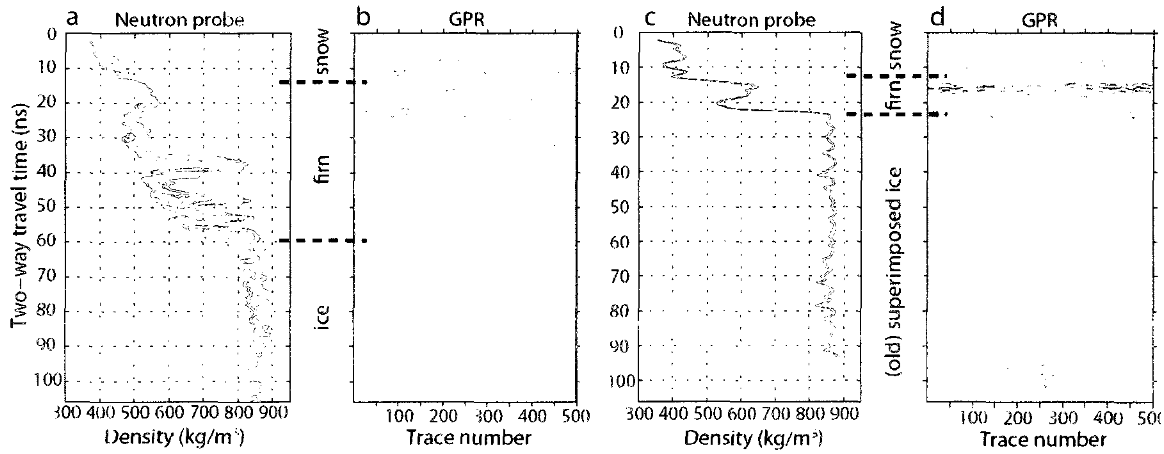

Figure 2.17 Snow thickness profiles on Austfonna for spring during 2004–07: along the (a) northwest–southeast and (b) southwest–east transects. Source: Dunse *et al.* (2008).

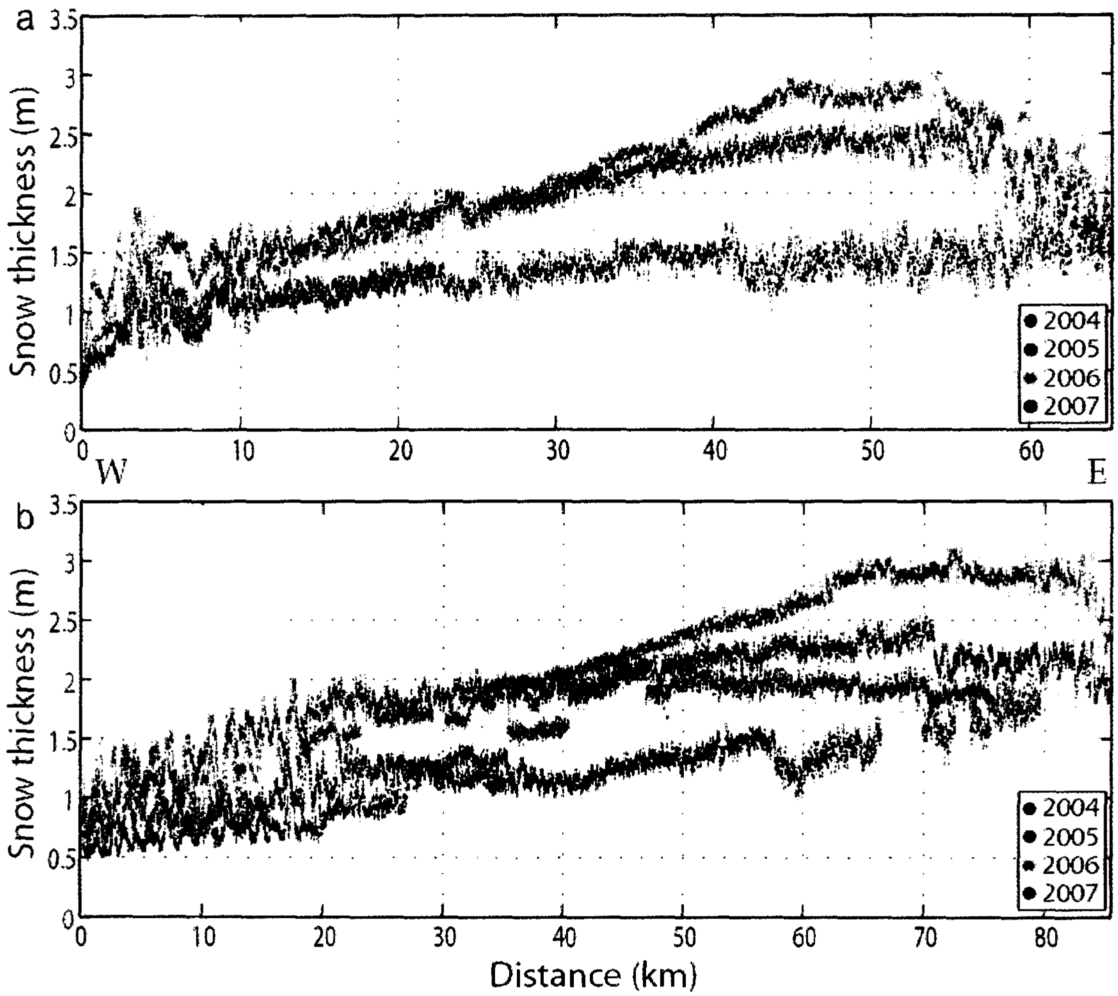

In addition, estimates of the equilibrium-line altitude have been made from a combination of SMB stakes on Etonbreen and GPR transects on Austfonna. The repeat GPR study by Dunse *et al.* (2009) shows that over the period 2003-6 the firn line decreased by about 40 to 100 m elevation in the north and west of Austfonna, and 150 to 230 m in the south and east. The authors show that this has lead to a lateral expansion of the firn area by up to 7.3 km along profiles in the north and west, and up to 13.3 km for the southern and eastern profiles (Fig. 2.17). Dunse *et al.* (2009) therefore demonstrate that GPR is a useful tool to map glacier facies and measure the amount of winter snow over long spatial extents.

Winther *et al.'s* (1998) study on Spitsbergen, Svalbard, used a 450-500 MHz GPR system combined with probing and snow pit stratigraphy to understand the controls on snow accumulation, and found that snow accumulation increased substantially with elevation. Similar accumulation – elevation trends established by Pinglot *et al.* (2001) in Svalbard also show that snow accumulation is highly variable within the accumulation zone of Austfonna Ice Cap over short (50 – 100 m) and long (1 – 10 km) distances. This study also showed that 25% of the variability in the snow accumulation zone on Austfonna Ice Cap is due to wind redistribution.

In another study on Svalbard, Pälli *et al.* (2002) used a 50 MHz GPR system along a profile on the Nordenskjoldbreen Glacier to accurately track accumulation layers identified in ice cores. Their study showed high spatial variability (40 – 60%) in snow accumulation at the local scale (100 m intervals). Combining the snow pit surveys with GPR transects, this type of analysis enabled the authors to compare snow accumulation rates between 1963-1986 and 1986-1999, over which time there was a 12% higher average accumulation rate in the more recent period.

Maurer (2006) used 1000 MHz GPR surveys conducted in a 100 x 100 m grid to determine snow accumulation variability at the local scale for two sites in the accumulation zone of the Greenland Ice Sheet. Stratigraphic layers were detected in the GPR traces due to the dielectric contrast between differing snow-crystal grain sizes in the subsurface caused by hoar frost variability (Maurer, 2006). The results suggest that spatial variability in layer depth at the sites is ±10 cm (1 S.D.), with a range of ±35 cm. This shows that it is possible to measure spatial variability in snow accumulation at the local scale and at relatively shallow depths using high-resolution GPR. However, the author cautions that even after his best filtering attempts, the remaining noise, echoes, near-field distortion zone, and exponential loss of signal with depth all challenge the accurate identification and absolute depth measurement of stratigraphic layers.

Demuth *et al.* (2007) describe the use of Broadband Microwave Frequency Modulated Continuous Wave (FMCW) radar measurements made during spring 2005 and 2006 on Devon Ice Cap (>1800 m a.s.l) to understand the processes that control internal layer development, densification and variability of the near-surface strata. The authors show that the primary factors of snow water equivalent (SWE) variability are post-depositional, via snow drifting forming sastrugi, and mass redistribution within the snow pack from internal melt water percolation and refreezing (Demuth *et al.* 2007). Profiles were taken over 1 km transects, at 5 cm horizontal resolution and ~1.5 cm vertical resolution. The authors developed a semi-automated layer picking routine to determine layer depths. Semi-variance analysis indicates a large change and range in several of the layers at 5 m, and 20 m in the deepest 3 layers. The depth to a given layer was shown to decrease in variability with depth (i.e. averaging over time; Fig. 2.18). Based on their analysis, Demuth *et al.* (2007) suggest that within the upper 2 m of the snowpack some process is causing variations that average themselves out over ~4-5 year time scales. This variability may be related to the process of sastrugi development and their subsequent burial, which promotes preferential horizontal pooling and vertical pathways for meltwater percolation.

Figure 2.18 Semi-variogram on Devon Ice Cap (>1800 m a.s.l) for five prominent reflectors shown in Figure 2.18. 5 m and 20 m separation distances (m) (*h*) highlighted for reference with black dashed lines. Source: Demuth *et al.* (2007)

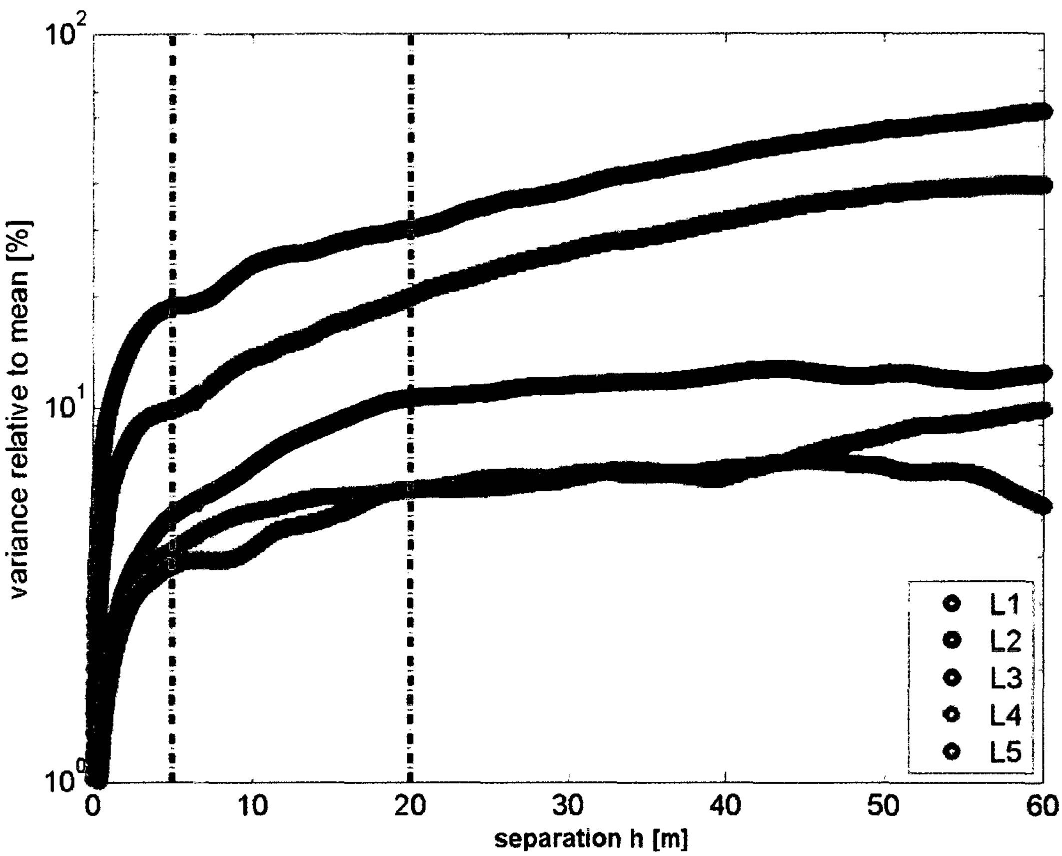

2.6 Summary

The review here has demonstrated that GPR can be used to effectively and accurately measure both snow depth and snow pack variability across large distances on glaciers. On the basis of IPCC (2007) and ACIA (2004) predictions with regards to increasing precipitation processes in a warming Arctic over the next century, snowpack variability on glaciers represents an important measure of climate change. Furthermore, GPR can also be used to map glacier facies beneath the winter snowpack and therefore provides a way to improve understanding of SMB changes on glaciers. In this thesis, GPR is used to determine snow pack variability across Belcher Glacier, Devon Ice Cap, Nunavut, as outlined in the next section (Chapter 3).

Chapter 3 - Spatial Patterns of Snow Accumulation across the Belcher Glacier Basin, Devon Ice Cap, Nunavut, Canada

3.1 Introduction

The Queen Elizabeth Islands (QEI) of northern Canada are characterized by large annual and seasonal variations in snow cover (ACIA, 2004). Surface meltwater runoff from the annual snow pack on High Arctic glaciers and ice caps has recently been linked to increases in glacier motion (Burgess and Sharp, 2008; Zwally *et al.* 2005). From a glacier mass balance perspective, increased ice velocities may provide a key mechanism for enhanced mass loss and thinning of QEI glaciers (Bingham et al. 2008; Burgess and Sharp, 2008). In light of current and projected high latitude climate warming, accurately quantifying the spatial distribution of snow is important both from a melt-modeling / hydrological forecasting viewpoint and a eustatic sea-level rise perspective (Burgess *et al.* 2005; Demuth *et al.* 2007). In order to calibrate and validate energy and mass balance models for glaciers in the QEI, this places a demand for detailed field data and studies of snow cover distribution.

At present, snow cover information on ice masses in the QEI has been largely derived from areal interpolations and extrapolations using a sparse network of annual point measurements including ablation stakes, firn cores, snow pits and manual probing. These measures usually reach the last summer's surface layer (LSS) to provide an indication of winter snow depth. These methods tend to be labor intensive and time consuming, however, and are largely unsuccessful at tracking continuous layers across large distances due to multiple ice lense intrusions (Kohler *et al.* 1997; Mair *et al.* 2005). Given the complexity of factors that control snow cover distribution on glaciers (e.g., accumulation and ablation processes, terrain features, distance from moisture sources, redistribution by wind and avalanching), extrapolation of point data across large areas may not be an effective way to characterize snow cover in these settings. These point measurement techniques provide very little information about the spatial and temporal distribution of snow or melt processes (Mair *et al.* 2005). This often makes it difficult to obtain measurements of snow depth distribution over a large area at a resolution that approximates the true variability present (Deems *et al.* 2007).

High frequency (200-1000 MHz) ground penetrating radar (GPR) has the ability to rapidly measure the spatial distribution of snow cover at high vertical and horizontal resolutions over large distances (Maurer, 2006; Pälli *et al.* 2002). This technique has been used previously to determine snow accumulation variability by finding datable internal reflector horizons (IRHs) on Austfonna Ice Cap, Svalbard (Dunse *et al.* 2009; Pälli *et al.* 2001; Taurisano *et al.* 2007), the Greenland Ice Sheet (Dunse *et al.* 2008; Maurer, 2006), and in Antarctica (Anschütz *et al.* 2006; Spikes *et al.* 2004). Transmitted radar waves are reflected at dielectric discontinuities (IRHs) that are typically related to density contrasts caused by refreezing of percolated meltwater in the snowpack.

In polar firn, ice layering due to the refreezing of percolated meltwater is mainly associated with patterns in the extent and magnitude of summer melt (Koerner, 1977, 2002; Wolken *et al.* 2009), but also depends on the initial snowpack properties such as temperature, depth and density (Bell *et al.* 2008; Dunse *et al.* 2008; Parry *et al.* 2007). Prior to the onset of summer melt, the winter snowpack is characterized by sub-freezing temperatures, low densities (<350 kg m^{-3}), and maximum annual depths. The depth of meltwater infiltration during the melt season in high elevation regions of ice caps and glaciers is limited by these snow pack properties. Percolating meltwater occurs in a uniform manner as snow temperature becomes isothermal, with infiltration tending to concentrate in the upper 0.5 m of the snowpack (Dunse *et al.* 2008; Koerner, 1977; Wolken *et al.* 2009). During anomalously warm summers with long and more pervasive melt, a wetting front may propagate deeper into the annual snow and accrete on the previous summer's surface, forming a thick ice lense upon refreezing. Annually, the homogenous freeze-up of percolating meltwater combined with wind action at the end of summer causes the near surface snowpack to form a distinct hard dense continuous crust across glaciers and ice caps in the polar regions (i.e. the LSS layer). During the following winter as snow accumulates on the LSS and submerges it, the layer maintains its summer signature over time. GPR radar waves are reflected at these layers since they contrast in density from the snow and firn above and below them. Measuring the vertical distance between LSS layers in a GPR profile can thus provide quantitative evaluations of snow accumulation rates. Changes in snow accumulation variability measured by high frequency GPR can further assist in assessing climatic changes over time. The potential of this snow depth measurement technique has not been fully realized in the QEI, however, as mass balance measurement programs typically still employ interpolations of point measurements.

The aims of this study are to:

1. Demonstrate that high frequency (500 MHz) GPR can effectively measure snow depths over large areas on a High Arctic ice cap, and provide a way to extrapolate and fill in data gaps between point measurements over annual and multi-year periods. This is undertaken by identifying IRHs as annual layers using GPR data combined with field measurements of depth and density. These results are further verified against remote sensing data collected by the SeaWinds Scatterometer on QuickSCAT (QSCAT), and overflights from the European Space Agency's Airborne SAR/Interferometric Radar Altimeter System (ASIRAS).
2. Map and determine the relationships between GPR-derived snow cover and DEM-derived terrain parameters across a High Arctic glacier. The significance of terrain factors (e.g., slope angle, elevation, curvature, aspect) on snow distribution on QEI glaciers is currently largely unknown, but is crucial to understand to enable proper extrapolation of point measurements, and to provide accurate inputs for hydrological and mass balance models.

3.2 Study Site

Belcher Glacier (82°W, 75°N) occupies the northeast sector of Devon Ice Cap, Nunavut, covers an area of 1180 km^2 and ranges in elevation from sea level to 1920 m a.s.l (Fig. 3.1). Glacier flow is dynamically driven by basal sliding and bed deformation, as indicated by surface flow stripes (Burgess and Sharp, 2004). The glacier bed lies below sea level in the lower 11 km of its length and reaches 400 m below sea level in an over-deepened basin located 2-5.5 km upglacier from the terminus (Burgess and Sharp, 2008). Ice thicknesses average ~300 m across the glacier, but reach a maximum of ~800 m in the over-deepened basin described above (Dowdeswell *et al.* 2004). Remote sensing studies show that Belcher Glacier accounts for approximately half of the iceberg calving loss from Devon Ice Cap and ~15% of the total mass loss since the 1960s (Burgess and Sharp, 2004; Burgess and Sharp,

Figure 3.1. Location of Belcher Glacier basin, Devon Ice Cap, Nunavut (Base image: Landsat 7, July 7, 2000).

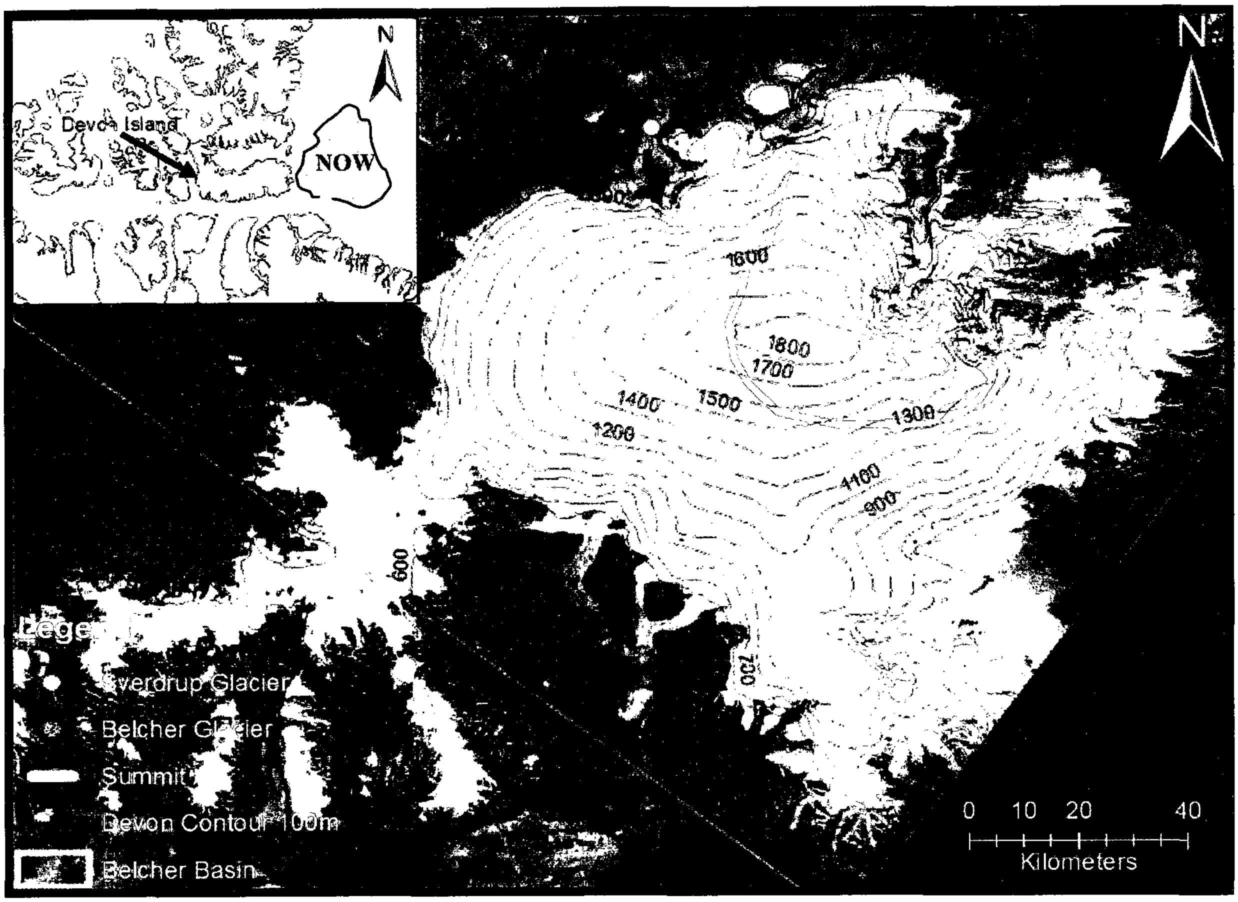

2008). The bed topography suggests that the terminus could become even more unstable in the event of further retreat and mass loss. The lower glacier is close to its primary moisture source region, the North Open Water (NOW) Polynya at the head of Baffin Bay, which promotes long melt seasons, with early melt onset and late freeze-up dates (Wang *et al.* 2005). Melt onset dates typically range from late May to mid-July, with freeze-up dates from mid-July to early September. The average melt season duration from 2000-2004 on the ice cap was 42.1 ± 6.3 days (Wang *et al.* 2005).

Snow accumulation on Devon Ice Cap and the Belcher Glacier Basin is primarily related to its proximity to the NOW Polynya, ~200 km to the northeast (Fig. 3.1). Open water traversed by low-elevation (<500 m) air masses transports moisture towards the ice cap (Colgan and Sharp, 2008). Sea ice coverage and its seasonal dynamics play a major role in the distribution of this moisture source (Burgess and Sharp, 2005; Colgan and Sharp, 2008). During summers (JJA) when sea ice coverage is low, warmer air masses traveling across the NOW Polynya en route to Devon Island can transport more moisture compared to the winter (NDJF) (Colgan and Sharp, 2008; Trenberth *et al.* 2003). As a result, Colgan and Sharp (2008) show that there is twice as much snow accumulation on Devon Ice Cap during the summer versus the spring, and less accumulation in the winter.

Glacier facies on High Arctic ice caps (including Devon Ice Cap and the Belcher Basin) consist of ordered zones of snow and ice mixtures which are distinguished on the basis of specific surface and near surface physical characteristics which are mainly related to elevation (Fig. 3.2) (Benson, 1960; Wolken *et al.* 2009). Facies correspond to transitions zones between ice, firn and snow content, with the quantity of each depending on melt processes at varying elevations. These zones are therefore an expression of SMB (Dunse *et al.* 2009). The boundaries between zones change from year to year on the basis of interannual variability in climate. As elevation increases, the lowest zone relates to the ablation facies, next is the superimposed ice zone, and then the percolation / accumulation facies is present in the upper parts of ice caps (Benson, 1960).

The ablation facies is composed of glacier ice with high densities at lower elevations and occupies ~37% of the Belcher Basin (Burgess and Sharp, 2008; Wolken *et al.* 2009). The upper boundary of this zone is marked by the equilibrium line which denotes the altitude of zero net accumulation (Paterson, 1994). This also represents the lower limit of the superimposed ice zone. The superimposed ice facies is characterized by the production of large volumes of meltwater, where ice accretes at the bottom of the snowpack upon refreezing. The upper limit of the superimposed ice facies marks the snow line and is the boundary between firn and ice. The snowline further represents the lower boundary of the wet snow facies in the percolation region. The wet snow facies is characterized by the snowpack reaching isothermal (0°C) temperatures during the summer, which facilitates the percolation of meltwater in these layers. Unlike the wet snow facies, meltwater infiltration in the percolation facies is limited to the upper part of the snowpack, owing to the fact that at higher altitudes snow temperatures are low (<0°C), and may rise above 0°C only in the warmest part of the summer. Also, meltwater infiltration is limited in this facies because downward propagation of the melting front may reach impermeable ice layers, forming a lateral coating on top of them. Dry snow zones are typically found in the coldest interior regions of the Greenland and Antarctic Ice Sheets, whereas in the Canadian High Arctic this zone is mainly classified as the percolation / accumulation facies (Dunse *et al.* 2009; Paterson, 1994).

3.2.1 Previous Snow Studies on Devon Ice Cap

Previous field studies on Devon Ice Cap since the 1960s have focused on quantifying surface mass balance (SMB) changes using point measurements including shallow and deep ice cores (Koerner, 1977), snow pits (Bell *et al.* 2008), gamma-spectrometry measurements (Colgan and Sharp, 2008; Mair *et al.* 2005), ablation stakes (Burgess and Sharp, 2004) and chemical ionic concentrations (Koerner and Russell, 1979; Koerner, 2005). Mair *et al.* (2005) mapped the spatial distribution of SMB along an elevation gradient (1325 – 1930 m a.s.l) over the period 1963-2000 via the detection of a distinctive 1963 radioactive layer with a gamma spectrometer in shallow boreholes in the NW, summit and SE areas of the ice cap. An accumulation rate of 0.241 ± 0.03 m we a^{-1} was found at the summit, with the 1963 horizon at 18 m depth. A non-linear pattern between accumulation and surface elevation was determined. Accumulation reduced dramatically from the summit to 1600 m in the SE, and then gradually decreased towards 1300 m at the equilibrium line. The pattern in the NW likely reflects wind redistribution of snow from higher altitude regions to lower elevations.

Figure 3.2. Glacier facies zones in the accumulation area of Arctic ice caps. With increasing altitudes, ablation zone, equilibrium line, superimposed ice zone, snow line, wet-snow zone, percolation zone, and dry snow zone. Source: modified from Paterson (1994).

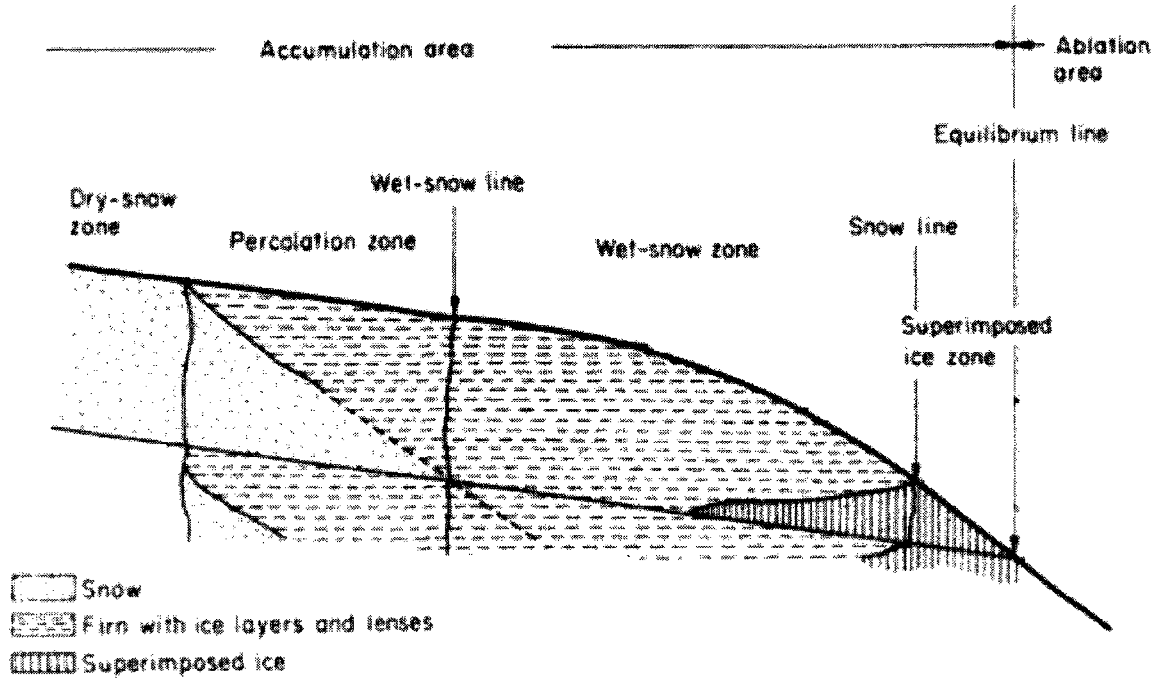

Colgan *et al.* (2008) report annual specific net accumulation rates over the 1963-2003 period for the entire ice cap above 1200 m a.s.l, and show that the southern basins (area-average: 0.22 ± 0.02 m w.e. a^{-1}) experienced significantly greater accumulation than the northern basins (area-average: 0.18 ± 0.02 m w.e. a^{-1}). The mean annual net accumulation rate for the Belcher Basin was predicted to be 0.19 ± 0.02 m w.e. a^{-1} based on an ice core at the summit (1920 m a.s.l) and two other cores <30 km to the west of the basin (Colgan *et al.* 2008). Overall, the main variation in net accumulation across the ice cap was found to be more related to latitude than elevation, with a strong north-south gradient.

As described above, long-term snow accumulation rates are reasonably well understood across several parts of Devon Ice Cap, yet none of these measurements have been focused in the Belcher Glacier (NE) region. Consequently, SMB in this area has been mainly interpolated from these remote point measurements. Considering that Devon Ice Cap has an area of 14010 km^2, and that the density of point data is low, using such a small sample size in interpolations from distant sites results in large uncertainties concerning the ability of these measurements to truly represent the conditions within the Belcher Glacier basin (Mair *et al.* 2005; Richardson-Näslund, 2004).

3.3 Field Data and Methods

3.3.1 Field Data Description

The data were collected in May 2008 prior to the onset of summer melt (Fig. 3.3). Over 306 km of snow surface was surveyed on skidoo, covering elevations ranging from 1000-1900 m in the upper ablation and accumulation regions of the basin. The GPR system was mounted in a sled and towed by the skidoo, which enabled access to the majority of the basin. Along each GPR transect, snow depths to the 2007 LSS (LSS-07) were determined every ~1-4 km with an avalanche probe, and ~1 m deep snow pits were dug to provide information on snow density. At each avalanche probe site five depth measurements were taken, and the average reported (Fig. 3.3). Snow density (ρ_{pit}) was measured at three equi-spaced intervals on each vertical snow pit wall using a 250 cm^3 snow scoop and digital scale. These values were averaged for each pit to provide a mean ρ_{pit} for the 2007-8 snowpack in units of kg m^{-3}. Bell

Figure 3.3. GPR transects, avalanche probe, and shallow borehole measurements for 2008 field season (Base image: Landsat 7, July 7, 2000).

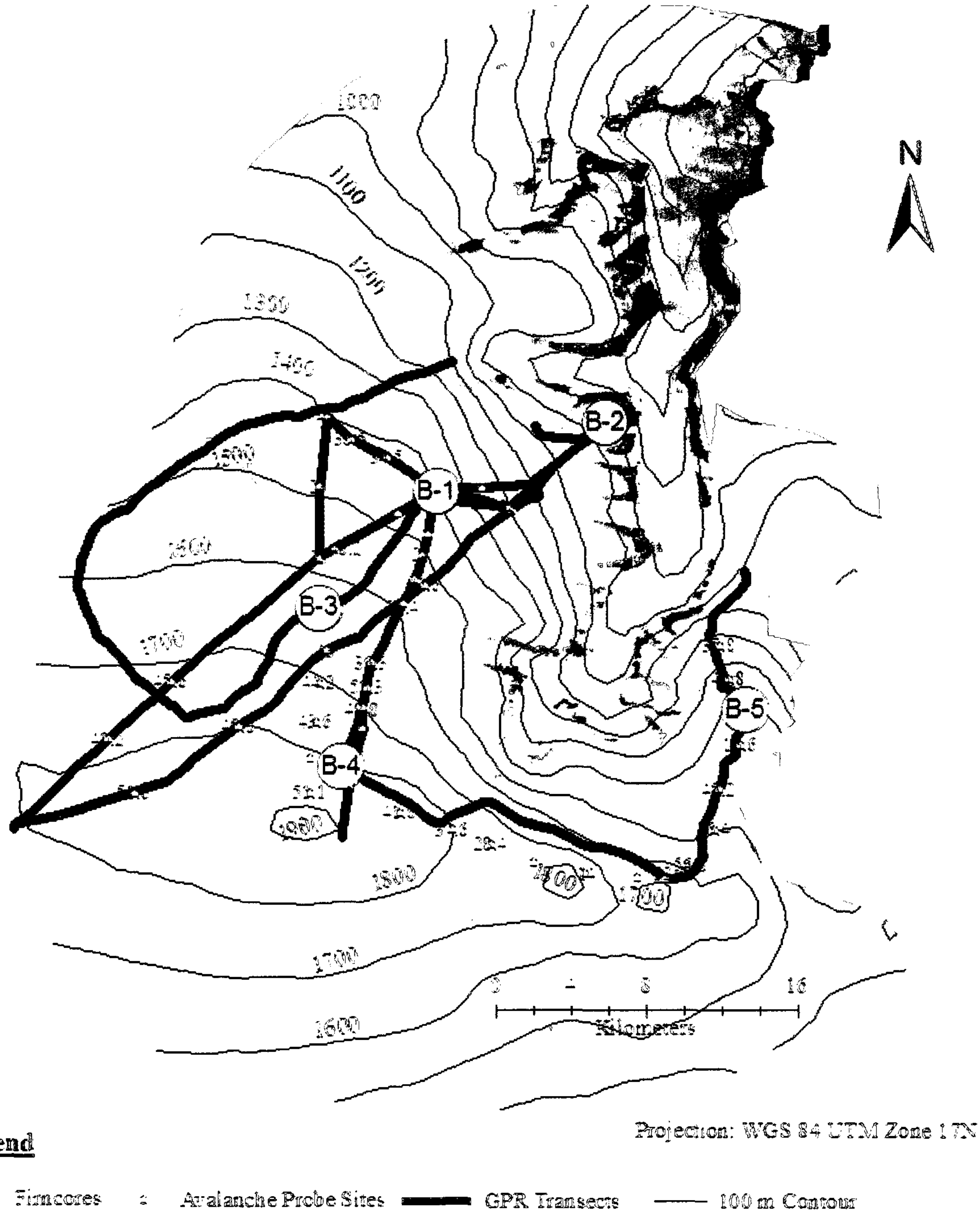

et al. (2008) suggest that measurement errors of 10% are associated with this type of density sampling.

Five shallow boreholes were drilled to depths of 7-12 m with a Kovacs Mark II ice coring system (core diameter 8.8 cm, barrel length 1.15 m) at elevations of 1060, 1390, 1515, 1640 and 1860 m a.s.l. In-situ bulk ρ_{core} were calculated using the weight, diameter and length of each core section. The location and thickness of ice lenses and ice layers in the cores were logged to establish visual stratigraphy for each core.

3.3.2 GPR and GPS acquisition and processing

In this study a 500 MHz Sensors and Software PulseEKKO Pro system was used to make the GPR measurements. The receiver and transmitter antennae were mounted in a sled and connected to a Digital Video Logger (DVL) for data viewing and recording (Fig. 3.4). Antenna separation was 0.25 m, with a total of 2500 points collected per trace. The time collection window was set to 500 ns (~40 m) and then clipped to 45 ns during post-processing to view the upper ~5 m of the snowpack. Radar wave speed v in snow is described by:

$$v = \frac{c}{\sqrt{\varepsilon_r'}} \qquad \text{(Eq. 1)}$$

where c is the speed of light in a vacuum and ε_r' is the dielectric permittivity. Kovacs *et al.* (1995) related density (ρ) with ε_r' using the empirical relationship

$$\varepsilon_r' = (1 + 0.000845\rho)^2 \qquad \text{(Eq. 2)}$$

which produces a calculated v in the near-surface snow of 0.20 m ns^{-1}. Velocity is verified by comparing snow depths calculated from GPR with those measured using the avalanche probe, where v here compares with estimates by Dunse et al. (2006) on Greenland of 0.21 m ns^{-1}.

The sled was towed by skidoo at a travelling speed of ~10 km h^{-1}, with GPS data collected at every 10th GPR trace (approximately every 5 m horizontally). The GPS data is accurate to about ±5 m in all spatial coordinates (x – latitude, y – longitude, and z - elevation). This

Figure 3.4. a) Field set up of PulseEKKO Pro 500 MHz ground penetrating radar housed in a sled and **b)** GPR and GPS antennae connected to skidoo.

a)

b)

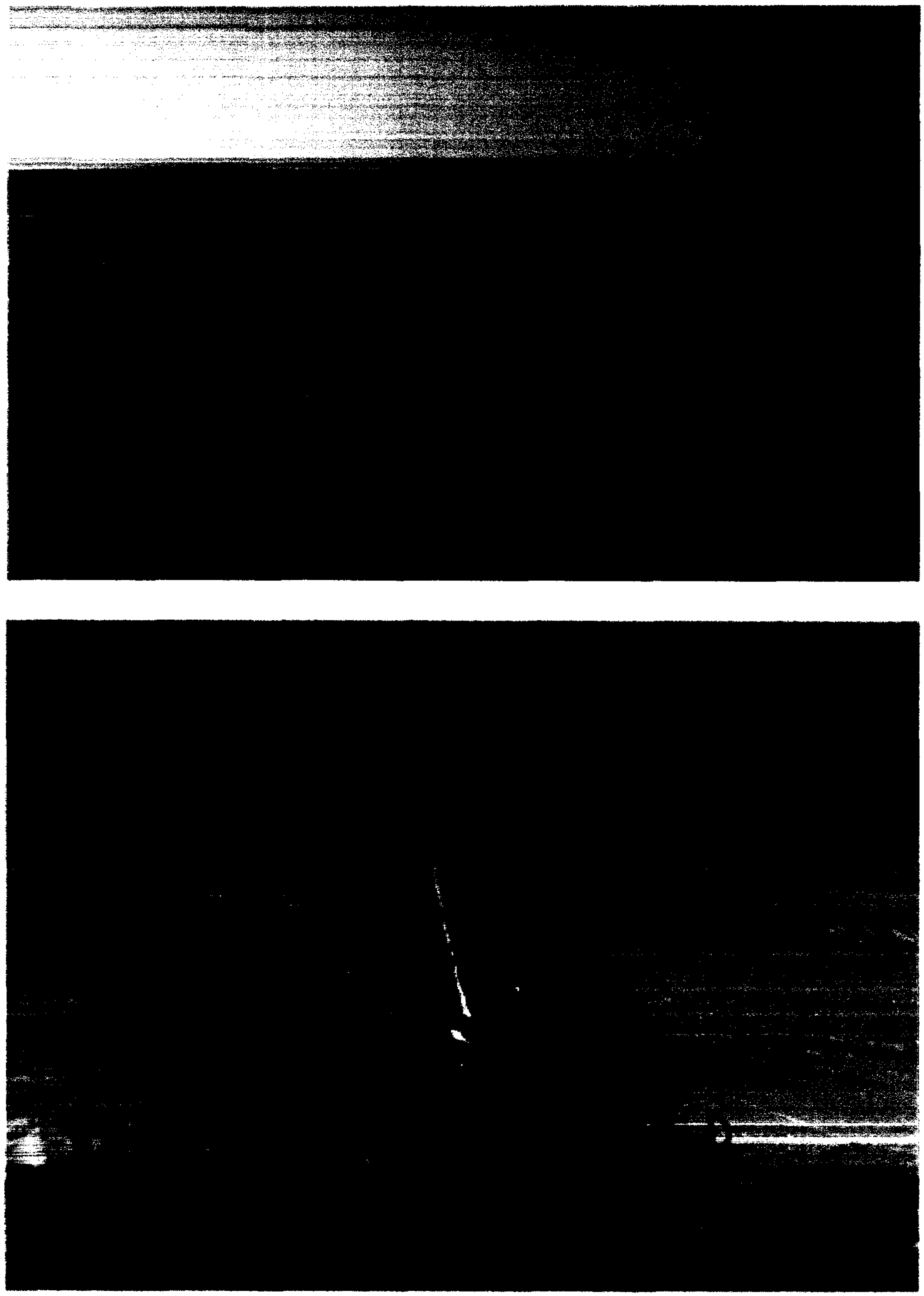

provides sufficient positional information over the length scales (10^0-10^3 m) at which snowpack features varied within the GPR traces.

During post-processing of the GPR data, unique coordinates were calculated for every GPR trace by assuming a constant travel speed between the GPS position provided at each 10^{th} trace.

Post-processing of GPR data involved the application of signal saturation corrections, frequency filtering, radar gain adjustments and trace editing (Fig. 3.5). The first received wavelet contains the most energy in a GPR trace, undergoing rebounding and echoing in the near surface (upper ~0.5 m) as it travels through the sled bottom, the groundwave, and interacts with near surface reflectors (Fig. 3.5a; Annan, 2002; Maurer, 2006; Plewes and Hubbard, 2001). These artifacts are removed by combining a Dewow filter with data editing (time window adjustment). The Dewow filter or "signal saturation correction" eliminates low frequency noise as a product of the near field echoing effect (Maurer, 2006), while preserving high frequency signals (Dunse *et al.* 2008; Kohler *et al.* 2003). Spherical Exponential Calibrated Compensation (SEC2) gain was used to enhance weak signals in the GPR trace by compensating for radar spherical spreading losses, and exponential ohmic dissipation of energy with increasing depth (Annan, 2002; Plewes and Hubbard, 2001). These post-processing steps provided a visually optimized image which allowed IRHs to be clearly identified as distinguishable bands of high reflectivity (compare Fig. 3.5a with Fig. 3.5b).

3.3.2.1 Layer depth determination using GPR

An automatic picking routine in Sensors and Software IcePicker R4 software was used to derive snow thickness measurements. This required 'training' of the software to determine the upper part of the highly reflective layer which corresponded to the LSS-07. To ensure that the LSS-07 depth was actually picked in the GPR traces, avalanche probe measurements were used to calibrate the LSS-07 depth. The learned wavelet was then used to digitize the layer as a series of points by automatically locating and picking the arrival time of the

Figure 3.5. a) Unprocessed raw radar profile showing the near field effect **b)** Post-processed GPR record after application of a DEWOW filter, trace analysis and editing, and SEC2 gain.

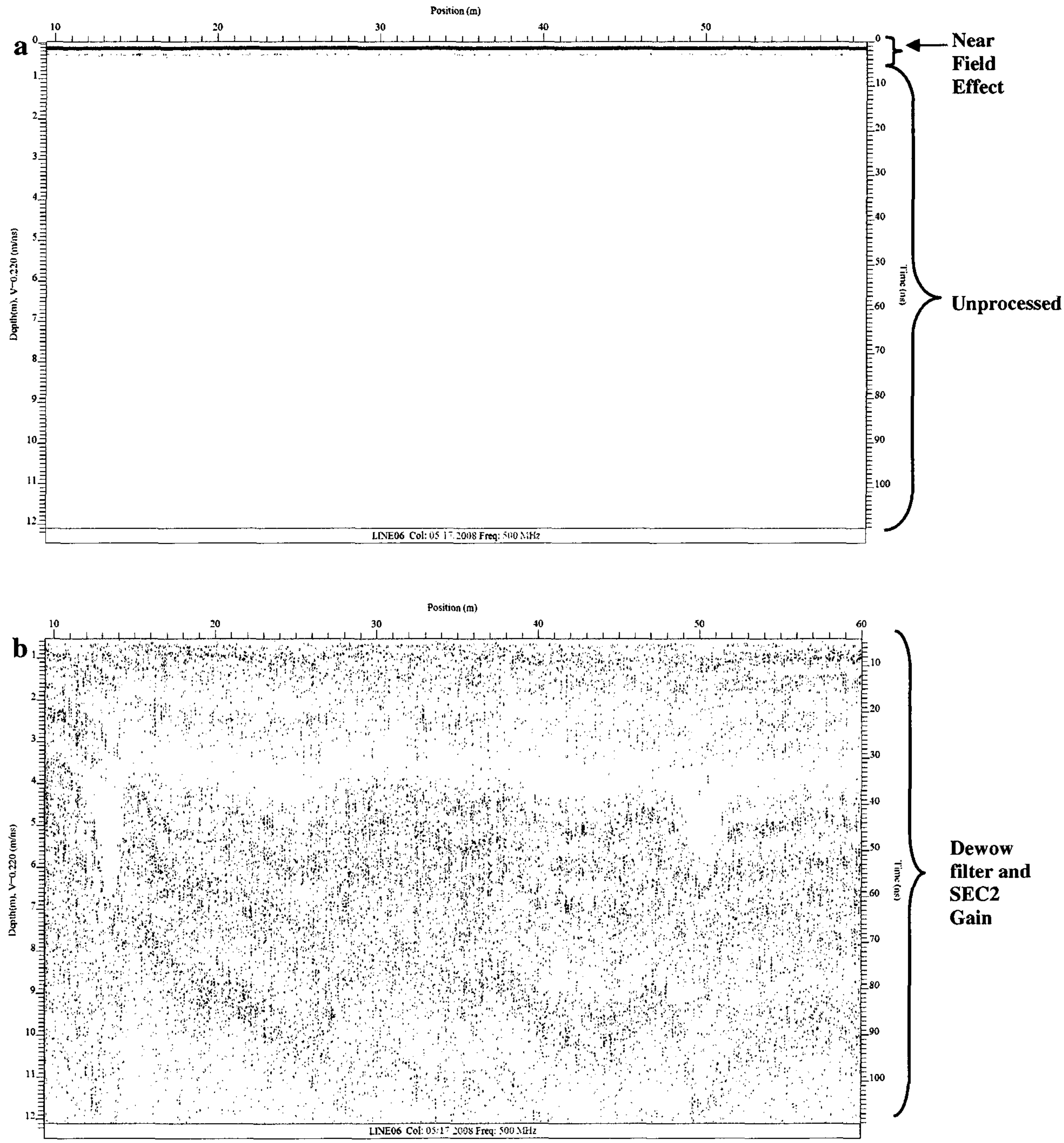

reflection from the IRH (Figs. 3.6 and 3.7). This wavelet is computed directly from the trace data representing the average reflected wavelet over the length of a survey line. IcePicker software derives ice thickness *T (m)* by computing the two-way-travel-time (*TWT*) for the pulse that is reflected from the IRH using the following:

$$T(m) = \left\{ \left[\left(t + \frac{s}{0.3} \right) \frac{V_l}{2} \right]^2 - \frac{s^2}{4} \right\}^{1/2} \qquad \text{(Eq. 3)}$$

Where t is the *TWT* (ns), V_l is the radar wave velocity in snow (0.20 m ns^{-1}) and s is the antenna separation (0.25 m). Measurements are converted by IcePicker software from the time domain to the depth domain.

3.3.2.2 Errors in depth determination

The accuracy of the automatic picking routine is affected by the roughness of the snow-firn transition as interference can arise from nearby intruding ice lenses and the dielectric contrast between firn and snow (Dunse *et al.* 2008; Pinglot *et al.* 2003). The picking routine is focused in a specified time window corresponding to the depth of the continuous IRH layer being followed. Inaccurate automatic picks were corrected manually and calibrated with avalanche probe measurements to ensure that the LSS was tracked. This procedure was undertaken for each GPR transect recorded in the basin.

The related error in IRH picking is difficult to assess, since manual picking is a somewhat subjective process (Anschütz *et al.* 2006; Dunse *et al.* 2008). The thickness error depends on a number of factors such as the accuracy of the radar wave velocity, the variability in the velocity along the survey line, the signal to noise ratio of the reflected event with respect to other clutter and ambient noise, and the ability to clearly identify the bottom of the snow layer (Parry *et al.* 2007; Pälli *et al.* 2002). Since these GPR measurements were made at the end of winter, the variability in radar velocity is assumed to be small, as density measurements obtained from the snow pits varied little with a value of 330 ± 0.05 kg m^{-3}. Meltwater intrusions which would create internal ice lenses and radar noise in the GPR returns were not present as the measurements were conducted in May, prior to the summer melt period (Wang *et al.* 2005). Given these factors, overall picking errors are assumed to lie between 1/20th and 1/10th of the wavelength used (Anschütz *et al.* 2006; Dunse *et al.* 2008).

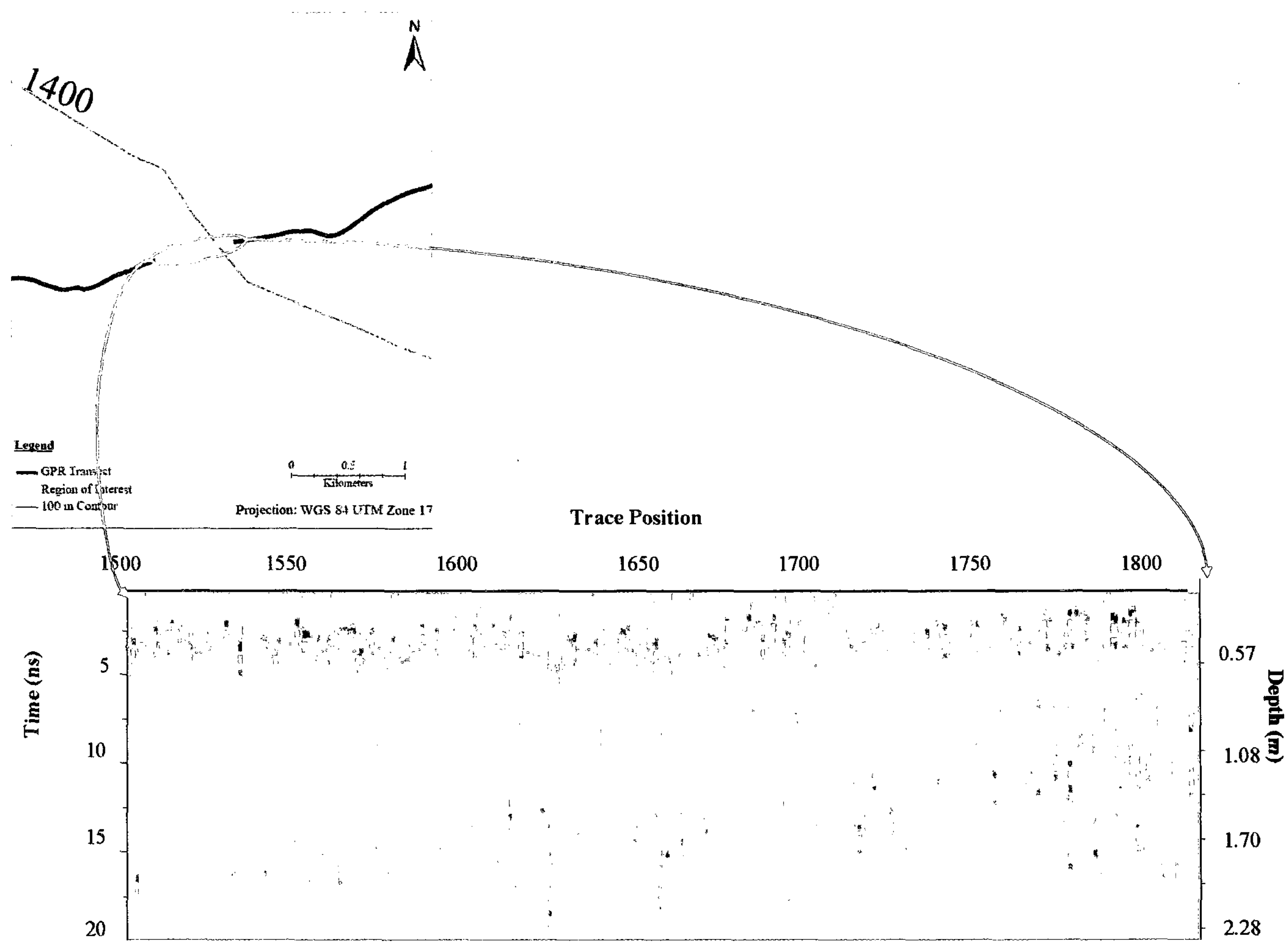

Figure 3.6. Radargram showing an example of GPR returns detected by IcePicker software from the last summer surface (LSS-07). Profile shown is ~1 km long by 2.30m deep. Position of picks along GPR transect shown between traces 1500 and 1800 are highlighted in turquoise in inset. (Base image: Landsat 7. July 7. 2000).

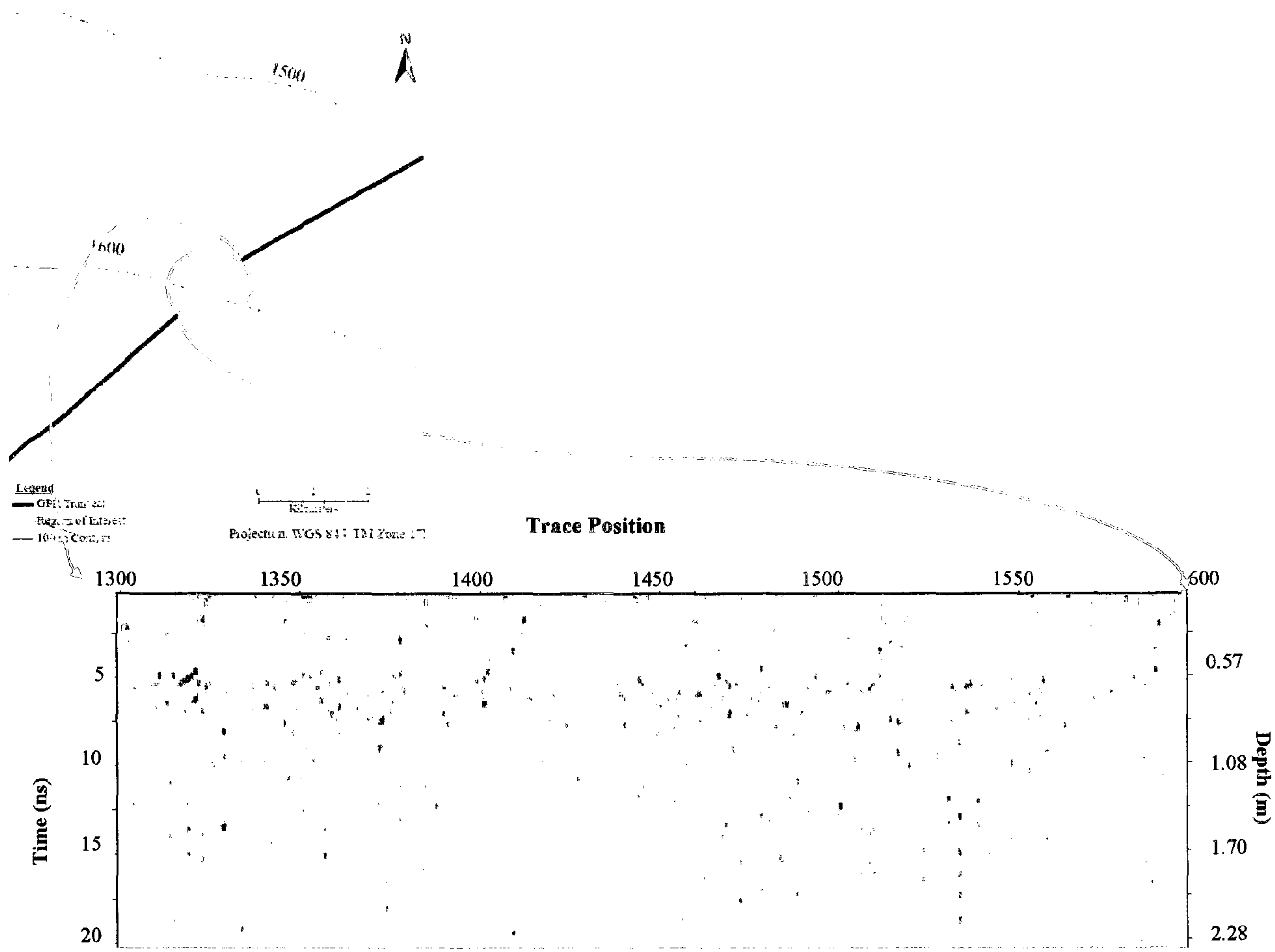

Figure 3.7. Radargram showing an example of GPR returns detected by IcePicker software from the last summer surface (LSS-07). Profile shown is ~1km long by 2.30 m deep. Position of picks along GPR transect shown between traces 1300 and 1600 are highlighted in turquoise in inset. (Base image: Landsat 7, July 7, 2000).

Based on the physical relationship between the velocity (v), wavelength (L), and center frequency (f):

$$v = Lf \qquad \text{(Eq. 4)}$$

This corresponds to depth errors on the order of ±0.02 to ±0.04 m with a 500 MHz center frequency and velocity of 0.20 m ns $^{-1}$. Radar wave velocity of 0.20 m ns^{-1} represents average velocity, and could locally be slower where there are numerous ice lenses in the superimposed ice region of the basin. Variations in velocity across the basin are encompassed within error estimates, which are estimated to be 10-15% of the depth reported. The upper and lower boundaries of layers are sometimes hard to distinguish along surveys. As depth increases the radar signal dissipates, and this further complicates the identification of layer depths.

3.3.3 High Resolution Density Profiles

High-resolution near surface density profiles were measured while raising a neutron probe from the bottom of each borehole. In the field the neutron probe is fixed to a cable, power console and winch motor, with data recorded on a laptop computer running GeoVista Platform Logger software. The probe is built with a ring-like radioactive source of fast neutrons surrounded by a cylindrical detector of slow (thermal) neutrons (Morris and Copper, 2004). Fast neutrons are scattered by hydrogen atoms absorbed in the snow and firn, and slowed down as they return to the detector (Dunse *et al.* 2008; Hawley *et al.* 2008; Morris and Cooper, 2004). The count rate of slow neutrons returned to the detector is related to the density of the snow (Hawley and Morris, 2006). Amplified pulses are shaped before passing up the cable, where the average count rate is reported in a 64 s time window. Scattering depends on the density and water content of the medium, and occurs throughout a sphere with a radius of ~15-30 cm surrounding the source detector.

The neutron probe returns a density profile for each borehole on the centimeter to decimeter scale. Previous studies show that neutron probe results can be used to determine an annual mass balance time series (Dunse *et al.* 2009; Hawley *et al.* 2008; Morris and Cooper, 2004). This is because peaks of high density are associated with summer ice/firn when more meltwater is produced, and troughs of low density are associated with autumn depth hoar when less meltwater is produced. Using the borehole diameter (12.2 cm) and distance from the wall of the borehole (probe centralization), calibration equations are used to convert the count rate to true density (Hawley and Morris, 2006). In this study the vertical density profiles are used together with visual stratigraphy to validate conclusions derived from the GPR record, since the boreholes cover the GPR depth range.

3.3.4 QSCAT Data

To interpret the origins of internal reflector horizons (IRHs) found in the GPR surveys, comparisons were made with maps of inter-annual changes in ice layer distribution on Devon Ice Cap derived from enhanced resolution data from the SeaWinds Scatterometer on the QuikSCAT (QSCAT) satellite. QSCAT makes observations of the polar regions multiple times per day (10 pm for descending pass, and 2 am for ascending pass) in the Ku-band frequency 12-18 GHz, with a nominal pixel spacing of 2.23 km and effective resolution of 5 km (Wang *et al.* 2005; Wolken *et al.* 2009). Ice layers are effective at scattering Ku band frequencies, which leads to an increase in backscatter (σ^0) at the end of each melt season. In the study of Wolken *et al.* (2009), melt mapping of changes in the distribution of ice layers formed by meltwater percolation and refreezing between 2000-2005 in the percolation zone was performed using bi-weekly averaged σ^0 values of each pixel following freeze-up periods in successive autumns. Decreases in σ^0 between successive melt seasons suggest reduced ice layer formation in the second summer. These maps represent a proxy for understanding recent summer climate variability, showing the annual melt extent and duration.

3.3.5 ASIRAS Data

Overflights with the Airborne Synthetic Aperture Radar/Interferometric Radar Altimeter System (ASIRAS) were undertaken across Devon Ice Cap along north-south and east-west transects in 2006. ASIRAS is a pulse-width limited radar altimeter which was developed in support of the European Space Agency's (ESA) CryoSat mission, and uses a radar frequency of 13.5 GHz, bandwidth of 1 GHz, and a sampling resolution of 4.5 m (Hawley *et al.* 2008). The radar can detect and track surface and subsurface layers, which enables mapping of snow accumulation patterns as it provides variation in reflectivity backscatter as a function of depth and off-nadir angle (Gray and Burgess, 2009; Hawley *et al.* 2008).

The first 30 km of the north-south flight line falls within <1 km of the western margin of the Belcher Glacier basin from 1400–1900 m elevation. The first 10 km of the east-west transect near the ice cap summit falls within the southwest portion of the basin between 1700 – 1900 m. ASIRAS transects cover the elevation range of the GPR transects, avalanche probe, snow pits, and firn cores collected during the 2008 field season. Annual layers determined in the ASIRAS record are compared with layers inferred via high frequency GPR surveys in this study. Strong annual melt layers of high density due to protracted summer melt conditions on Devon Ice Cap identified by ASIRAS should be readily identified in the GPR since variations in near surface density dominate the GPR returns in the accumulation and percolation zones of the ice cap (Wolken *et al.* 2009; Koerner, 1977).

3.3.6 Terrain Analysis

Surface topography of the Belcher Glacier basin was obtained from a DEM with 20 m nodal spacing derived from 2007 SPOT-5 stereo satellite imagery. The accuracy of the DEM was determined by checking the difference between points in the SPOT grid with ground control points (GCPs) based on GPS elevations measured during the GPR surveys. Fifty GCPs are used across the basin, and these show that the SPOT DEM is accurate to ±15 m in the vertical dimension with a mean difference of 5.78 ±5.86 m. An Inverse Distance Weighting (IDW) interpolation routine was performed on the SPOT DEM to provide a smoothed raster DEM surface.

The terrain factors of slope angle, profile curvature, planform curvature and aspect were calculated as raster surface files from the DEM using ESRI ArcGIS 9.0 software. These terrain data were plotted in both two dimensions (Fig. 3.8) and three dimensions (Fig. 3.9) to illustrate how they are distributed across the basin. It is expected that the terrain factors might play a role in the spatial variability in SWE because:

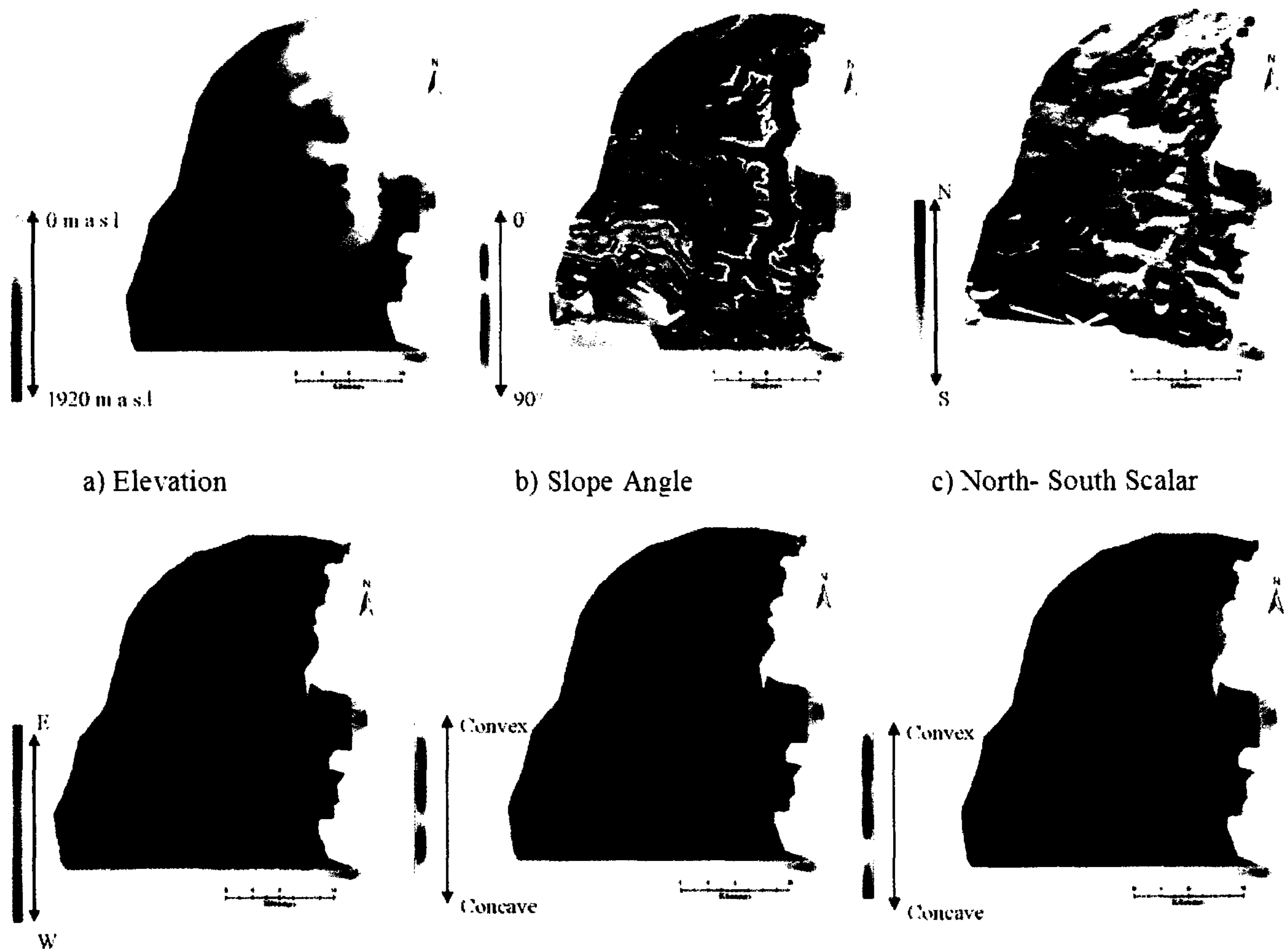

a) Elevation b) Slope Angle c) North- South Scalar

d) East-West Scalar e) Profile Curvature f) Planform Curvature

Figure 3.8. 2-Dimensional terrain factors based on SPOT DEM with ±20 m vertical resolution displayed in ArcMap 9.0 for **a)** elevation (0 – 1911 m a.s.l) **b)** slope angle (0° to 90°) **c)** North-South Scalar Aspect (1° to 180° **d)** East-West Scalar Aspect (90° to 270°) **e)** profile curvature **f)** planform curvature. (Base image: Devon Ice Cap Landsat 7, July 7, 2000 – 15 m resolution)

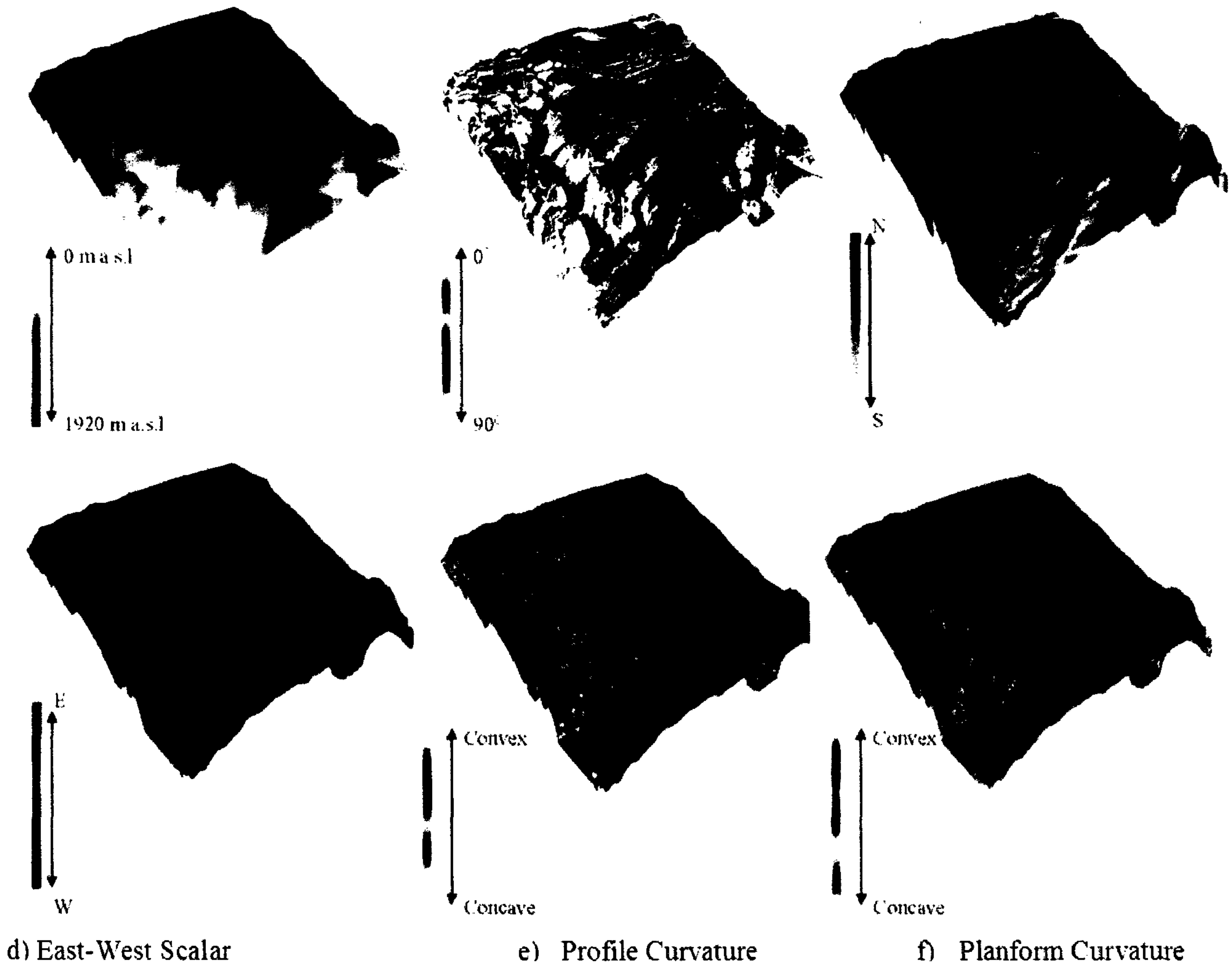

Figure 3.9. 3-Dimensional display of terrain factors **a)** elevation (0 – 1911 m a.s.l) **b)** slope angle (0° to 90°) **c)** North-South Scalar Aspect (1° to 180° **d)** East-West Scalar Aspect (90° to 270°) **e)** profile curvature **f)** planform curvature; b – e overlain on SPOT DEM with ±20 m vertical resolution displayed with a vertical exaggeration of 10 and hillshade effect of 3 in ESRI ArcScene Software.

(i) Slope angle frequently corresponds to variability in snow depth since snow tends to erode in areas of convergent wind flow, and accumulate in areas of divergent flow (Copland, 1998; Elder *et al.* 1991; Kattelmann and Elder, 1993). The slope tool in ArcMap calculates slope angles by determining the maximum change in elevation between the eight neighbors around a given cell using the equations of Zevenbergen and Thorne (1987). Lower slope values identify areas of flat terrain, while high slope values correspond to steep terrain.

(ii) Aspect relates to variations in SWE due to variability in solar radiation and wind direction (Copland, 1998; Kattelmann and Elder, 1993). Aspect is defined as the direction of steepest slope, and calculated in ArcMap from the change in elevation across the eight cells surrounding the point of interest (Zevenbergen and Thorne, 1987). It is provided as a value from 0^{o} to 359.9^{o}, measured clockwise from north. After Copland (1998), the aspect data was modified for statistical analyses because two slopes with aspects of 3^{o} and 358^{o} are similar physically, yet at the extremes of a range from 0^{o} to 360^{o} mathematically. To address this, we created a north-south scalar by computing the cosine of the aspect (i.e., 0^{o} corresponds to 1 and 180^{o} to -1), and an east-west scalar by computing the sine of the aspect (i.e., 90^{o} represented by 1 and 270^{o} by -1).

(iii) Curvature often corresponds to SWE redistribution because low SWE is found in convex areas where wind flow diverges, and high SWE is associated with concave areas where flow converges (Woo *et al.* 1983). We calculated profile and planform curvature surfaces from the SPOT DEM using the Spatial Analyst tool in ArcMap. Profile curvature describes the rate of change of slope in the aspect (i.e., steepest slope) direction, with a negative value corresponding to a convex surface, and a positive value where the surface is concave. Planform curvature relates to curvature in the direction perpendicular to the aspect, with negative values denoting a concave surface, while positive values denote a convex surface.

(iv) Elevation typically relates to increases in precipitation with altitude. Orographic precipitation tends to increase on steeper windward slopes owing to enhanced lifting, although this process is currently poorly understood in the QEI (Jiang, 2003; Roe, 2005).

The values of the terrain factors were extracted at every location where snow depth was determined in the GPR data. The final data set for each GPR snow depth location therefore had x, y and z coordinates, a SWE value from 2007-2008 and 2005-2007, slope, profile curvature, planform curvature, north-south scalar and east-west scalar aspect values. These surfaces provide a means to understand how surface terrain features affect the spatial distribution of SWE across the Belcher Glacier basin.

Previous studies that have examined the effects of terrain factors on SWE patterns have mainly focused in alpine and low elevation areas. For example, Elder *et al.* (1991) determined the distribution of SWE across a small alpine basin by identifying and mapping areas with similar snow properties on the basis of terrain controls using slope, elevation and radiation as controlling factors. They show that the quantification of slope and elevation enabled the successful modeling of SWE in the basin, with radiation providing both a physically based and temporally dynamic variable which helped to explain the variation in SWE distribution throughout the melt season. The study of Woo *et al.* (1983) in the McMaster River Catchment near Resolute Bay, Nunavut, further showed the variability in SWE as a function of terrain. They demonstrated that SWE varied from 30% of average on ridges or hilltops to 300% in gullies when compared with flat terrain. These studies highlight the importance of terrain in determining the redistribution of SWE. Although these evaluations indicate that understanding terrain variability may improve parameterizations of melt models, these types of terrain studies and analyses have not previously been evaluated on glaciers or ice caps in the QEI.

3.3.7 Principal Component Analysis

Terrain factors across glaciers are typically highly collinear (Copland, 1998). For example, elevation is often negatively correlated with slope on ice caps since there is a tendency for upper elevation regions to have gentler slope angles. A Principal Component Analysis (PCA) was therefore performed on the terrain variables to remove the effects of statistical interdependencies between factors. The data set was reduced to a set of mutually orthogonal eigenvectors, termed components (Aguado, 1990). PCA creates a set of new linear components between variables from the original data in the correlation matrix (Smith, 2002). The new variables or projections are uncorrelated with one another, and are weighted by the eigenvector representations of the original data set. The new variables also have maximum variance (Aguado, 1990). A significant component is taken to be one that has an eigenvalue >1, because this corresponds to the variance of the original variables, and limits the discussion to the most important terrain factors.

We use Pearson's correlation coefficient to understand the statistical relationship between SWE derived by GPR transects and principal components based on terrain parameters for the basin. To identify the most important terrain factors on basin-wide SWE we chose a significance level of 99%.

3.4. Results

In the GPR records, the first continuous lateral IRH was observed between the surface and a depth of 1 m, and was related to the density contrast formed during freeze-up at the end of summer 2007 (LSS-07) (Figs. 3.7 and 3.8). This layer is characterized by a band with a distinct highly reflective upper boundary and a diffuse lower boundary. In addition to density differences, this high reflectivity is also related to wind redistribution of dust and dirt during summer and the entrainment of this particulate in the snowpack during freeze-up at the end of the summer melt season. This causes the LSS to be dirty and enhances its dielectric contrast. The depth of undisturbed low density snow above this reflective layer represents accumulation for winter 2007-8.

To calibrate the radar wave velocity, and to verify that the LSS-07 layer identified in the GPR data was chosen correctly, a comparison of probing depths with the GPR LSS-07 layer data was undertaken (Fig. 3.10). A positive and statistically significant ($p<0.01$, $R^2 = 0.98$) correlation was found between the avalanche probe depths (cm) and the GPR derived depths

Figure 3.10. Scatter plot of avalanche probe depths to the 2007 last summer surface versus GPR derived depths to the same surface. Linear trend line is statistically significant at 99% level of significance.

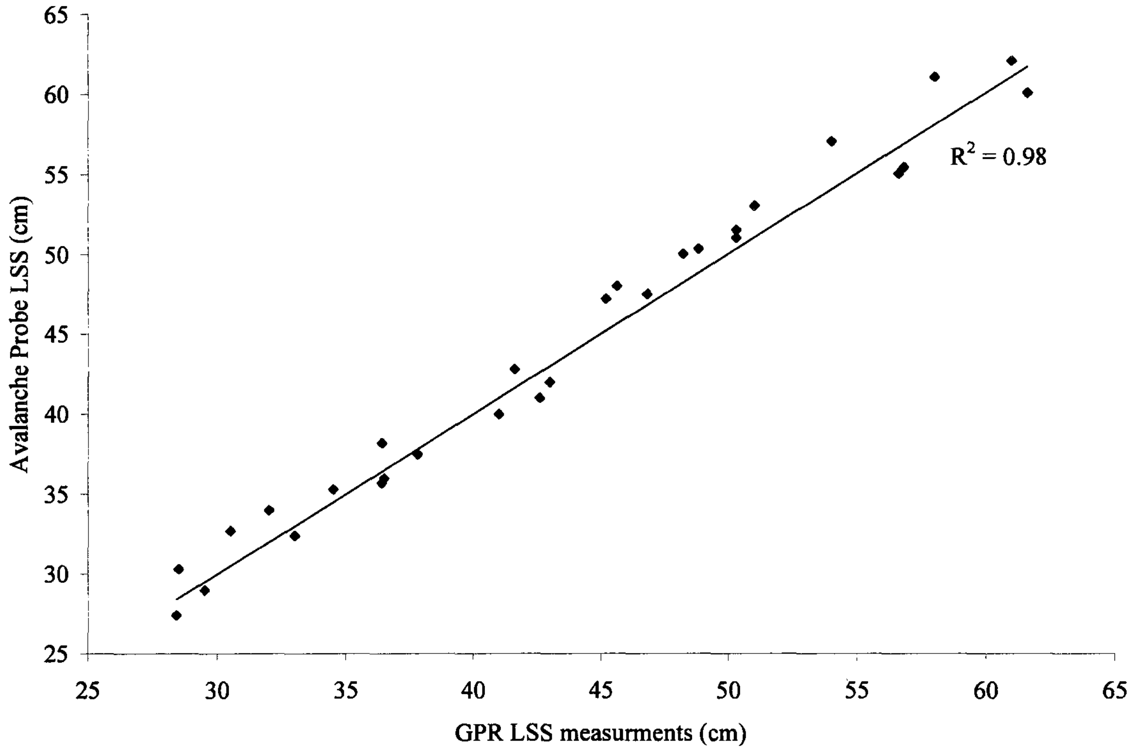

(cm) using a radar wave velocity of 0.20 m ns^{-1} in IcePicker software. This information helps reduce error in manually picking the layer. Field observations indicate outliers in Figure 3.10 relate to local variations in snow depth above the LSS due to post depositional processes such as wind redistribution and interaction with local topography.

3.4.1 Winter SWE Patterns 2007 – 2008

Based on the verification given above, it is possible to derive winter 2007-8 snow thickness measurements for every one of the 94,778 locations where GPR traces were recorded between 1000-1900 m a.s.l. across the Belcher Glacier basin. To convert snow thickness measurements to SWE values, they must be multiplied by the snow density. The manual and GPR measurements consistently showed that depth varied much more than density, with average snow pit densities (ρ_{pit}) of 330 ± 0.05 kg m^{-3}. The density value varied little about this mean (± 0.05 SD), and therefore was used as a standard factor to convert the depths to SWE values. Using ArcMap 9.0 software, maps of the winter SWE distribution were then produced for the basin (Fig. 3.11). The following is a discussion of these patterns.

The winter 2007-8 accumulation varied spatially across Belcher Glacier, with a clear elevation gradient shown in Figure 3.11. All transects that show predominantly low values (0.03-0.17 m w.e.) are in the lowest elevations of the basin (1000-1200 m), with a low degree of spatial variability. There is a larger degree of spatial variability with low to moderate SWE as elevations increase from 1400-1700 m when compared with lower elevations. Transects in the central part of the basin show moderate increases between 1400-1700 m, however the patterns in the east and west at similar elevations are markedly different. GPR transects in the western-most part of the basin (1000-1700 m) show SWE values typically lower than transects at similar elevations separated by ~10-15 km in the central part of the basin (Fig. 3.11). The spatial variation of SWE in the western part of the basin is also low which does not resemble the central region at similar elevations; rather the entire elevation range in the west compares more with SWE in the ablation region (1000-1200 m a.s.l pattern). The eastern transect shows both higher SWE values and greater spatial variations in SWE for the same elevations when compared to the other parts of the basin. A pronounced elevation accumulation gradient from 1000-1450 m a.s.l is revealed in the east with values

Figure 3.11. 2007 – 2008 Winter SWE map for the Belcher Basin based on 500 MHz GPR transects. SWE (m w.e.) calculated based on the product of IcePicker derived depth (m) to the LSS-07 via GPR traces, and mean basin-wide snow pack density (330 kg m^{-3}). Values classified as low: 0.03 – 0.17 m w.e. (green), Medium / Moderate: 0.18 – 0.33 m w.e. (olive green to orange), High: 0.34 – 0.49 m w.e. (dark orange to red). (Base image: Devon Ice Cap Landsat 7, July 7, 2000 – 15 m resolution).

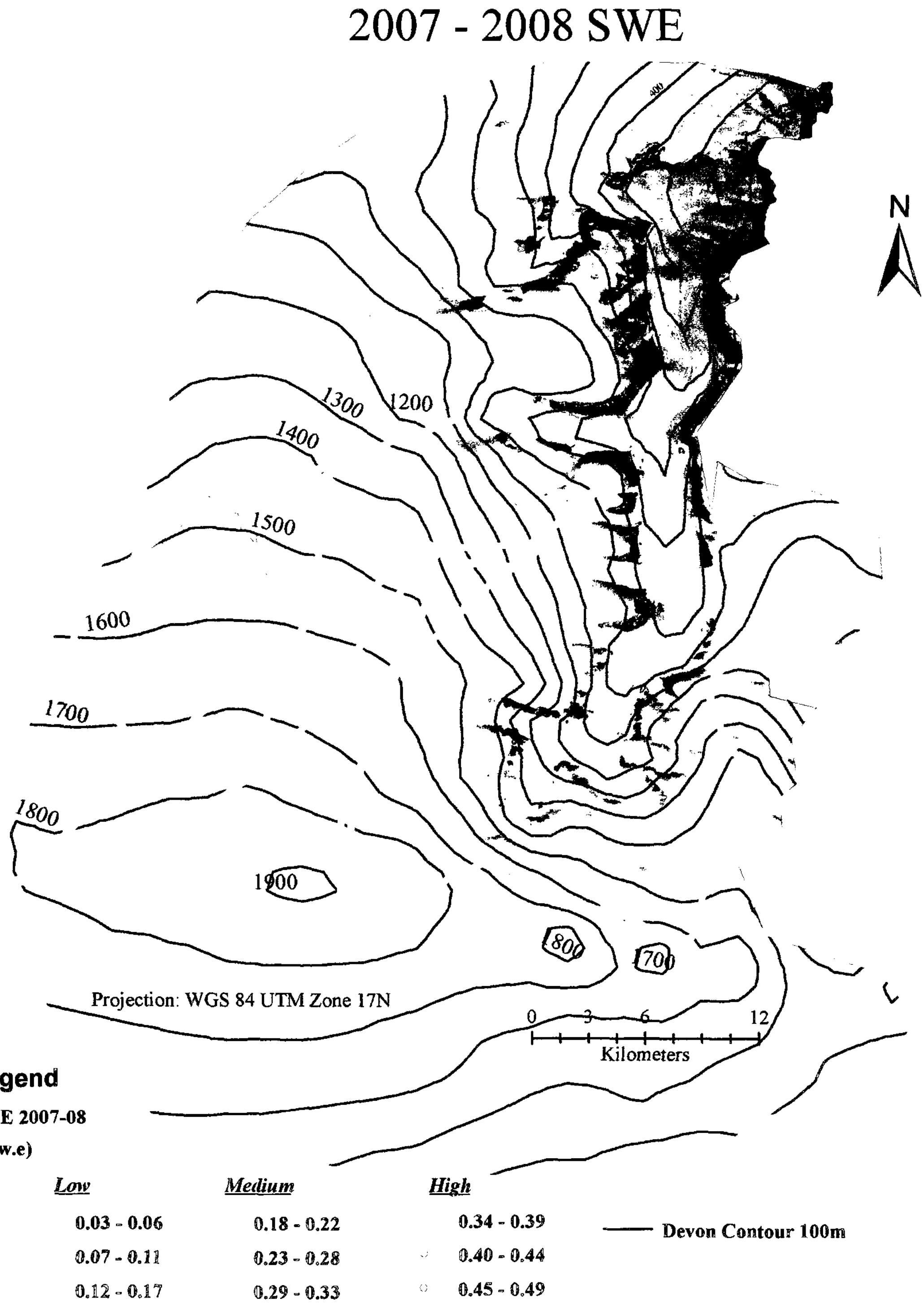

ranging from 0.03-0.49 m w.e. within a ~10 km distance. The largest SWE values are found in the SW part of the basin (1700-1900 m a.s.l) near the summit region, with transects showing average values above 0.23 to 0.39 m w.e. which locally reach 0.40 to 0.48 m w.e.

The E-W transect at the southern headwall of the Belcher Glacier varies little in elevation from 1600-1800 m a.s.l. There are, however, considerable spatial variations in SWE along this transect, with low, moderate, and high values (Fig. 3.11). Little change in accumulation with elevation is observed in this area, suggesting that some other factor may be important in determining the spatial pattern in SWE. Field observations along the headwall transect indicate that surface topography is highly variable with a series of ridges and gullies. These appear to influence local snow patterns, and can explain how high and low SWE values can occur over distances of <1 km horizontally.

3.4.2 Multiyear Snow Depths

In addition to the LSS-07 layer discussed above, other deeper internal layers are also visible in the GPR traces. The next layer below the LSS-07 is quite faint, inferred to be the LSS-06 when less melting occurred than in 2005 and 2007. Decadal ranking of summer June, July, August (JJA) temperatures at the 700 hPa pressure surface using the National Centers for Environmental Prediction/National Center for Atmospheric Research (NCEP/NCAR) reanalysis data since 2000 shows that 2006 was the 5th warmest year on record for QEI Caps, with 2007 and 2005 ranked 2nd and 3rd respectively (Sharp, personal communication, 2009). The latter two years would have produced a thick layer upon refreezing at the end of summer. Evidence of a thick 2005 layer is provided using information from QSCAT and ASIRAS as described below.

3.4.2.1 QSCAT

To understand the origins of the internal layers in the GPR record, comparisons can be made with the QSCAT maps of melt-refreezing history of Devon Ice Cap (Wolken *et al.* 2009). This information helps to date the ages of observed melt layers, and brings meaning to the vertical layering in the GPR data. These results show that from 2000-2005 there was high spatio-temporal variability in ice layer formation in both the ablation and percolation zones of the ice cap (Fig. 3.12). The spatial patterns in ice layer formation are statistically significantly ($p < 0.05$) and highly correlated with elevation ($r = 0.78$). The most extensive ice layer formation occurred in 2001 and 2005, with the large magnitude backscatter (σ^0) changes in 2005 compared to the previous year's values occurring at nearly all elevations on the ice cap. Wolken *et al.* (2009) show that areas which experienced large magnitude + σ^0 changes from the previous year (i.e. 2004 to 2005), are likely to be associated with the greatest changes in the density profile of the snowpack (Fig. 3.12). The refreezing of large quantities of meltwater produced during the warm summer of 2005, combined with wind action at the end of the melt season, likely produced a thick continuous ice lense across the ice cap.

3.4.2.2 ASIRAS

Complementing the QSCAT records, results from ASIRAS overflights in April/May 2006 show that 2005 was an anomalously warm year on both the north-south (N-S) and east-west (E-W) transects (Fig. 3.13). This is indicated by high reflectivity of the second layer found at ~0.50-0.75 m and ~0.75-1.00 m depths in the N-S and E-W transects respectively (the first layer represents the snow surface at the time of the overflight). Comparing the relative strength of the annual horizons across each transect, the strongest reflections from 2005 in the N-S line occur within 10 km of the north side of the summit, between ~1700-1800 m a.s.l. Similar strong reflections from 2005 are shown in the first 20 km of the E-W transect between ~1800-1900 m a.s.l. These findings suggest that the highest reflection returns from the 2005 layer shown in the ASIRAS data occur near the Belcher Glacier basin, since both flightlines occurred close to the outline of the basin in the west and southwest. The distinct density contrast produced by the strong annual melt year of 2005 facilitates the identification of the LSS-05 layer in the GPR record.

3.4.3 2005 – 2007 SWE Patterns

If it is assumed that the next major reflector beneath the LSS-07 surface relates to LSS-05, then it becomes possible to determine what the net mass balance was across the glacier for the period 2005-7. This is different from the 2007-8 records, which represented winter accumulation, as the 2005-7 series has undergone a two year melt cycle and indicates what

Figure 3.12. QSCAT post-freeze up bi-weekly averaged backscatter (σ^0) change between successive melt seasons for Devon Ice Cap 2000 – 2005. Yellow to red represent positive σ^0 values and indicate an increase in ice layer formation since the end of the previous melt season. Dark red values show the highest σ^0 change, which is indicative of ubiquitous ice layer formation across the ice cap. Light to blue σ^0 values suggest that ice layer formation was either limited, or that there was considerable snowfall at the end of the melt season. Source: Wolken et al. (2009).

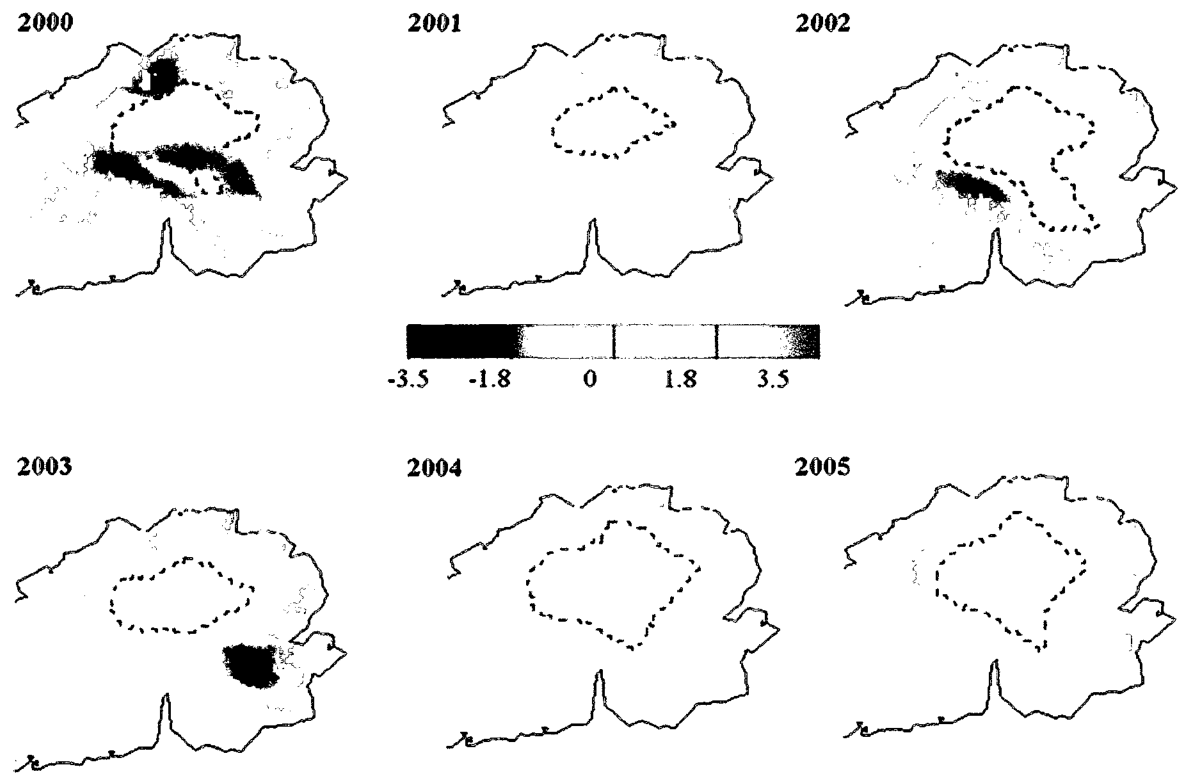

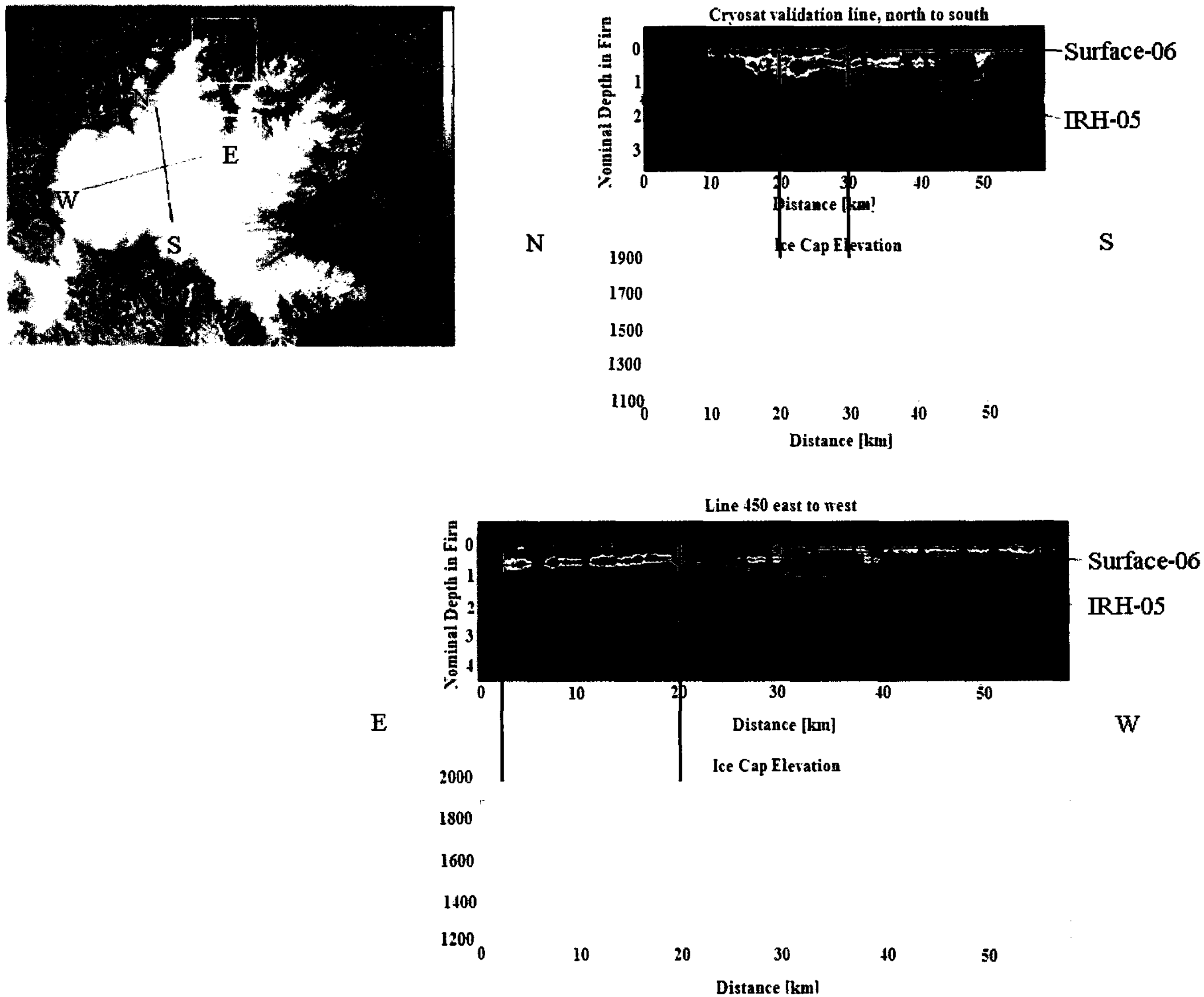

Figure 3.13. ASIRAS overflights in April/May 2006; north-south, and east-west transects on the Devon Ice Cap. Clearest Internal Reflector horizons (IRHs) for both transects is the 2nd layer corresponding to the 2005 summer surface melt layer. The 2006 and 2005 internal layers are pointed to by arrows

has remained at the end of full annual cycles (i.e., net mass balance). The reflections produced by the LSS-05 layer are quite strong and complex in the GPR records, with picks of this surface made for locations which occurred above the ELA (>1260 m a.s.l.). The GPR picks to the LSS-05 layer provided 81,359 snow depth measurements, and were differenced from the 2007-8 snow depth series to provide a new 2005-7 SWE data set.

The 2005-7 snow depth data are converted to snow water equivalent (SWE) values using the mean density of the firn-snow matrix between the LSS-05 and LSS-07 layers determined from the neutron probe records. These measurements ranged between 300-360 kg m^{-3}, so the same mean density value of 330 kg m^{-3} was applied to the 2005-7 snow depth measurements as the 2007-8 data. This enables the production of a 2005–2007 SWE map for the entire basin above the ELA (Fig. 3.14).

The spatial pattern of SWE for the multi-year time series exhibits considerable spatial variability across the basin (Fig. 3.14). The lowest values occur between the ELA and 1400 m a.s.l in the central part of the basin, however for both east and western transects SWE tends to be much higher for these contours. There is a considerable increase in both amounts and spatial variability of SWE above 1700 m a.s.l (Fig. 3.14), with the largest values in these transects found in the southwest between 1700 and 1900 m a.s.l near the ice cap summit. The most western transect (1300-1600 m a.s.l) shows SWE values which are consistently in the moderate range from 0.30 to 0.57 m w.e, with very little spatial variability (Fig. 3.14). This contrasts with the central part of the basin, as similar elevations showed typically lower values. SWE in the west slightly reflects an elevation accumulation gradient, however is considered minimal when compared with the extremely pronounced trend observed in the central portion of the basin at similar elevations. The spatial pattern of SWE in the eastern transect is different from the west in that there is more of an elevation accumulation relationship in this region. These spatial patterns were also demonstrated in the 2007-8 winter SWE data series.

The E-W headwall transect at the southern end of the Belcher Glacier is characterized by significant spatial variations in SWE over short horizontal scales (<10^2 m) (Fig. 3.14). This

Figure 3.14. Multi-year SWE (m w.e.) map 2005 – 2007 of the Belcher Basin based on 500 MHz GPR transects. SWE (m w.e.) calculated based on the product of IcePicker derived depth (m) to the LSS-05 via GPR traces, and mean basin-wide snow pack density (330 kg m^{-3}). Calculations based on the difference between 2005 – 2008 SWE and 2007 – 2008 SWE. Values classified as low: 0.03 – 0.29 m w.e. (green), Medium / Moderate: 0.30 – 0.57 m w.e. (olive green to orange), High: 0.58 – 0.84 m w.e. (dark orange to red). (Base image: Devon Ice Cap Landsat 7, July 7, 2000 – 15 m resolution).

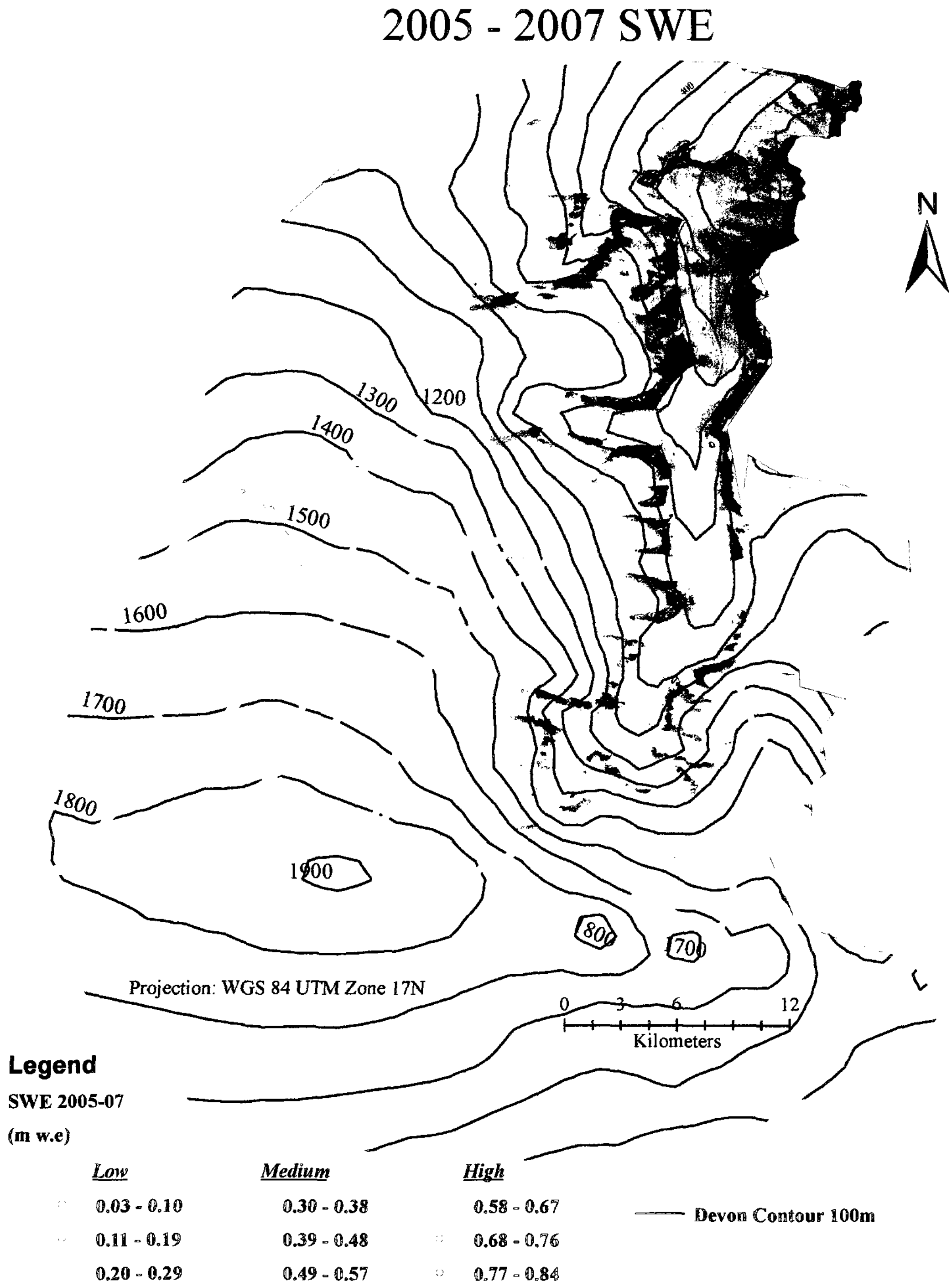

is demonstrated over a 2 km section by a single patch of extremely low values of 0.03 to 0.10 m w.e., which rises sharply to 0.39 – 0.48 m w.e. nearby. This region experiences typically low SWE values with considerable spatial variability, which is also observed in the 2007-8 winter SWE data (Fig. 3.11). This transect does, however, have considerably lower values when compared with the western part of the basin at similar elevations.

3.4.4 Terrain Analysis

With SWE evaluated across the basin for winter 2007-8 and annual 2005-7 time series, these observations suggest that terrain factors have an important control on the spatial pattern of SWE. These factors are now quantified in the following sections.

3.4.4.1 2007-8 Terrain Analysis and Principal Component Analysis (PCA)

Collinearity between the terrain variables was removed using a PCA at the 94,778 locations where 2007-8 snow depths were determined from the GPR transects, with the results provided in Table 3.1. Principal component 1 (PC1) was the most significant with an eigenvalue (λ) of 1.52, explaining 25.28% of the total variance in the terrain data. PC1 is classified as an elevation (positive eigenvector), slope (negative eigenvector), and north-south scalar (positive eigenvector) component. The percent variance of elevation, slope and north-south scalar aspect in PC1 combine to explain 96.76% of the total variance in this component. This suggests that as elevation increases, slope angles decrease, and that these features are predominantly found on north facing slopes. These terrain patterns have been plotted and can be observed in Figs. 3.8 a-c and 3.9 a-c.

Principal component 2 (PC2) is primarily a profile and planform curvature component with an λ of 1.32, explaining 22.00% of the total variance in the terrain data. Profile (49.26%) and planform (46.85%) curvature represent 96.11% of the total variance in this component, with the two inversely related. A negative profile curvature value combined with a positive sign for planform curvature both suggests a convex surface (Figs. 3.8 e-f and 3.9 e-f).

Principal component 3 (PC3) is dominated by east-west scalar aspect with an λ of 0.99, explaining 16.51% of the total variance in the terrain data. A positive east-west scalar aspect

Component	1	% Variance	2	% Variance	3	% Variance	4	% Variance	5	% Variance	6	% Variance
Elevation	**0.66**	**43.76**	-0.02	0.35	0.09	0.4	-0.07	1.19	-0.09	0.04	**0.73**	**54.25**
Slope Angle	**-0.58**	**34.93**	-0.01	0.79	-0.09	0.26	**0.56**	**25.37**	-0.02	0.37	**0.59**	**38.27**
N-S scalar	**0.45**	**18.07**	-0.03	0.71	0.09	1.32	**0.82**	**71.94**	0.09	0.63	-0.33	7.33
E-W scalar	-0.15	1.11	0.07	2.03	**0.98**	**93.85**	-0.01	0.2	-0.11	2.79	0.01	0.01
Profile curvature	-0.02	1.01	**-0.71**	**49.26**	-0.03	0.07	0.03	0.33	**-0.7**	**49.27**	-0.07	0.07
Planform curvature	0.03	1.12	**0.7**	**46.85**	-0.12	4.1	0.07	0.96	**-0.69**	**46.9**	-0.07	0.07
Explained variance (%)	**25.28**		**22**		**16.51**		15.19		11.29		9.72	
Eigenvalue	**1.52**		**1.32**		**0.99**		0.91		0.68		0.58	

Table 3.1. Principal component analysis of the terrain variables present at the 2007-2008 snow depth locations. The explained variance and corresponding eigenvalue for each component are shown, with significant components, eigenvectors, and eigenvalues highlighted in bold.

represents 93.85% of the total component variance in PC3 and indicates aspects are more easterly. The first three components explain 63.79% of the total variance and are considered to be representative of the original data.

3.4.4.2 2007-8 SWE and PCA Terrain Variability

To determine the relationship between SWE and terrain, the projections of the first three principal components (Table 3.1) were correlated with the 2007-8 SWE values determined from the GPR traces (Table 3.2). The resulting correlation coefficients are all statistically significant at the >99% significance level. SWE is significantly positively correlated ($r = 0.62$) with PC1 (elevation, slope angle, and N-S scalar aspect), which indicates that SWE increases as elevation increases (since the eigenvector for elevation is positive in PC1: 0.66). This is also shown in Figure 3.11. Slope angle has a negative eigenvector in PC1, which indicates that higher SWE is present on lower slope angles. Finally, North-South scalar aspect has a positive eigenvector in PC1 showing that north facing slopes receive more SWE than south facing ones.

SWE is significantly negatively correlated ($r = -0.26$) with PC2, the factor that mainly represents surface curvature. This indicates that higher SWE values are related to concave surfaces since PC2 in Table 3.1 is composed of negative profile curvature values and positive planform curvature values (which both indicate a convex surface). This indicates that gullies or topographic troughs on the surface retain more snow than ridges, likely relating to wind action redistributing freshly deposited snow off ridges and depositing it in topographic hollows on the surface. These findings complement those of Woo *et al.* (1983) near Resolute Bay, where annual snow deposits were found to be shallowest (<0.1 m) on windswept hilltops or convex ridges, and thickest (>1.0 m) in concave gullies and valleys.

SWE is significantly positively correlated with PC3, the component dominated by East-West scalar aspect, which indicates that SWE tends to increase on easterly facing aspects. This is shown in Figure 3.11, with 2007-8 SWE values being much larger near the summit area in the southwest and western parts of the basin at high elevations (>1700 m) when compared with the east.

Table 3.2. Correlation coefficients (r-value) of SWE with terrain variable significant components 2007 – 2008

Component	SWE
PC1 - Elevation, Slope Angle and N-S Scalar	0.62
PC2 - Profile and Planform Curvature	-0.26
PC3 - E-W Scalar	0.62

3.4.4.3 2005-07 Terrain Analysis and PCA

A PCA was performed using terrain variables at 81,359 snow depth locations above the ELA (>1260 m a.s.l) where 2005-7 snow depths could be determined (Table 3.3). In general, the 2005-7 PCA results show many similarities with the 2007-8 terrain results. The first three components are significant, explaining 62.00% of the total variance in the terrain data. Each component is characterized by the same terrain factors found in PCA with the 2007 – 2008 data.

Principal component 1 (PC1) represents an elevation, slope angle and north-south scalar aspect component, explaining 23.52% of the total variance in the terrain data. For the 2005-7 period elevation and slope angle contribute 46.24% and 33.65% of the variance, respectively, with north-south scalar aspect contributing an additional 17.64%. Together, these three factors contribute 97.52% of the total variance in PC1. Elevation and north-south scalar aspect factors have positive eigenvectors, while slope angle is negative.

Principal component 2 (PC2) is again a planform and profile curvature component which explains 21.45% of the total variance in the terrain data (Table 3.3). PC2 profile and planform curvature account for 47.61% and 49.00% of the variance in PC2 respectively, corresponding to 96.61% of the total component variance. Profile curvature has a negative relationship with PC2 but planform curvature has a positive relationship. Principal component 3 (PC3) is an east-west scalar aspect component with λ of 1.02 and explains 17.03 % of the total variance. A negative east-west scalar aspect dominates the total variance of PC3, representing 84.64% of the total component variance.

Component	1	% Variance	2	% Variance	3	% Variance	4	% Variance	5	% Variance	6	% Variance
Elevation	**0.68**	**46.24**	-0.09	0.64	0.02	0.04	-0.07	0.49	-0.17	2.89	**-0.71**	**50.41**
Slope Angle	**-0.58**	**33.64**	0.14	1.96	-0.22	4.84	**0.47**	**22.09**	-0.22	4.84	**-0.57**	**32.49**
N-S scalar	**0.42**	**17.64**	-0.05	0.25	-0.3	9	**0.79**	**62.41**	0.01	0.01	-0.32	10.24
E-W scalar	0.02	0.04	0.01	0.01	**-0.92**	**84.64**	-0.35	12.25	0.19	3.61	0.02	0.04
Profile curvature	-0.13	1.69	**-0.69**	**47.61**	0.08	0.64	0.13	1.69	**0.66**	**43.56**	0.21	4.41
Planform curvature	0.1	1	**0.7**	**49**	0.12	1.44	0.09	0.81	**0.67**	**44.89**	-0.16	2.56
Explained variance (%)	**23.52**		**21.45**		**17.03**		15.65		11.71		10.64	
Eigenvalue	**1.41**		**1.29**		**1.02**		0.94		0.7		0.64	

Table 3.3. Principal component analysis of the terrain variables present at the 2005-2007 snow depth locations. The explained variance and corresponding eigenvalue for each component are shown, with significant components, eigenvectors, and eigenvalues highlighted in bold.

3.4.4.4 2005-7 SWE and PCA Terrain Variability

Correlations of the 2005-7 SWE data with the PCA projections showed similar patterns to the 2007-8 correlations, with statistically significant results at the >99% level (although the overall correlations are lower compared to the 2007-8 data) (Table 3.4). PC1 indicates that elevation was still the single most important component across the basin, with SWE increasing in tandem with increasing elevation (Figs 3.11 and 3.14). Lower slope angles were also characterized by higher SWE, as also seen 2007-8. N-S scalar aspect has a positive eigenvector in PC1 and positively correlated with SWE, which suggests that increasing SWE occurs more on north facing slopes.

For PC2, the curvature component, it was found that higher SWE values were again related to concave surfaces. The correlation coefficient was weaker in the 2005-7 PCA correlations ($r = -0.21$) than in the 2007-8 results ($r = -0.26$), although the same patterns still held. In relation to PC3, SWE is significantly related, although with higher SWE values on more westerly facing aspects in 2005-7 compared to higher values on more easterly aspects in 2007-8.

Table 3.4. Correlation coefficients (r-value) of SWE with terrain variable significant components for 2005 – 2007

Component	SWE
PC1 - Elevation, Slope Angle and N-S Scalar	0.23
PC2 - Profile and Planform Curvature	-0.21
PC3 - E-W Scalar	0.22

3.4.5 Average Annual Accumulation Patterns

Terrain analyses combined with transect evaluations of winter 2007-8 (Fig. 3.11) and annual 2005-7 (Fig. 3.14) SWE consistently show elevation as the most significant factor in determining SWE depth. To provide a general pattern of SWE across the basin, the average annual snow accumulation (SWE) patterns for the Belcher Glacier basin were calculated by dividing the 2005-7 SWE series by two for each elevation contour above the ELA (1260 m a.s.l.). The average annual SWE value is then applied to its respective elevation contour (Fig. 3.15). Like the transect evaluation above, the average annual spatial pattern of SWE in the basin is largely controlled by elevation.

There is a pronounced elevation accumulation gradient from north to south across the basin for the average annual pattern, similar to the 2007-8 winter accumulation series (Fig. 3.11). The lowest average annual rate of 0.09 m w.e. a^{-1} is shown in the superimposed ice region (1260 – 1400 m a.s.l) and then progressively increases towards the 1800-1920 m contour to 0.21 m w.e. a^{-1}. The 1400-1500 m contour, however shows notably higher values for the average annual series (0.18 m w.e. a^{-1}) when compared with the 1300-1400 m (0.13 m w.e a^{-1}) and 1500-1600 m (0.15 m w.e a^{-1}) contours. For 2005-7, the 1400-1500 m contour in the east and west parts of the basin shows significant areas with much higher SWE values when compared with central transects (Fig. 3.14). Although more transects were sampled in the central part of the basin, these significant outlier areas potentially increase the average annual rate for this contour. The average annual pattern shows SWE increases only slightly between 1500-1700 m, but increases substantially towards the ice cap summit region (Fig. 3.15).

The mean SWE recorded at each elevation band can also be calculated for the 2007-8 winter series, which enables comparisons with the 2005 to 2007 SWE patterns (Fig. 3.16). In both cases, a clear increase in accumulation with elevation is observed, although this relationship is not linear in the lower parts of the accumulation area (<1500 m a.s.l.). If it is assumed that

Figure 3.15. Average Annual Accumulation map 2005 – 2007. Derived by dividing values from GPR transects in Figure 21 by 2. Values applied to elevation contours above the ELA – 1260 m a.s.l (Base image: Devon Ice Cap Landsat 7, July 7, 2000 – 15 m resolution).

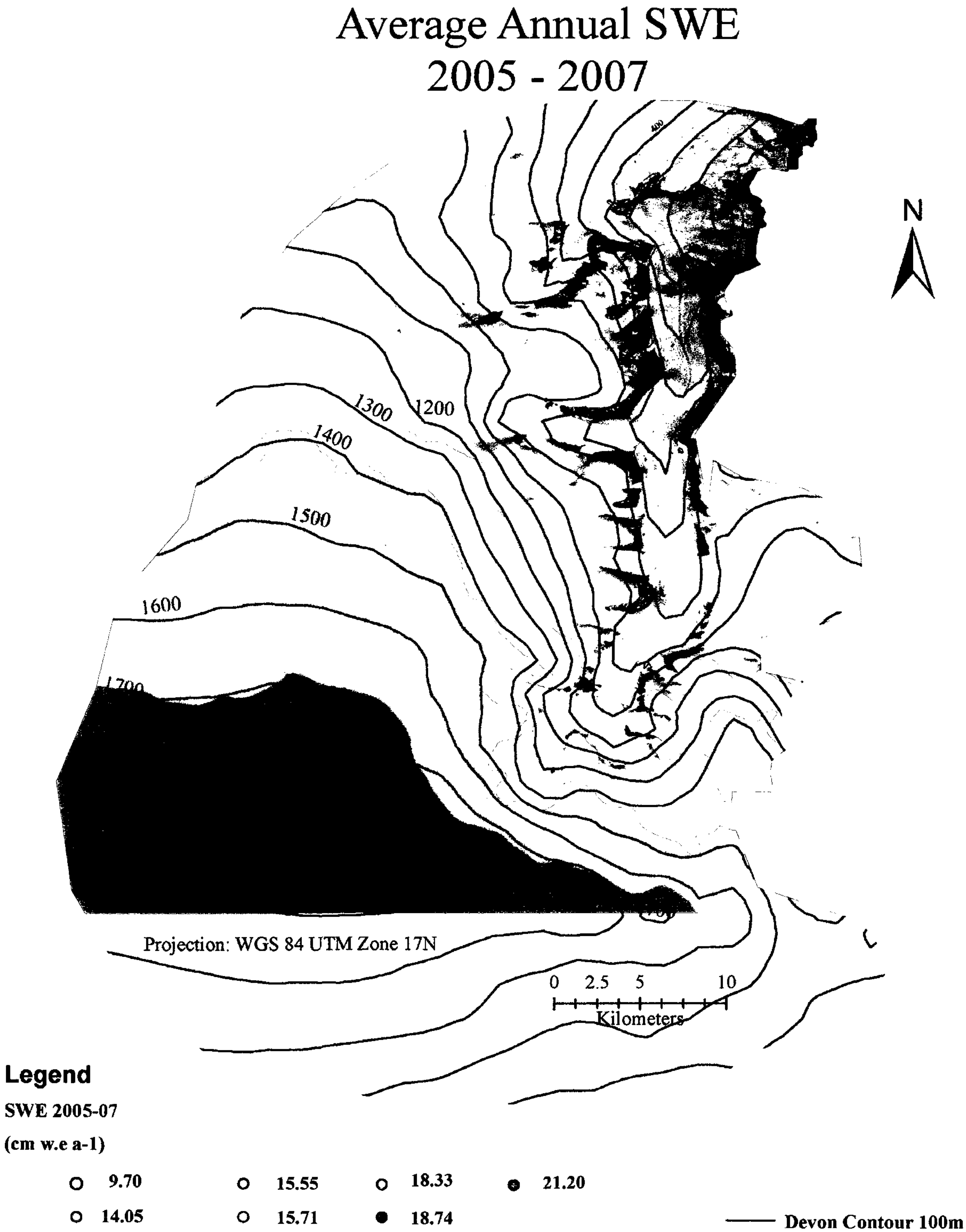

Figure 3.16. Average annual accumulation (SWE m w.e. a^{-1}) based on the 2005 – 2007 SWE series with winter snow accumulation 2007 – 2008 (SWE m w.e.) plotted against elevation contours between 1200 – 1920 m a.s.l

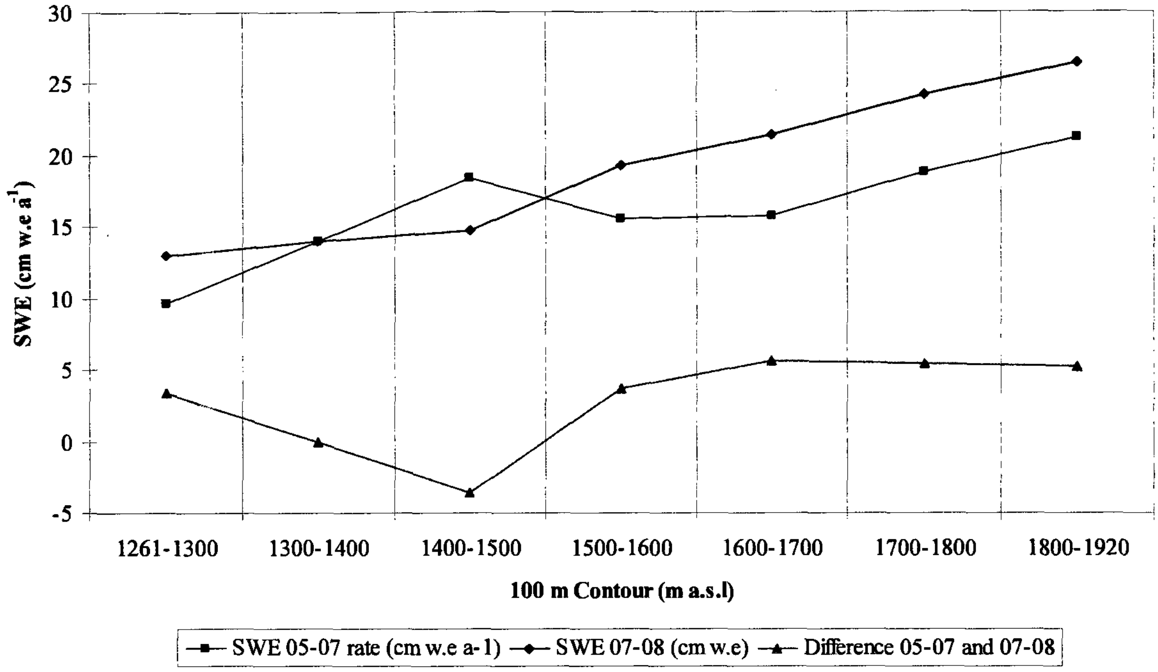

total snowfall amounts are comparable between years, the difference in values mainly relates to the fact that the 2005-7 series had undergone summer melt processes, whereas the winter 2007-8 series had not. There is a higher rate of SWE increase in the winter series between 1400 and 1900 m a.s.l when compared with the average annual accumulation rate. The largest change in SWE between the winter and the average annual rate occurs between 1500 to 1900 m a.s.l., suggesting that melt processes combined with wind redistribution removes ~0.03 m w.e. a^{-1} from each 100 m elevation contour in this range.

3.4.6 Comparison between GPR derived snow depths and borehole records

Validation of the characteristics of the LSS-05 and LSS-07 layers is made possible by combining the GPR record with visual stratigraphy of core sections and the high resolution neutron probe borehole density measurements (Figs. 3.17-3.21). This is because density peaks in the neutron probe record correspond to annual changes in the snow pack caused by summer melt, while low densities relate to snow from the fall/winter. It is these density changes that provide the dominant control on dielectric discontinuities that are detected in the GPR record, and which allow layers to be tracked throughout the basin. Results are presented from 0.45 m to 3 m depth, in order of borehole surface elevation. The 0.45 m constant offset is used because the probe (1 m length) needed to be fully contained in the borehole to provide accurate measurements. The exception was BH-2, where density returns were only captured in the 4.90-6.30 m depth range due to technical problems (Fig. 3.17). This core's visual stratigraphy displayed ice throughout this depth range, and also from the surface to 6.30 m, which is expected given its location in the ablation zone. The neutron probe data from BH-2 showed variability at the decimeter scale, although densities ranged little between 584-691 kg m^{-3}, with a mean of 641 kg m^{-3}. Layers were not detected in the GPR profile at this depth.

Neutron density returns for BH-1 at 1390 m a.s.l. showed a high degree of variability from the surface to 3 m depth (Fig. 3.18). The LSS-07 is identified as a prominent density peak of ~720 kg m^{-3} in between 0.59-0.62 m depth, which correlates with the first layer found in the GPR profile. Densities are much lower from 0.62-1.10 m depth, except for a moderate peak between 0.90-1.00 m, which we interpret to be the 2006 summer melt surface. From 1.30-1.85 m depth the upper boundary of LSS-05 is clearly identifiable in both the neutron probe

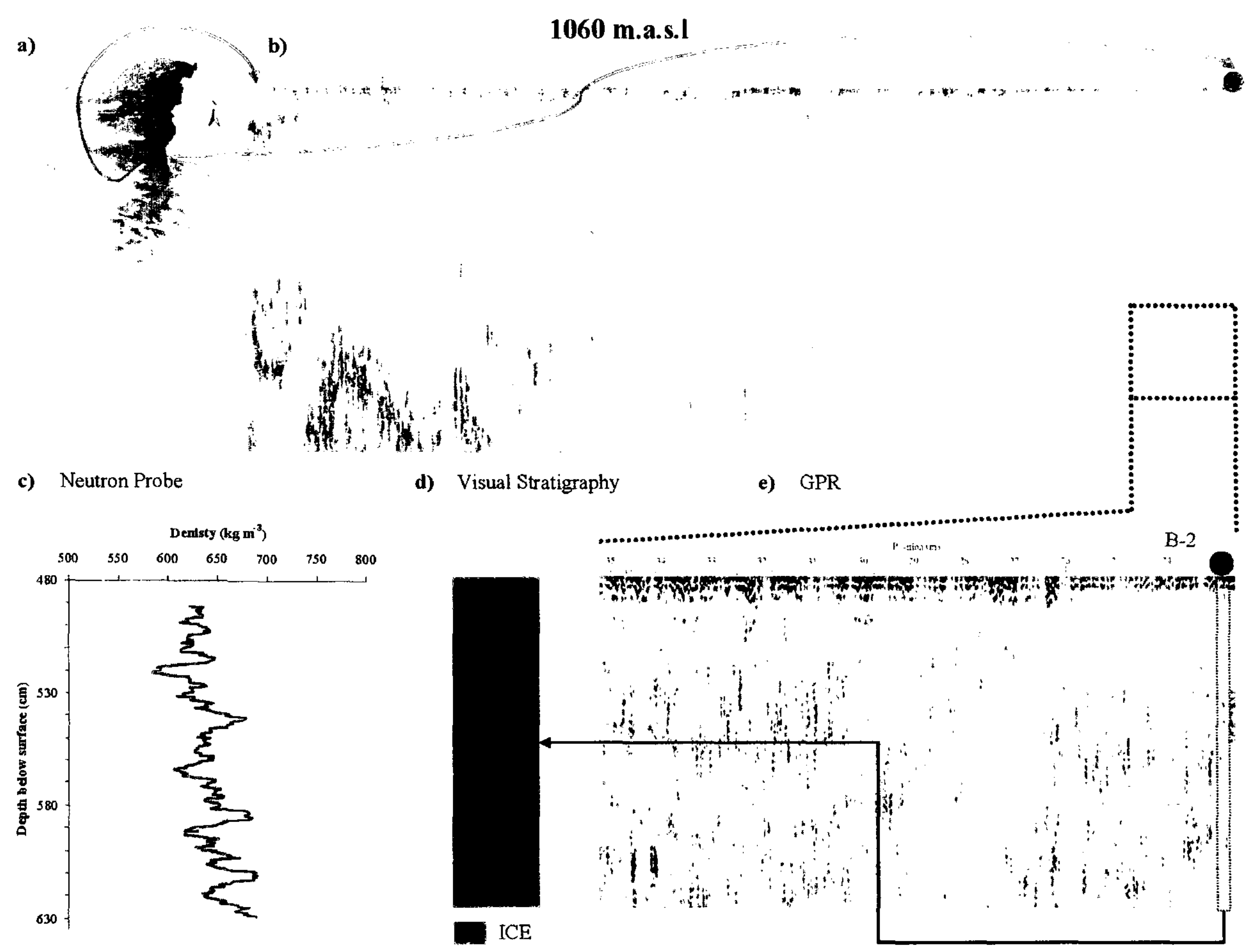

Figure 3.17. a) Borehole 2 (BH-2) at 1060 m indicated by green dot on inset map (Base image: Landsat 7, July 7, 2000); **b)** Upper panel GPR trace (~15 km by 7 m deep) with green dot on trace corresponding with the borehole location found on the inset map (arrows from the map to trace indicate start and end points of the trace); **c)** Visual core stratigraphy section for 4.90 – 6.30 m; **d)** High resolution neutron density probe data showing relationship between density (kg m^{-3}) and depth (4.90 – 6.30 m); **e)** Hatched square on upper panel indicates 1 km long GPR trace corresponding to the neutron density probe and visual stratigraphy depths.

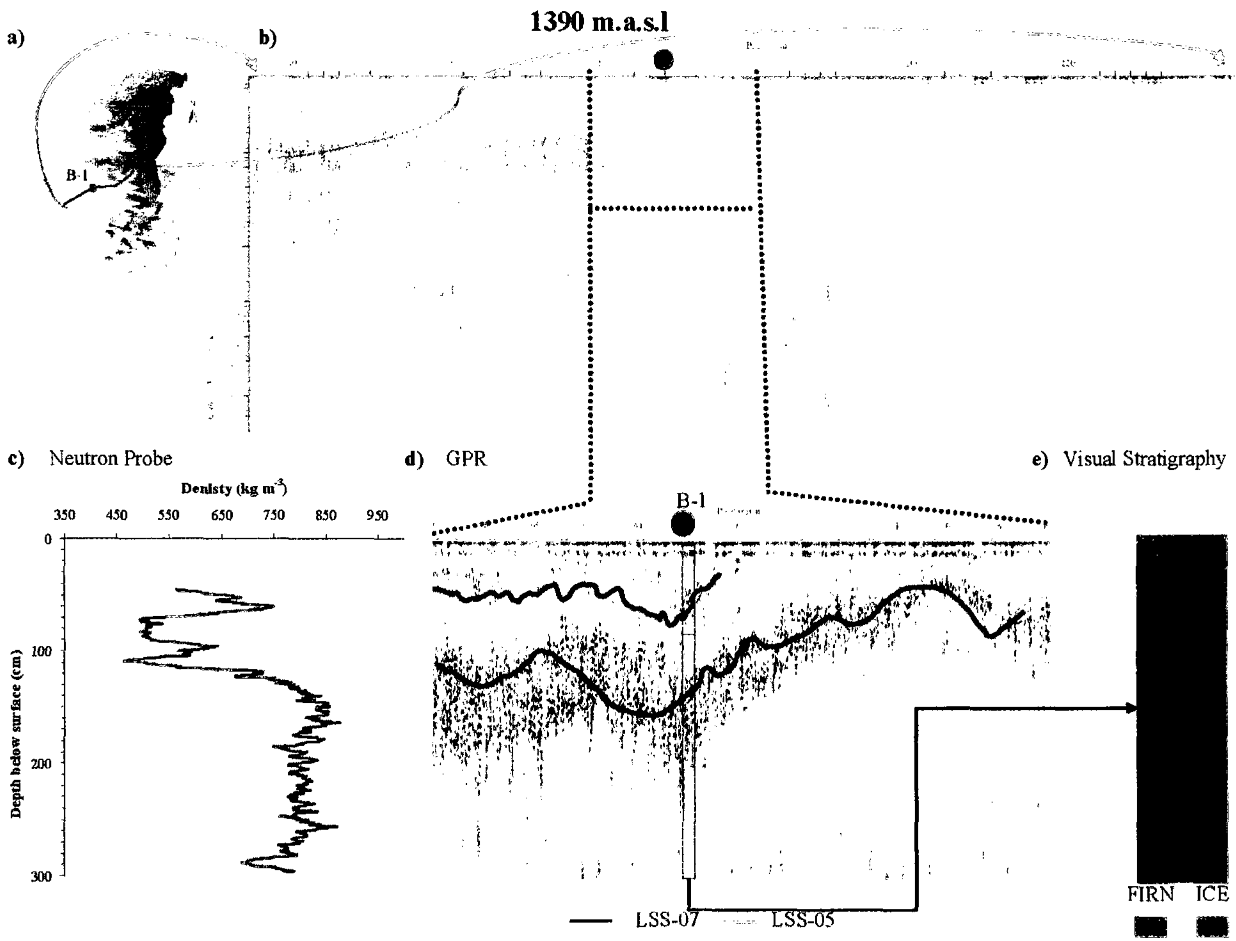

Figure 3.18 a) Borehole 1 (BH-1) at 1390 m indicated by green dot on inset map (Base image: Landsat 7, July 7, 2000); **b)** Upper panel GPR trace (~15 km by 7 m deep) with green dot on trace corresponding with BH-1 found on the inset map (arrows from the map to trace indicate start and end points of the trace); **c)** High resolution neutron density probe data showing density (kg m^{-3}) and depth (0.45 – 3.00 m) relationship; **d)** Visual core stratigraphy section for 0 – 3.00 m; **e)** Hatched square on upper panel indicates 1 km long GPR trace corresponding to the neutron density probe and visual stratigraphy depths.

and GPR profile, with the densities almost doubling from 450 to 825 kg m^{-3} across the upper part of this zone. High densities continue below this depth, with extensive ice lensing also found in this depth range in visual stratigraphy of this core section.

East of the main trunk of the glacier at BH-5 (1515 m a.s.l) densities increased rapidly from 400 to 550 kg m^{-3} at a depth of ~0.65 m (Fig. 3.19). This relates to the LSS-07 layer, which is clearly identified as a strong reflection in the GPR profile. The density peak is 0.07 m thick, which is approximately the same vertical distance between the upper highly reflective boundary and lower diffuse boundary of the first layer in the GPR data. These measurements also agree with ice layering found in the borehole visual stratigraphy at this depth. In the 0.94-1.30 m depth range of the neutron probe profile, the density increased sharply from 337 kg m^{-3} to 527 kg m^{-3}. At this core site, a second reflective layer in the GPR profile matches the depth of this density increase. The visual stratigraphy record at this depth shows a series of ice lenses of varying thickness. We infer this second reflection to be the 2006 LSS. Below this layer, the neutron probe record shows a third density peak, rising from 399 kg m^{-3} to 496 kg m^{-3} between 1.74-1.85 m depths. This peak is clearly related to a distinct reflector horizon in the GPR record at this depth, and corresponds well with ice lenses and layers in the visual stratigraphy record in this depth range. This 0.11 m thick layer of high density likely relates to the extreme 2005 melt year observed in QSCAT and ASIRAS records.

The greatest coherency between all field data was found at BH-3 (1640 m a.s.l.) in the percolation region of the basin (Fig. 3.20). The LSS-07 is clearly identified as a sharp peak of 502 kg m^{-3} to 532 kg m^{-3} in the density profile at the 0.45-0.50 m depth range. The density peak relates to a continuous band of high reflectivity in the GPR trace at the same depth. Manual snow probe measurements confirm that this is the depth associated with the LSS-07, which also agrees with ice layering found in the borehole visual stratigraphy. There is a moderate density peak from 0.80 to 0.95 m depth in the neutron probe record, which is likely associated with the weak 2006 summer melt season. A faint, but continuous, internal layer also appears at this depth in the GPR record, although no ice layers in the visual stratigraphy were recorded at this position. The neutron probe record shows the next prominent density peak at a depth between 1.05-1.40 m. Visual core stratigraphy of this section showed that ice

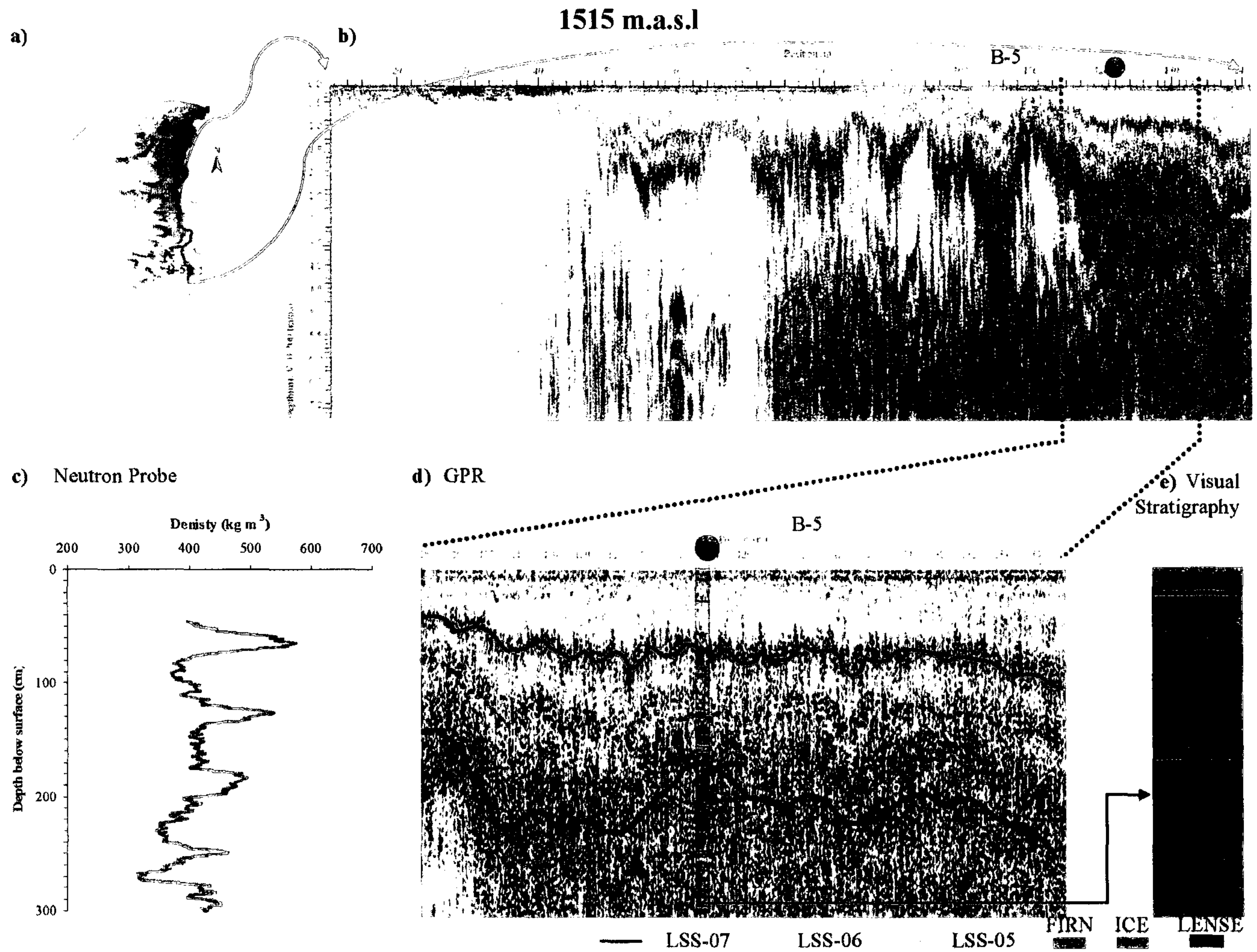

Figure 3.19. **a)** Borehole 5(BH-5) at 1515 m indicated by green dot on inset map (Base image: Landsat 7, July 7, 2000); **b)** Upper panel GPR trace (~15 km by 7 m deep) with green dot on trace corresponding with BH-1 found on the inset map (arrows from the map to trace indicate start and end points of the trace); **c)** High resolution neutron density probe data showing density (kg m^{-3}) and depth (0.45 – 3.00 m) relationship; **d)** Visual core stratigraphy section for 0 – 3.00 m; **e)** Hatched square on upper panel indicates 1 km long GPR trace corresponding to the neutron density probe and visual stratigraphy depths.

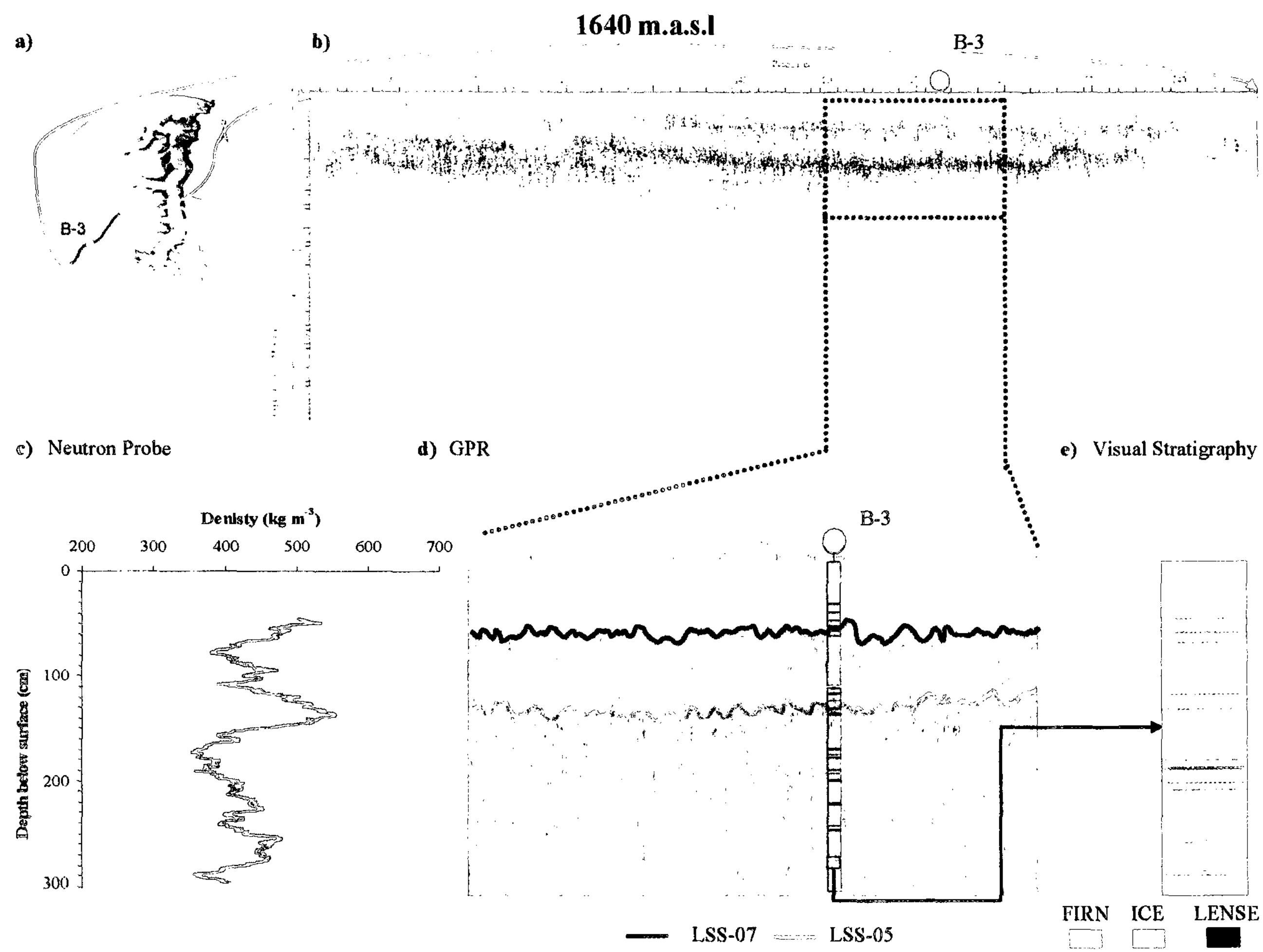

Figure 3.20.a) Borehole 3 (BH-1) at 1640 m indicated by green dot on inset map (Base image: Landsat 7, July 7, 2000); **b)** Upper panel GPR trace (~15 km by 7 m deep) with green dot on trace corresponding with BH-1 found on the inset map (arrows from the map to trace indicate start and end points of the trace); **c)** High resolution neutron density probe data showing density (kg m^{-3}) and depth (0.45 – 3.00 m) relationship; **d)** Visual core stratigraphy section for 0 – 3.00 m; **e)** Hatched square on upper panel indicates 1 km long GPR trace corresponding to the neutron density probe and visual stratigraphy depths.

layers and lenses were also present here. In the GPR record a thick band of high reflectivity backscatter at ~1.3 m is shown, which correlates well with the both high resolution density profiles and the visual stratigraphy. We take this layer to represent the LSS-05.

At BH-4 in the accumulation / percolation zone of the basin, there is similar coherency between GPR, high-resolution density profiles and visual stratigraphy records for both the LSS-07 and LSS-05 (Fig. 3.21). Both layers are clearly identified with sharp density peaks in the neutron probe data. Between 0.45 and 0.50 m depths the LSS-07 is represented by a marked density peak. A clear and continuous IRH is detected in the GPR record at this same depth, which was also confirmed by the snow pits and avalanche probe measurements at this location. The ice core record shows a few ice lenses in this depth range as indicated by black stripes in the visual stratigraphy. A second density peak occurs between 1.10-1.40 m in the neutron probe record and is shown as a second continuous IRH in the GPR trace. This is inferred to be the LSS-05. Neutron probe densities are high at 457-468 kg m^{-3} for some 0.30 m in relation to this layer, with a distinctive 0.30 m thick band of high reflection amplitudes also present in the GPR profile across this transect. The visual core record did not detect ice layering or lensing at these depths, although this is not particularly surprising since the density peaks in this core are the lowest in absolute value compared to any of the other cores. This reflects its high altitude location in the percolation/firn snow zone, and means that most density increases must be accommodated by internal snow densification rather than ice layer formation.

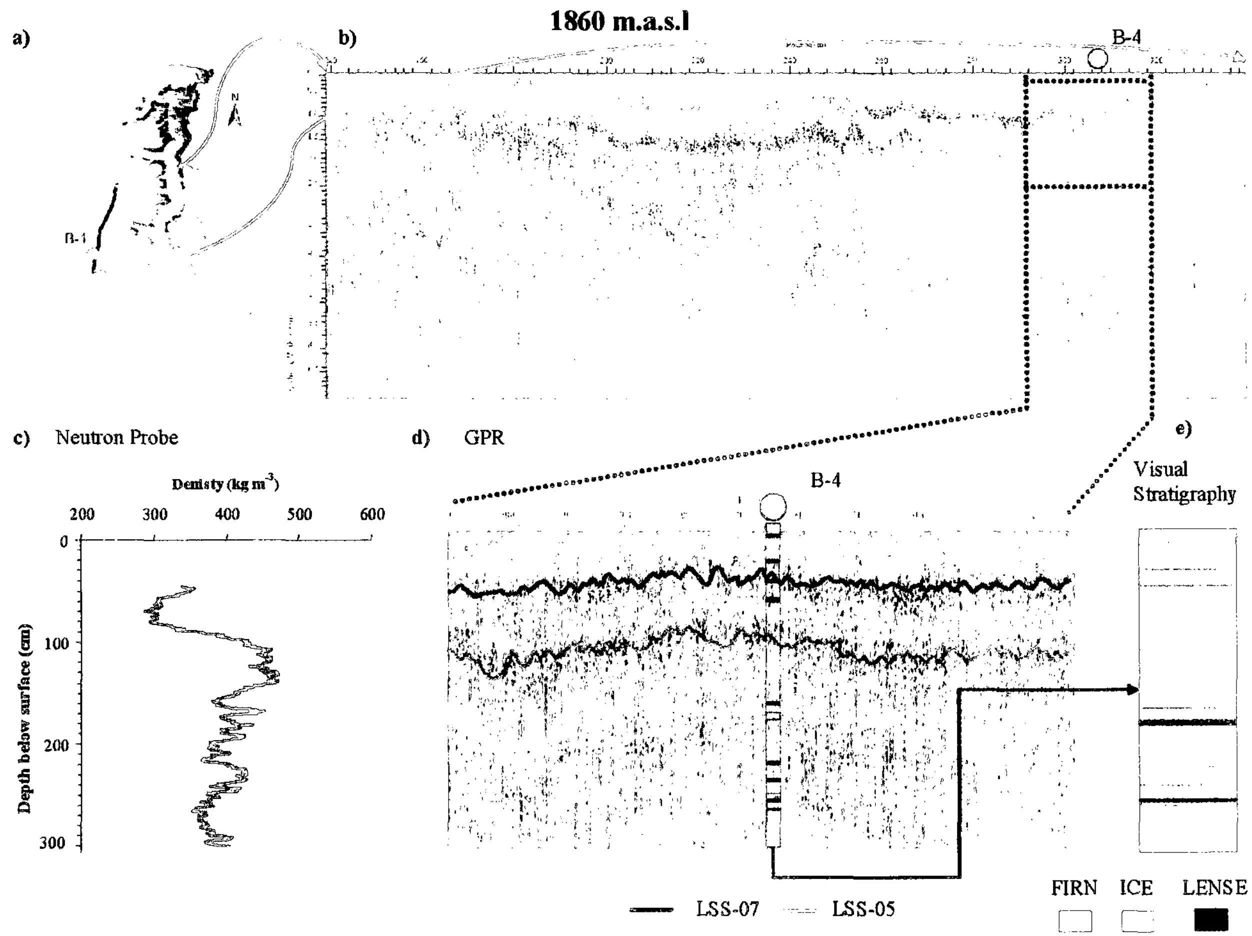

Figure 3.21. a) Borehole 4 (BH-1) at 1890 m indicated by green dot on inset map (Base image: Landsat 7, July 7, 2000); **b)** Upper panel GPR trace (~15 km by 7 m deep) with green dot on trace corresponding with BH-1 found on the inset map (arrows from the map to trace indicate start and end points of the trace); **c)** High resolution neutron density probe data showing density (kg m^{-3}) and depth (0.45 – 3.00 m) relationship; **d)** Visual core stratigraphy section for 0 – 3.00 m; **e)** Hatched square on upper panel indicates 1 km long GPR trace corresponding to the neutron density probe and visual stratigraphy depths.

3.4.7 Determination of glacier facies with GPR

High frequency GPR enables the identification of the snow line across the Belcher Glacier Basin. This is defined as the upper limit of the superimposed ice zone and separates firn from ice. The equilibrium line altitude (ELA) is below the location of the snow line, since it is the lower limit of the superimposed ice zone. In general, snow thickness above the LSS-07 decreases from the accumulation area towards the ablation zone, as shown in Figure 3.22. This is demonstrated by two distinct layers emerging at the surface in the central, eastern and western parts of the Belcher Glacier basin (Fig. 3.23). These layers rise to the surface in the GPR traces (Fig. 3.24 a) at elevations between 1260 and 1300 m a.s.l (Fig. 3.23 b-d). At elevations <1260 m a.s.l. the first layer (i.e. LSS-07) can be seen intermittently, although the snow depths can still be determined. The second layer (LSS-05), or any deeper ones, cannot be tracked at elevations <1260 m a.s.l. The LSS-05 and deeper layers rise at a steep angle to the surface here and become cut off between 1260 to 1300 m a.s.l (Fig. 3.23 b-d). This indicates the zone of net snow gain, with net accumulation below this altitude due to superimposed ice. GPR transects which cross the location where internal accumulation layers rise to the surface are able to provide point positions of the snow line. Using this method, the snow line in the Belcher Glacier basin occurs between ~1260-1300 m a.s.l., with contour lines drawn to connect between known points (green contour in Fig. 3.23 a).

Using the GPR traces it is possible to map out glacier facies distribution. The superimposed ice, snow line, and percolation facies (i.e. >1260 m a.s.l.) are mainly composed of a firn/snow matrix and detected by high backscatter in GPR records (Fig. 3.23 b-d). Decimeter scale variations in near surface density in the upper part of the accumulation zone causes the GPR signal to be reflected and attenuated at the multiple interfaces between compacted firn, ice lenses and snow. The contrast in density between each of these materials produces a series of dielectric discontinuities leading to noisy and high backscatter in the GPR returns in the accumulation region. There is a dramatic difference in radar returns at lower elevations in the ablation and superimposed ice zones (i.e. <1260 m a.s.l.), as these areas coincide with areas of low backscatter (Fig. 3.23 b-d). The solid ice in these areas is almost transparent to the GPR wave, with few internal discontinuities and therefore few internal radar reflections. The location of the transition between firn and ice facies is clear in the GPR profiles in the

Figure 3.22 500 MHz GPR line (16 km by 5.5 m deep) in the accumulation area (1350 – 1780 m a.s.l.) with elevation data superimposed on GPR trace; inset map showing location of May 25 Line00 profile (Base Image; Landsat 7, June 7, 2000).

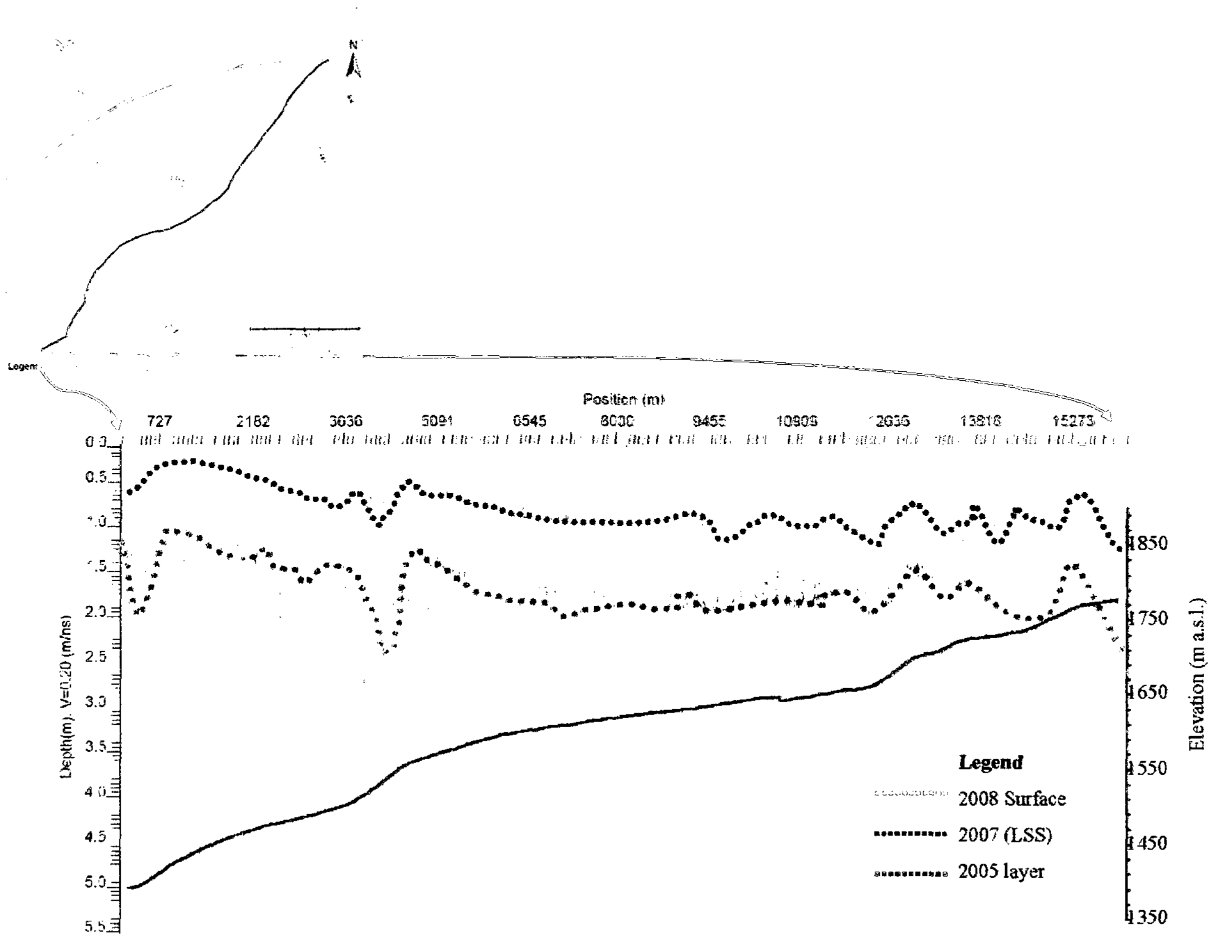

Figure 3.23. a) Inset map showing point locations (orange dots) of snow line derived from 500 MHz GPR lines; green line connects snow line positions based between 1250 to 1300 m a.s.l contour indicating position of snow line across the Belcher Basin (Base Image; Landsat 7, June 7, 2000); **b)** 500 MHz GPR trace ~23 km by 5.5 m deep; snow line found at 1275 m a.s.l **c)** 500 MHz GPR line collected on ~8.5 km by 5.5 m deep; snow line found at 1264 m a.s.l **d)** 500 MHz GPR line collected ~ 24 km by 5.5 m deep; snow line found at 1271 m a.s.l;

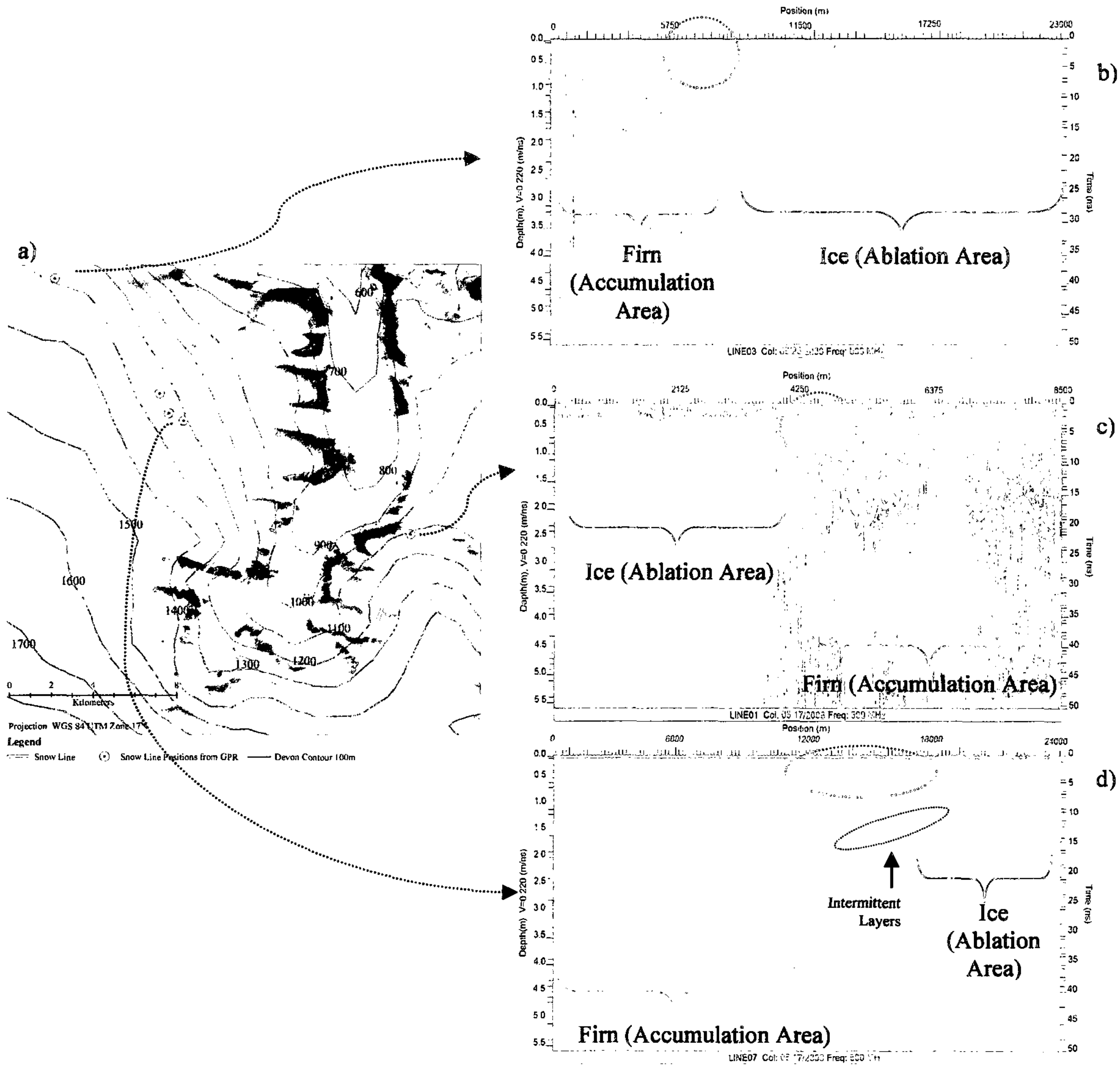

central, eastern and western areas of the Belcher Glacier basin. Dunse *et al.* (2009) on the Austfonna Ice Cap, Svalbard showed GPR traces in the ablation facies with characteristic low reflection amplitudes and little radar attenuation, while the transition between the superimposed ice and percolation facies composed of a mixture of firn snow and ice layers showed significantly higher and noisier returns. GPR traces in the Belcher Basin compare well with this previous study.

3.5.0 Discussion and Conclusions

3.5.1 Age-Depth Relationships and GPR

Density contrasts in the near surface (0-5 m) firn provide the dominant cause of reflections in the GPR signal between 1000–1900 m a.s.l in the Belcher Glacier basin. Distinctive high density layers observable in high frequency GPR records in the upper 3 m of the snow pack in May 2008 were related to previous year melt records. The near surface (<1 m) reflector in our GPR traces equates to the melt event corresponding to the last summer (2007) surface. The layer is clearly shown across the basin as a band of high reflectivity with a distinct highly reflective upper boundary and diffuse lower boundary (Dunse *et al.* 2008). The strong density contrast between the less dense snow accumulated during the 2008 winter on top of the LSS-07 ice lense has enabled the basin-wide snow depth to be quantified and mapped (Fig. 3.11). The depth of winter snow determined by GPR agrees well with manual point measurements observed in avalanche probe data (Fig. 3.10), and high resolution neutron density probe records (Figs. 3.17-3.21).

This study has shown that high-frequency GPR is both highly effective and successful at providing detailed winter snow depths across large distances and broad elevation ranges in a basin by accurately defining information between sites. This technique provides a method to fill in substantial data gaps between sparse point measurements.

Across the entire elevation range of the Belcher Glacier basin, above average summer temperatures in 2005 led to extreme ice layer formation, as shown in both QSCAT (Fig. 3.12) and ASIRAS (Fig. 3.13) records. In the GPR record, a thick high density layer in the 1 to 2 m depth range is likely related to the protracted summer melt season of 2005 (Fig. 3.22).

A wetting front produced during summer 2005 enabled deeper penetration of percolating meltwater in the near surface snow pack, whereupon refreezing produced a thick high density layer. As winter snow accumulated and buried the 2005 melt layer, it maintained its refrozen summer characteristics, which enables the depth of winter snow for 2005-7 to be determined across the basin. The depth of the LSS-05 layer is validated by high resolution neutron density records, visual stratigraphy of core sections, and confirmed by ASIRAS overflights in April/May 2006. The 2005-7 SWE data represents snow accumulation which has been metamorphosed by meltwater percolation over a two year melt cycle, whereas winter snow accumulated above the LSS-07 has not yet undergone melt processes.

Unusual melt conditions or rainy events can also complicate the apparent results and interpretation of the causes of the LSS-05 layer. A major rain event of ~3.8 cm occurred over Devon Ice Cap in August 2006, which likely caused water to percolate and pooled above the 2005 melt layer (Sharp, personal communication, 2009). The refreezing of this percolated meltwater would then enhance the expression of the 2005 IRH in the GPR traces. Overall, summer 2006 was not a well-defined melt season, however, which means that it is not easily identifiable in the GPR traces and neutron probe record. Consequently, unusual rain events in an otherwise cool summer such as 2006 may mean that in particular years a direct link between internal ice layer formation and summer conditions is too simplistic.

Successfully determining the depth to the distinctive LSS-05 using high frequency GPR shows that this technique is also feasible at determining multi-year sequences of snow depth in the presence of strong melt years. Quantifying long term variability of snow using GPR can also help to address significant gaps in understanding climatic changes in Northern Canada, since the region is characterized by sparse meteorological data. Variations in snow depth represent a good interannual proxy for climate changes in the QEI, since it is one of the most highly variable cryospheric variables (ACIA, 2004).

The greatest coherency between GPR transects, high resolution density records and visual core stratigraphy was found in moderate to upper altitude ranges of the basin (1600-1900 m a.s.l) near BH-3 (1640 m a.s.l) and BH-4 (1840 m a.s.l) (Figs. 3.20 and 3.21). This relates to the fact that higher elevations annually contain a mixture of ice and snow, with the proportion of each depending on temperature conditions during the summer. The patterns are particularly distinctive at these elevations because these regions tend to only experience melt in the warmest part of the summer. QSCAT records suggest that snow pack conditions during the 2005 melt year resemble those in the wet snow zone rather than the percolation zone across the entire elevation range of the Devon Ice Cap (Wolken *et al.* 2009). Very warm years like 2005 and 2007 with a pervasive melting front producing large volumes of meltwater generate broad peaks in the neutron probe record, and distinct IRHs in the GPR record which can be followed between traces. Colder summers such as 2006 have less expression in these records due to minimal melt and reduced density increases at these elevations.

3.5.2 Control Factors

The SPOT DEM has enabled the quantitative determination of slope angle, profile curvature, planform curvature, north-south scalar aspect and east-west scalar aspect for the entire Belcher Basin in ArcMap 9.0 GIS software. SWE is affected by the same terrain control factors for both the 2007-8 winter and the 2005-7 annual data sets, although the relationships for the 2005-7 data are lower than for the 2007-8 data. This likely due to the influence of summer melt processes reducing the impact of topographic variation on accumulation. The eigenvalues for both time series show that PC1 is the most important factor in controlling SWE patterns across the Belcher Glacier basin. This is an elevation, slope angle, and northerly aspect factor, with SWE increasing as altitudes increase and slope angles decline, which leads to greatest snow depths in the upper, gently sloping regions of the basin. These slopes are predominantly north facing, in the direction of the NOW Polynya moisture source.

Elevation has previously been recognized as an important influence on variations in snow depth distribution for the Devon Ice cap and QEI. For example, Mair *et al.* (2005) and Colgan *et al.* (2008) highlight the influence of elevation in their studies in the North West, summit and south east regions of the ice cap. The reason for increasing SWE with elevation relates to the forced mechanical lifting of air (Elder *et al.* 1991), on the predominantly north facing slopes of the Belcher. Air masses originating from the NOW Polynya moisture source ascend from lower elevations in the north towards the south, causing the rising column of air to cool, condense and form precipitation as elevations increase. The lower snow thicknesses found on steeper slopes was expected as these slopes tend to retain less snow due to wind scouring, with redeposition on slopes with gentle angles. In addition, Figs. 3.8 b and 3.9 b both show high slope angles are more characteristic in the lower reaches of the basin, while slope angles tend to be low in the upper elevations of the basin.

The significance of PC-2 showed that SWE values are higher in concave areas such as gullies. Wind flow speeds up over convex ridges, leading to pronounced surface scouring and redistribution as slope angles increase down-slope, while wind diverges slowing down in surface depressions. This causes greater snow depths in concave hollows at the base of slopes. The pattern for the 2005-7 data set and 2007-8 datasets combined with field observations imply concave features enhance SWE depth locally.

Maps of 2007 – 2008 winter SWE (Fig. 3.11) and 2005 – 2007 multiyear SWE (Fig. 3.14) showed that snow distribution is largely controlled by distance from the moisture source as indicated by east-west scalar aspect data. Although PC3 is an east-west scalar aspect component in both the winter and multi-year period, the effect of this component on SWE distribution is notably different. Higher winter SWE values are significantly positively correlated in the western part of the basin when compared with the east. This is because the western part of the basin mainly faces the easterly direction and likely relates to the fact that more transect sampling was done in the west. Eastern transects also never exceed 1700 m, while western transects consistently showed the largest average winter SWE values above 1700-1920 m in the southwest part of the basin. The multi-year period (2005 – 2007) shows SWE is more positively related in the eastern part of the basin with more westerly facing aspects. During the melt season, warm air masses would have a greater effect in the east than the west, since the east is closer and more directly influenced by the warm moisture source. Wang *et al.* (2005) suggest that ice cap margins facing Baffin Bay have significantly longer melt season durations than margins facing the interior of the QEI. Our results explain this as well, since the more maritime eastern region of the basin would be under a greater influence of summer melt and for longer durations when compared with the west.

3.5.3 Snowline and Facies identification using GPR

Approximate locations and transitions between of the ablation, superimposed ice, snowline and percolation zones in the Belcher Glacier basin is made possible by observing distinct radar return patterns in the GPR record. Rising layers which are cut-off at distinct altitudes are taken to represent the location of the snow line. The superimposed ice zone lies below this. Since the snowline is not a fixed altitude, but rather crosses a range of altitudes depending on the intensity and duration of the melt season, it is quite possible the long-term snowline could extend below the superimposed ice zone in some years. This is evident in the GPR returns as intermittent layers are observed beyond the positions of the rising 2005 and 2007 LSS layers (Fig. 3.23 d black oval). Dunse *et al.* (2009) on Austfonna Ice Cap, Svalbard, showed the ELA lowered up to 250 m on some parts of this ice cap between 2003 and 2006 combined with a lateral expansion of the firn area of up to 13.3 km over the same period.

For the Belcher Basin, the superimposed ice facies likely extends into the wet snow zone / percolation facies to ~ 1450 m a.s.l. Burgess and Sharp (2008) using aerial photography and field observations revealed a system of meltwater channels that begin at 1500 m a.s.l and terminate in crevasse fields and moulins at lower elevations. Surface meltwater in these channels at the end of the summer melt season would refreeze on the surface at the end of summer, causing a series of thick ice layers, lenses and ice glands of high density in this region. Consequently, the GPR record tends to be cluttered by noisy returns at 1260-1450 m altitudes. These findings suggest the importance of superimposed ice formation in the Belcher Basin.

The upper limit of the superimposed ice facies, defined as the snow line, marks the lower boundary of the percolation facies. Using GPR, we show the wet snow / percolation facies extending from ~1450 m towards the ice cap summit at ~1920 m in the southwest part of the Belcher Glacier basin. As snow reaches isothermal (0^{o}C) temperatures during the warmest part of the summer, surface meltwater infiltrates within the snowpack and refreezes at the end of the melt season (Paterson, 1994). The mixture of both wet and dry snow clearly produces a series of dielectric discontinuities leading to noisy high backscatter in the GPR record. Layering is also more distinct in this zone, since at higher altitudes the magnitude and duration of the melt season is not as severe when compared with the ELA / superimposed ice region of the basin.

Similar to the Dunse *et al.* (2009) study on Austfonna Ice Cap, we show that high frequency GPR is an effective way to identify and approximate glacier facies for the Belcher Basin on Devon Ice Cap. The locations and transitions between zones are identifiable due to distinct dielectric and density contrasts of ice, snow, and firn which produce characteristic signal reflection patterns using high frequency GPR.

3.5.4 Comparisons with previous studies on Devon Ice Cap

The average annual accumulation rate and mass balance at each elevation contour found in this study is in good agreement with past work on the Devon Ice Cap (Fig. 3.15 and Table 3.5). For example, Mair *et al.* (2005) used down borehole gamma spectrometry techniques to estimate ice cap wide mass balance and accumulation for the 1963-2000 period at similar elevation contours as this study. Near the summit (>1900 m a.s.l,), they calculated an average annual accumulation rate of 0.24 m w.e a^{-1}. The average annual accumulation rate derived via GPR showed a rate of 0.212 m w.e. a^{-1} for 2005 – 2007 for 1800-1920 m. For the 1300-1400 m a.s.l, 1500-1600 m, and 1600-1700 m ranges we determined rates of 0.141 m w.e. a^{-1}, 0.155 m w.e a^{-1}, and 0.157 m w.e. a^{-1} respectively. For these same elevations bands in the northern basins of the Devon Ice Cap, Mair *et al.* (2005) showed 1963 – 2000 average accumulation rates of 0.128 m w.e a^{-1}, 0.138 m w.e. a^{-1}, and 0.159 m w.e a^{-1}. These findings also agree with the study of Colgan *et al.* (2008), which used point measurement techniques to show that the northern basins of Devon Ice Cap experience average annual accumulation rates of 0.19 m w.e. $a\text{-}^{1}$.

The consistency between the findings of this study and others suggests that derivation of the average annual accumulation rate using high frequency GPR is both accurate and well defined. Furthermore, this assessment reveals that the more recent (2005-7) average annual accumulation rate across the Belcher Glacier basin hasn't changed significantly compared to the long-term 1963-2000 rates reported by Mair *et al.* (2005). These findings are also supported by Koerner's (1977) climate-stratigraphic study based on ice cores from Sverdrup Basin in the northeast sector of the ice cap, which showed that average annual accumulation rates in the upper elevation regions between 1600 and 1800 m a.s.l vary very little, and that summer melt governs mass balance patterns for this elevation range.

Table 3.5. Comparisons between average annual accumulation rates (cm w.e. a^{-1}) with previous Devon Ice Cap Studies

Elevation Contour (m a.s.l)	GPR (2005 – 2007) (Mean ± S.D.)	Mair *et al.* 2005 (1963 – 2000)	Colgan *et al.* 2008 (1963 – 2003)	Koerner (1977)
1200 – 1300	9.70 ± 6.5			
1300 – 1400	14.05 ± 8	12.80		
1400 – 1500	18.33 ± 5.7	21.80		
1500 – 1600	15.55 ± 4.7	13.80		
1600 – 1700	15.71 ± 4.1	15.90		
1700 – 1800	18.74 ± 4.9			
1800 – 1900	21.20 ± 6	24.10	19.00	22

Chapter 4

4.0 Conclusions

In this study high frequency 500 MHz GPR measurements were analyzed from ~306 km of skidoo surveys in the Belcher Glacier basin in May 2008. The distinct characteristics of the GPR record from the surface to 3 m depth were related to the 2007 and 2005 summer surfaces. GPR derived depths to these surfaces and the assessment of the average annual accumulation rate across this basin correlate well with previous snow accumulation assessments in other parts of Devon Ice Cap (Mair *et al.* 2005, Colgan *et al.* 2008 and Koerner 1977). The complex radar returns in the LSS-05 depth range are clearly related to extensive melt processes during summer 2005 which produced large quantities of meltwater at all elevations on Devon Ice Cap. Evidence for this is provided by NCEP-NCAR climate reanalysis, QSCAT satellite records, airborne ASIRAS data, and in situ neutron density probe records. The results of this study underscore the importance of strong melt years and their impact on near surface density patterns.

Unlike previous studies which have relied on point measures and interpolation techniques to determine snow depth on Devon Ice Cap (e.g., Mair et. al, 2005; Colgan and Sharp, 2008), this study used high frequency GPR to directly measure snow depths along continuous transects. These measurements have enabled a detailed quantification of SWE for an entire high arctic glacier basin. Continuous snow depth coverage provided across transects ranging from 1000-1900 m a.s.l significantly improves upon traditional snow depth measurements using point data. The potential of GPR as a snow depth measurement technique is clearly demonstrated in this study by relating point measurements separated by several kilometers, and accurately expanding the physical characteristics at these points across large distances. Inputs here will benefit future modeling efforts which will focus on mass balance, hydrological and velocity patterns at Belcher Glacier in response to current and predicted climate warming. This study provides spatially comprehensive snow depth information and quantifies the control factors which affect this variability. Furthermore, this study proves that high frequency GPR can be used as an effective and accurate technique to determine snow depths for not only annual periods, but also for multi-year periods.

Results show that the main factor in controlling snow depth variability across the Belcher Glacier basin is elevation. A characteristic elevation-accumulation relationship is revealed in both SWE maps for 2005-7 and 2007-8, and quantified by using principal component analysis of terrain factors. Abrupt irregularities in topography, such as the interchange between surface ridges and gullies combined with wind redistribution processes play an important role in determining local snow depth variability. This is shown by the high degree of spatial variability across GPR transects and supported by principal component 2. This study also showed the impact of the moisture source area on determining snow depths in the Belcher Basin via east-west scalar aspect data for both annual and multi-year periods. Terrain analysis provides useful insights into both small and broad scale features affecting the accumulation in the Belcher Basin. This information is crucial to understand to enable proper extrapolation of point measurements, and to provide accurate inputs for hydrological and mass balance models.

The use of high frequency GPR has also enabled the evaluation of glacier facies/zones across the Belcher Basin. The approximation of the basin-wide snow line is made possible by identifying layers which emerge at the surface in the central, western and eastern parts of the basin. The specific radar backscatter properties relating to contrasts in density between facies is distinct when analyzing GPR traces which cover broad elevation ranges. The importance of the superimposed ice zone as an intermediary transition between the ablation and percolation facies is verified with GPR.

This study is thus of interest to not only the glaciological community, but also for both climate and water resource management purposes. Climatically this study clearly demonstrates that quantifying the spatial variability in snow on a high arctic glacier can provide insights into the recent melt and refreezing history of the ice cap. Although the QEI region is characterized by sparse meteorological information, this study shows that high frequency GPR can be used to derive detailed continuous information with regards to snow accumulation and thus climate, for both annual and multi-year periods.

References

Aguado, E., 1990. Elevational and latitudinal patterns of snow accumulation departures from normal in the Sierra Nevada. *Theoretical & Applied Climatology,* **42**(3), 177-185.

Annan, A.P. 2002. GPR – History, Trends, and Future Developments. *Subsurface Sensing Technologies and Applications* **3** (4), 253 – 270

Anschütz, H., Steinhage, D., Eisen, O., Oerter, H., Horwath, M. and Ruth, U., 2008. Small-scale spatio-temporal characteristics of accumulation rates in western Dronning Maud Land, Antarctica. *Journal of Glaciology*, **54**(185), 315-323.

Arctic Climate Impact Assessment (ACIA). 2004. Impacts of a Warming Arctic. Cambridge University Press, New York, New York ACIA (2004). Scientific Report.

Arnold, N.S. and Rees, W.G., 2004. Self-similarity in glacier surface characteristics. Journal of Glaciology, **49**(167), 547-554.

Bell, C., Mair, D., Burgess, D., Sharp, M., Demuth, M., Cawkwell, F., Bingham, R. and Wadham, J., 2008. Spatial and temporal variability in the snowpack of a High Arctic ice cap: Implications for mass-change measurements. *Annals of Glaciology*, **48**, 159-170.

Benn, D.I., and Evans, D.J., 1998. Glaciers and Glaciation. Hodder Arnold Publication.

Benson, C.S, 1960. Stratigraphic Studies in the Snow and Firn of the Greenland Ice Sheet. Doctor of Philosophy Degree Thesis. California Institute of Technology, Pasadena, California.

Bingham, R.G., Hubbard, A.L., Nienow, P.W. and Sharp, M.J., 2008. An investigation into the mechanisms controlling seasonal speedup events at a High Arctic glacier. *Journal of Geophysical Research F: Earth Surface*, **113**(2).

Blöschl, G. and Kirnbauer, R., 1992. An analysis of snow cover patterns in a small alpine catchment. *Hydrological Processes*, **6**(1), 99-109.

Blöschl, G., Kirnbauer, R. and Gutknecht, D., 1991. A spatially distributed snowmelt model for application in alpine terrain. Snow, hydrology and forests in high alpine areas. Proc.symposium Vienna, 1991, 51-60.

Boon, S., Sharp, M. and Nienow, P., 2003. Impact of an extreme melt event on the runoff and hydrology of a high Arctic glacier. *Hydrological Processes,* **17**(6), 1051-1072.

Braun, C., Hardy, D.R. and Bradley, R.S., 2004. Mass balance and area changes of four high arctic plateau ice caps, 1959-2002. *Geografiska Annaler, Series A: Physical Geography,* **86**(1), 43-52.

Burgess, D. and Sharp, M.J., 2008. Recent changes in thickness of the Devon Island ice cap, *Canada. Journal of Geophysical Research B: Solid Earth,* **113**(7).

Burgess, D.O. and Sharp, M.J., 2004. Recent changes in areal extent of the Devon Ice Cap, Nunavut, Canada. *Arctic, Antarctic, and Alpine Research,* **36**(2), 261-271.

Burgess, D.O., Sharp, M.J., Mair, D.W.F., Dowdeswell, J.A. and Benham, T.J., 2005. Flow dynamics and iceberg calving rates of Devon Ice Cap, Nunavut, Canada. *Journal of Glaciology,* **51**(173), 219-230.

Colgan, W., Davis, J. and Sharp, M., 2008. Is the high-elevation region of Devon Ice Cap thickening? *Journal of Glaciology,* **54**(186), 428-436.

Colgan, W. and Sharp, M., 2008. Combined oceanic and atmospheric influences on net accumulation on Devon ice cap, Nunavut, Canada. *Journal of Glaciology,* **54**(184), 28-40.

Copland, L. 1998. The use of terrain analysis in the evaluation of snow cover over an alpine glacier. Landform Monitoring, Modelling and Analysis, 385-404. Wiley, New York

Copland, L., Mueller, D.R. and Weir, L., 2007. Rapid loss of the Ayles Ice Shelf, Ellesmere Island, Canada. *Geophysical Research Letters,* **34**(21), 1-6.

Copland, L., Sharp, M.J., Nienow, P. and Bingham, R.G., 2003. The distribution of basal motion beneath a High Arctic polythermal glacier. *Journal of Glaciology,* **49**(166), 407-414.

Deems, J.S., Fassnacht, S.R. and Elder, K.J., 2006. Fractal distribution of snow depth from lidar data. *Journal of Hydrometeorology,* **7**(2), 285-297.

Demuth, M.N., and Pietroniro, A., 2007. Climate Change Impacts on Canadian Glaciers: Why Worry? Workshop on Adapting to Water Supply Issues in a Changing Climate: Earth Science Contributions.

Demuth, M.N., Marshall, H-P., Morris, E.M., 2007. High-Resolution Near-Surface Snow Stratigraphy Inferred From Ground-Based 8-18 GHz FMCW Radar Measurements: Devon Ice Cap, Nunavut, Canada 2005-06, Cryosat Validation Experiment. *64th Eastern Snow Conference.* St. John's Newfoundland, Canada, 2007.

Dowdeswell, E.K., Dowdeswell, J.A. and Cawkwell, F., 2007. On the glaciers of Bylot Island, Nunavut, Arctic Canada. *Arctic, Antarctic, and Alpine Research,* **39**(3), 402-411.

Dowdeswell, J.A., Hagen, J.O., Bjornsson, H., Glazovsky, A.F., Harrison, W.D., Holmlund, P., Jainia, J., Koerner, R.M., Lefauconnier, B., Omanney, C.S.L. and Thomas, R.H., 1997. The Mass Balance of Circum-Arctic Glaciers and Recent Climate Change. *Quaternary Research,* **48**(1), 1-14.

Dunse, T., Eisen, O., Helm, V., Rack, W., Steinhage, D. and Parry, V., 2008. Characteristics and small-scale variability of GPR signals and their relation to snow accumulation in Greenland's percolation zone. *Journal of Glaciology*, **54**(185), 333-342.

Dunse, T., Schuler, T.V., Hagen, J.O., Eiken, T., Brandt, O. and Høgda, K.A., 2009. Recent fluctuations in the extent of the firn area of Austfonna, Svalbard, inferred from GPR. *Annals of Glaciology*, **50**(50), 155-162.

Elder, K., Dozier, J. and Michaelsen, J., 1991. Snow accumulation and distribution in an alpine watershed. *Water Resources Research*, **27**(7), 1541-1552.

Gardner, A.S., Sharp, Koerner, R.M., Labine, C., Boon, S., Marshall, S.J., Burgess, D.O., Lewis, D. 2009. Near-Surface Temperature Lapse Rates over Arctic Glaciers and Their Implications for Temperature Downscaling. *Journal of Climate.* **22**(16), 4281-4289.

Gray, L. and Burgess, D., 2009. Radar Results from the Devon Ice Cap. IASC-NAG – Kananasksis Country, Alberta. February 16, 2009

Gregoire, L., 2008. Cold Warriors. *Canadian Geographic.* October 2008, 128(5) – The Need to Be Cold.

Hagen J.O., Melvold, K., Pinglot, F. and Dowdeswell, J.A., 2003. On the net mass balance of the Glaciers and Ice Caps in Svalbard, Norwegian Arctic. *Arctic, Antarctic, and Alpine Research,* **35**(2), 264-270.

Hawley, R.L., Brandt, O., Morris, E.M., Kohler, J., Shepherd, A.P. and Wingham, D.J., 2008. Techniques for measuring high-resolution firn density profiles: Case study from Kongsvegen, Svalbard. *Journal of Glaciology,* **54**(186), 463-468.

Hawley, R.L. and Morris, E.M., 2006. Borehole optical stratigraphy and neutron-scattering density measurements at Summit, Greenland. *Journal of Glaciology*, **52**(179), 491-496.

Hawley, R.L., Morris, E.M., Cullen, R., Nixdorf, U., Shepherd, A.P. and Wingham, D.J., 2006. ASIRAS airborne radar resolves internal annual layers in the dry-snow zone of Greenland. *Geophysical Research Letters*, **33**(4).

Huss, M., Stöckli, R., Kappenberger, G. and Blatter, H., 2008. Temporal and spatial changes of Laika Glacier, Canadian Arctic, since 1959, inferred from satellite remote sensing and mass-balance modelling. *Journal of Glaciology*, **54**(188), 857-866.

IPCC. 2007. Climate Change 2007: The Physical Science Basis: Summary for Policy Makers: Contributions of Working Group I to the Fourth Assessment Report of the Intergovernmental Panel On Climate Changes, 5-10.

Irvine-Fynn, T.D.L., Moorman, B.J., Williams, J.L.M. and Walter, F.S.A., 2006. Seasonal changes in ground-penetrating radar signature observed at a polythermal glacier, Bylot Island, Canada. *Earth Surface Processes and Landforms*, **31**(7), 892-909.

Jiang, Q., 2003. Moist dynamics and orographic precipitation. *Tellus, Series A: Dynamic Meteorology and Oceanography*, **55**(4), 301-316.

Kattelmann, R. and Elder, K., 1993. Accumulation and ablation of snow cover in an alpine basin in the Sierra Nevada, USA. Snow and glacier hydrology.Proc.international symposium, Kathmandu, 1992, 297-307.

Koerner, R.M., 2005. Mass balance of glaciers in the Queen Elizabeth Islands, Nunavut, Canada. *Annals of Glaciology*, **42**, 417-423.

Koerner, R.M., 2002. Glaciers of the High Arctic islands. US Geological Survey Professional Paper, (1386 J), J111-J146.

Koerner, R.M. and Lundgaard, L., 1995. Glaciers and Global Warming. *Géographie Physique et Quaternaire*, **49** (3), 429 – 434.

Koerner, R. and Russell, R.D., 1979. Delta18O variations in snow on the Devon Island ice cap, Northwest Territories. *Canadian Journal of Earth Sciences*, **16**(7), 1419-1427.

Koerner, R.M., 1977. Devon Island ice cap: Core stratigraphy and paleoclimate. *Science*, **196**(4285), 15-18.

Kohler, J., Moore, J., Kennett, M., Engeset, R. and Elvehøy, H., 1997. Using ground-penetrating radar to image previous years' summer surfaces for mass-balance measurements. *Annals of Glaciology*, **24**, 355-360.

Kohler, J., Moore, J.C. and Isaksson, E., 2003. Comparison of modelled and observed responses of a glacier snowpack to ground-penetrating radar. *Annals of Glaciology*, **37**, 293-297.

Kovacs, A., Gow, A.J. and Morey, R.M., 1995. The in-situ dielectric constant of polar firn revisited. *Cold Regions Science and Technology*, **23**(3), 245-256.

Langley, K., Hamran, S.-., Høgda, K.A., Storvold, R., Brandt, O., Kohler, J. and Hagen, J.O., 2008. From glacier facies to SAR backscatter zones via GPR. IEEE Transactions on Geoscience and Remote Sensing, **46**(9), 2506-2516.

Lewkowicz, A.G., 2007. Dynamics of active-layer detachment failures, Fosheim Peninsula, Ellesmere Island, Nunavut, Canada. *Permafrost and Periglacial Processes*, **18**(1), 89-103.

Lundberg, A., Richardson-Näslund, C. and Andersson, C., 2006. Snow density variations: Consequences for ground-penetrating radar. *Hydrological Processes*, **20**(7), 1483-1495.

Mair, D., Burgess, D. and Sharp, M., 2005. Thirty-seven year mass balance of Devon Ice Cap, Nunavut, Canada, determined by shallow ice coring and melt modeling. Journal of *Geophysical Research F: Earth Surface*, **110**(1).

Maslanik, J.A., Fowler, C., Stroeve, J., Drobot, S., Zwally, J., Yi, D. and Emery, W., 2007. A younger, thinner Arctic ice cover: Increased potential for rapid, extensive sea-ice loss. *Geophysical Research Letters*, **34**(24),

Maurer, IV, J.A. 2006. Local-scale snow accumulation variability on the Greenland ice sheet from ground-penetrating radar (GPR). Master's thesis, University of Colorado at Boulder.

Morris, E.M. and Cooper, J.D., 2004. Instruments and methods density measurements in ice boreholes using neutron scattering. *Journal of Glaciology*, **49**(167), 599-604.

NASA., 2007. "Greenland's Ice Island Alarm." *NASA Earth Observatory.* 28 Aug 2007. NASA, Web. 15 Sep 2009. <http://earthobservatory.nasa.gov/Features/Greenland/>.

Pälli, A., Kohler, J.C., Isaksson, E., Moore, J.C., Pinglot, J.F., Pohjola, V.A. and Samuelsson, H., 2002. Spatial and temporal variability of snow accumulation using ground-penetrating radar and ice cores on a Svalbard glacier. *Journal of Glaciology*, **48**(162), 417-424.

Paterson, W.S.B. 1994. The physics of glaciers. 3rd edition. Pergamon, Oxford.

Parry, V., Nienow, P., Mair, D., Scott, J., Hubbard, B., Steffen, K. and Wingham, D., 2007. Investigations of meltwater refreezing and density variations in the snowpack and firn within the percolation zone of the Greenland ice sheet. *Annals of Glaciology*, **46**, 61-68.

Pinglot, J.F., J.O. Hagen, K. Melvold, T. Eiken, AND C. Vincent. 2001. A mean net accumulation pattern derived from radioactive layers and radar soundings on Austfonna, Nordaustlandet, Svalbard. *Journal of Glaciology*. **47**(159), 555-566.

Pinglot, J.F., Vaikmae, R.A., Kamiyama, K., Igarshi, M., Fritzche, D., Wilhelms, F., Koerner, R., Henderson, L., Isaksson, E., Winther, J., Van De Wal, R.S.W., Fournier, M., Bouisset, P. and Meijer, H.A.J., 2003. Ice cores from Arctic sub-polar glaciers: Chronology and post-depositional processes deduced from radioactivity measurements. *Journal of Glaciology*, **49**(164), 149-158.

Plewes, L, A., and Hubbard, B., 2001. A review of the use of radio-echo sounding in glaciology. *Progress in Physical Geography,* **25** (2), 203-236.

Prach, R.W. and Smith, A.R., 1992. Breeding distribution and numbers of black guillemots in Jones Sound, NWT. *Arctic,* **45**(2), 111-114.

Richardson-Näslund, C., 2004. Spatial characteristics of snow accumulation in Dronning Maud Land, Antarctica. *Global and Planetary Change*, **42**(1-4), 31-43.

Rignot, E. and Kanagaratnam, P., 2006. Changes in the velocity structure of the Greenland Ice Sheet. *Science,* **311**(5763), 986-990.

Roe, G.H., 2005. Orographic precipitation. *Annual Review of Earth and Planetary Sciences,* **33**, 645-671

Robertson, G.P. 2008. *GS+: Geostatistics for the Environmental Sciences.* Gamma Design Software, Plainwell, Michigan USA.

Sharp, M.J., 2009. Discussion on NCEP-NCAR Reanalysis Data for Devon Ice Cap for 2000-2009. [Letter] (Personal Communication, 10 June, 2009).

Shepherd, A., Du, Z., Benham, T.J., Dowdeswell, J.A. and Morris, E.M., 2007. Mass balance of Devon Ice Cap, Canadian Arctic. *Annals of Glaciology,* **46**, 249-254.

Smith, L. I. 2002. A tutorial on Principal Component Analysis. Cornell University, USA, 1 – 26

Sneed, W.A., Hooke, R.L. and Hamilton, G.S., 2008. Thinning of the south dome of Barnes Ice Cap, Arctic Canada, over the past two decades. *Geology,* **36**(1), 71-74.

Spikes, V.B., Hamilton, G.S., Arcone, S.A., Kaspari, S. and Mayewski, P.A., 2005. Variability in accumulation rates from GPR profiling on the West Antarctic plateau. *Annals of Glaciology*, **39**, 238-244.

Taurisano, A., Schuler, T.V., Hagen, J.O., Eiken, T., Loe, E., Melvold, K. and Kohler, J., 2007. The distribution of snow accumulation across the Austfonna ice cap, Svalbard: Direct measurements and modelling. *Polar Research*, **26**(1), 7-13.

Trenberth, K.E., Dai, A., Rasmussen, R.M. and Parsons, D.B., 2003. The changing character of precipitation. *Bulletin of the American Meteorological Society,* **84**(9), 1205-1217+1161.

Wang, L., Sharp, M.J., Rivard, B., Marshall, S. and Burgess, D., 2005. Melt season duration on Canadian Arctic ice caps, 2000-2004. *Geophysical Research Letters,* **32**(19), 1-4.

Winther, J.-G., O. Bruland, K. Sand, Å. Killingtveit, and D. Marechal 1998, Snow accumulation distribution on Spitsbergen, Svalbard, in 1997. *Polar Research.* **17**(2), 155-164.

Woo, M-k., Heron, R., Marsh, P., and Steer, P., 1983. Comparison of Weather Station Snowfall with Winter Snow Accumulation in High Arctic Basins. *Atmosphere-Ocean* **21**(3), 312 – 325.

Wolken, G.J., Sharp, M., Wang, L., In Press. Snow and ice facies variability and ice layer formation on Canadian Arctic ice caps, 1999 – 2005. *Journal of Geophysical Research – Earth Surface*

Zeverbergen, L. W., and C. R. Thorne. 1987. Quantitative Analysis of Land Surface Topography. *Earth Surface Processes and Landforms* **12**: 47–56.

Zwally, H.J., Abdalati, W., Herring, T., Larson, K., Saba, J. and Steffen, K., 2002. Surface melt-induced acceleration of Greenland ice-sheet flow. *Science,* **297**(5579), 218-222.

Appendix

A.1 Spatial Scales and Variability in Snow Depth

Snow depth measurements inferred via GPR picks (LSS-07, LSS-05) exhibit high spatial variability at both short and long (10^0 – 10^3 m) spatial scales in the basin. Semi-variograms were created to evaluate statistical properties and fractal behavior of the variability in snow depth of these scales (Arnold and Rees, 2003; Deems *et al.* 2006). Semi-variograms graph semivariance $\gamma(h)$ vs. separation distance (h) of measurements. Semivariance is an autocorrelation statistic i.e. measurements separated by less distance share more similarities than measurements further apart, defined as:

$$\gamma(h)=\frac{1}{2N(h)}\sum_{i=1}^{N(h)}\left[z_i - z_{i+h}\right]^2 \qquad \textit{(Eq. A1)}$$

where $\gamma(h)$ is the semivariance for interval distance h, z_i is the measured sample value at point i, z_{i+h} is the measured sample value at point $i+h$, and $N(h)$ is total number of sample couples for the lag interval h (Robertson, 2008). The curve of snow depth semivariance $\gamma(h)$ against separation h distance is composed of the sill and range, which can provide useful information about the spatial variability of the measured snow depth via GPR. The sill represents the maximum $\gamma(h)$ of depth at a particular separation h and demarks the transition of snow depth values which are not autocorrelated as h increases. Range parameter h_0, defines the separation distance h between short and long scale semi-variance (γ) in snow depth (Arnold and Rees, 2003; Robertson, 2008). Semivariogram plots were modeled using an exponential relationship of snow depths defined as:

$$\gamma(h)=C_0+C\left[1-\exp\left(-h/h_0\right)\right] \qquad \textit{(Eq. A2)}$$

where $\gamma(h)$ is the semivariance for interval distance h, h is the lag interval, C_0 is the nugget variance, C is the structural variance, and h_0 is the range. The strength of the variogram model is assessed based on the lowest value of the Residual Sums of Squares (RSS) which is fit to the variogram data (Robertson, 2008).

For analyzing basin-wide variance in snow depth for the 2007 - 2008 a maximum h of 4.2×10^3 m, corresponding to the diameter of the largest possible circle that could be fitted on the spatial plane of the data extent (Fig. A1) (Deems *et al.* 2006). The large scale distribution factor on snow depths, elevation, was not removed for basin-wide analysis. Removing this large-scale trend would create a bias in the calculated $\gamma(h)$ toward short scale variability (Deems *et al.* 2006). For this data set, 50 uniform bins as the lag class distance interval was used.

This analysis is taken a step further, where a single GPR transect with a length of 11.60 km is used to assess local scale snow depth variability (Fig. A2). Semivariance $\gamma(h)$ is calculated using half of the active transect lag distance h of 5.8 x 10 ^{3} m. This transect is not under the direct influence of the broad scale elevation factor since the transect ranges only by 64 m from 1688 to 1752 m a.s.l. For this dataset 50 uniform bins as the lag class interval is also used.

A.2 Results

<u>*Broad Scale Variability*</u>

The 2007 semivariogram shows clear changes in snow-depth distribution (Fig. A3). Variance increases at short spatial separations and then reaches a sill of maximum $\gamma(h)$ of 0.06 m^2. For 2007, the calculated h_0 where the variance in snow depths is autocorrelated occurs at 9.29×10^3 m separations. At the basin scale this suggests similar distribution processes may be controlled at these length scales to determine snow depth variability. Depth measurements from 0 – 9.29×10^3 m are spatially autocorrelated but measurements where h > 9.29×10^3 m are no more related than measurements at 42 km, the maximum h. Beyond this range or increasing the separation distance snow depth distribution becomes random. These results clearly suggest that snow depth variance over the Belcher basin shows higher autocorrelation at short separation distances (h) (Arnold and Rees, 2003). Arnold and Rees (2003) have observed these patterns on Lovénbreen, a 6 km^2 valley glacier in northwest Svalbard, and also Deems *et al.* (2006) in Colorado, at the Buffalo Pass, Walton Creek, and Alpine Intensive Study Areas.

Figure A1. Belcher Basin Map showing GPR transects and maximum separation distance (h) between transects (red line). Maximum separation distance was then applied to semivariance analysis to determine spatial scales of variability.

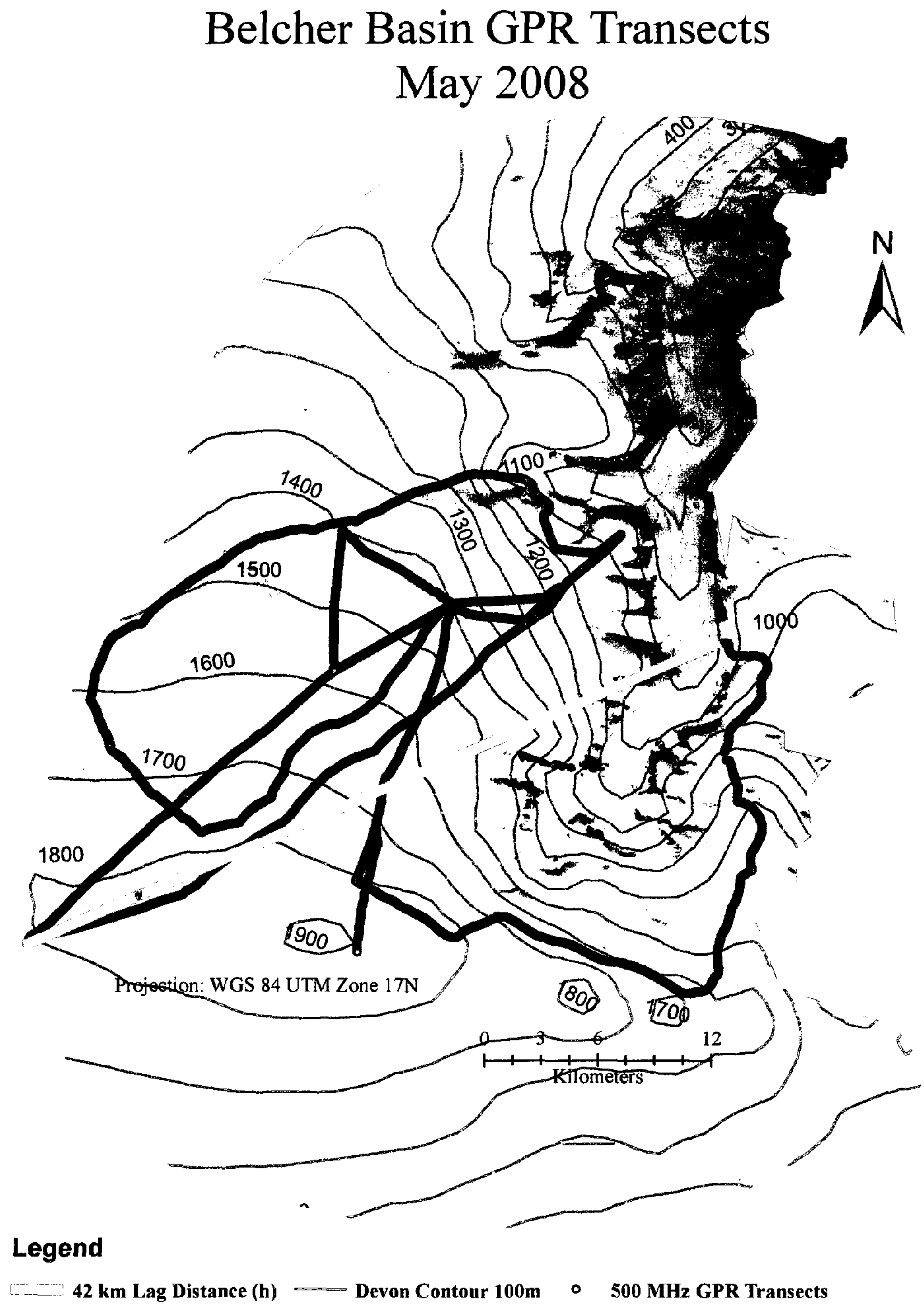

Figure A2. Belcher Basin Map showing the part of GPR transect used (red) in semivariance analysis. This transect is shown to vary little in terms of elevation between the 1600 and 1700 m contour.

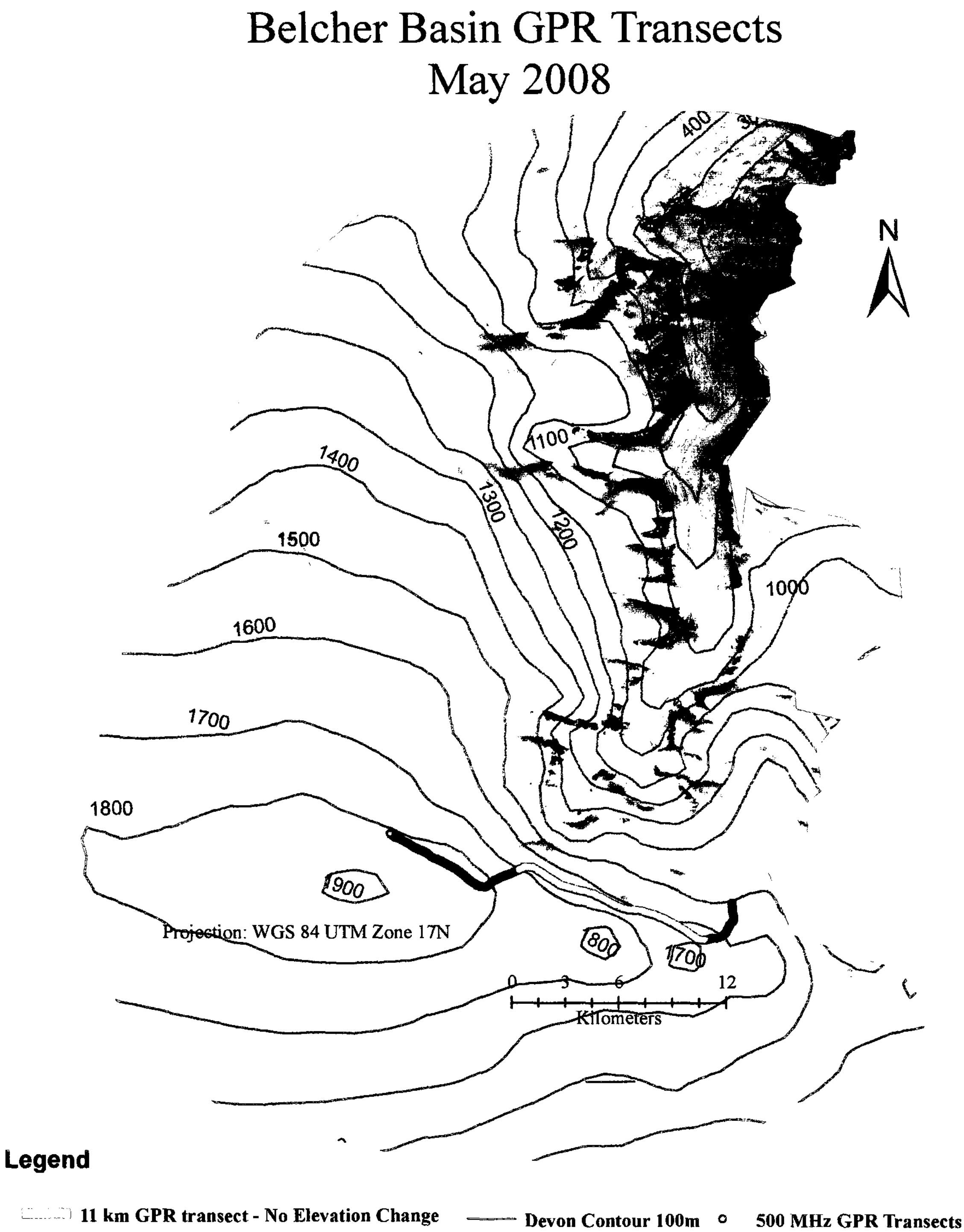

Figure A3. Modeled Exponential Semivariogram of 2007 – 2008 snow depth measurements inferred via 500 MHz GPR transects found in Fig A1.

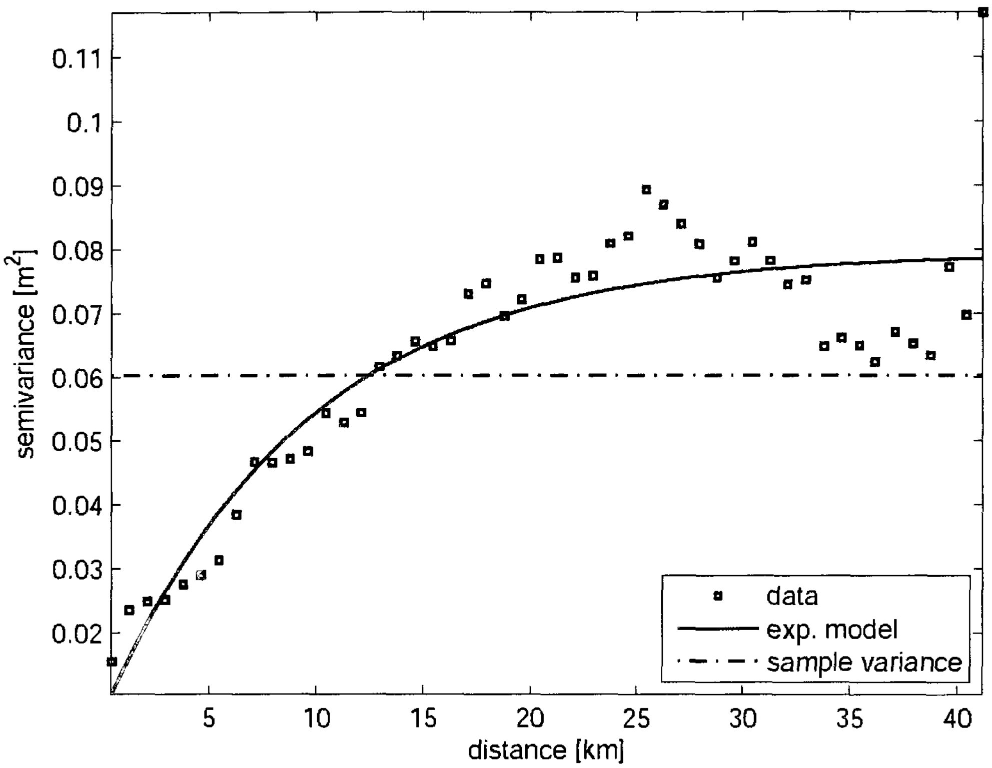

Local Scale Variability

The semivariogram shows clear changes in snow depth distribution at the local scale when elevation as a major terrain factor is removed (Fig. A4). Variance increases until it reaches a sill of maximum $\gamma(h)$ 0.026 m^2. For this transect, at h_0 where the variance in snow depths is autocorrelated occurs at separation distances of 7.2 x 10^2 m. This suggests at the local scale, similar distribution process may be controlled at these length scales to determine snow depth variability. At greater separation distances, snow depth measurements are no more related than measurements separated by the maximum separation distance of 5.8 x 10^3 m.

These findings suggest that perhaps when elevation is not impacting snow depth, that some other process may be dominant. Based on the findings with PCA of terrain factors, curvature may be an important factor at the local scale in controlling snow depth distribution. Field observations at elevations of 1600 – 1900 m a.s.l show that the primary agents of stratigraphic/SWE variability are post depositional through snow drifting/sastrugi formation (Demuth *et al.* 2007). Sastrugi locally produces rolling dune like topography which would lead to complex series of concave hollows and convex ridges. These features were shown to change markedly over the surface ranging from the 10^0 to 10^2 m scales (Fig. A5).

A.3 Conclusions

Snow depth distribution shows self-similarity in snow depth at both local (7.2 x 10^2 m) and broad (9.29×10^3) spatial scales in the Belcher Basin. For greater separation distances, snow depths are considered to be randomly distributed as indicated by the semivariograms. Broad scale evaluations here, combined with information determined via PCA of terrain factors, indicates that snow depth is controlled largely by elevation. Depth characteristically increases as elevation increases from north to south across the basin. At the local scale, however, for transects which do not change in elevation markedly, these results suggest that perhaps curvature as a terrain factor may play a large role in determining the snow depth variability and distribution. Snow depth is largely controlled by post-depositional processes in the upper elevations of the basin, as wind scours and redistributes snow across the surface. The complexity and ruggedness of sastrugi development and rolling topographic features

Figure A4. Modeled Exponential Semivariogram of 2007 – 2008 snow depth measurements inferred via the 500 MHz GPR transect found in Fig A2.

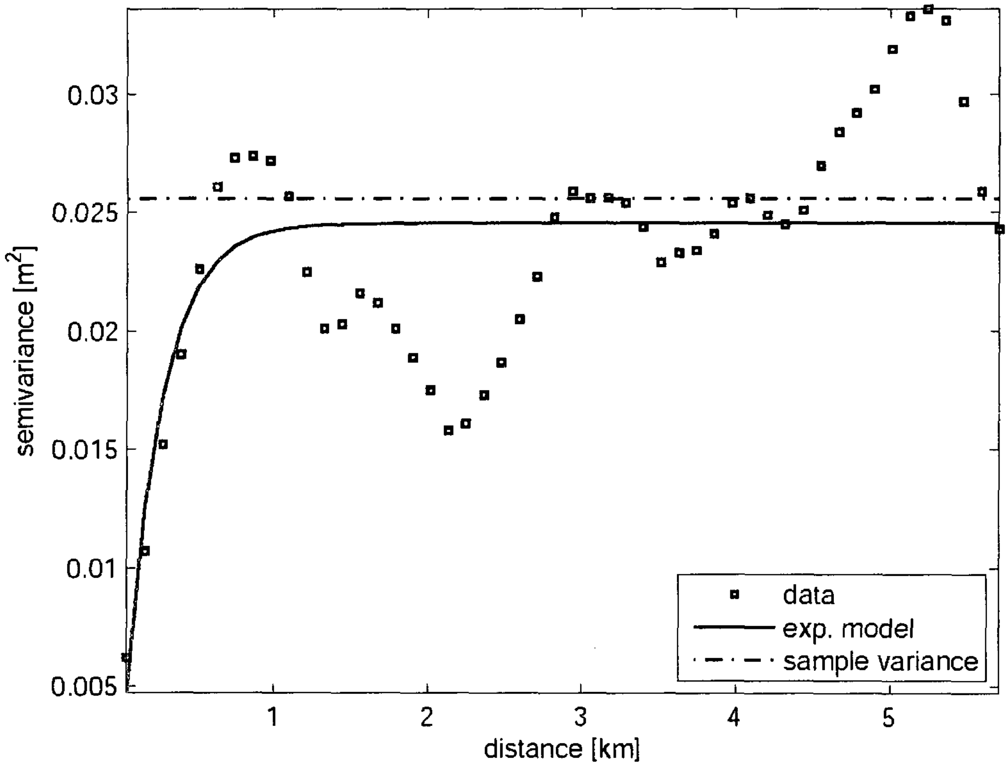

Figure A5. Photo (May 17, 2008) near the Belcher Glacier Camp Site 1060 m a.s.l. Arrows point to sastrugi fields on the surface. There is a clear interchange between concave and convex features over short horizontal distances.

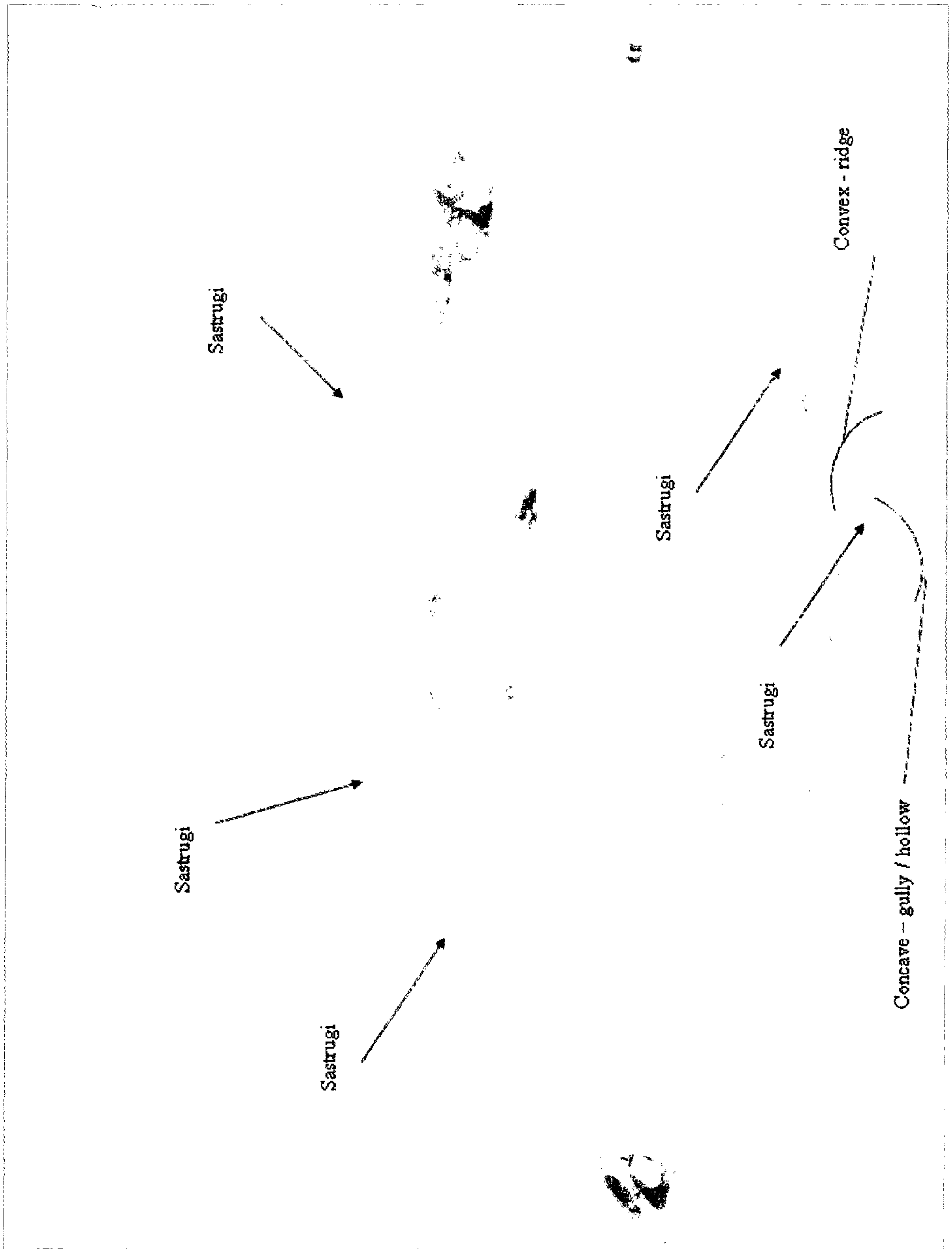

facilitates preferential collection of snow in gullies and hollows, when compared with ridges and rounded shapes.